PPPL-3250, Preprint: June 1997, UC-420, 426, 427

FEEDBACK STABILIZATION INITIATIVE

(Contributors as listed in report)

Abstract

Much progress has been made in attaining high confinement regimes in magnetic confinement devices. These operating modes tend to be transient, however, due to the onset of MHD instabilities, and their stabilization is critical for improved performance at steady state. This report describes the Feedback Stabilization Initiative (FSI), a broad-based, multi-institutional effort to develop and implement methods for raising the achievable plasma betas through active MHD feedback stabilization. A key element in this proposed effort is the Feedback Stabilization Experiment (FSX), a medium-sized, national facility that would be specifically dedicated to demonstrating beta improvement in reactor relevant plasmas by using a variety of MHD feedback stabilization schemes.

Table of Contents

Section 6: Proposed Modifications for FSX

Section 7: Research Plan and Summary

Acknowledgment of Contributors

Princeton Plasma Physics Laboratory
C. Ancher, H. Anderson, S. Bernabei, J. Bialek, M. Chance, Z. Chang, R. Ellis Jr., H. Ji, J. Chrzanowski, E. Fredrickson, R. Goldston, R. Hatcher, R. Hawryluk, P. Heitzenroeder, S. Jardin, D. Johnson, R. Kaita, T. Kozub, H. Kugel, K. McGuire, D. Majeski, J. Manickam, R. Nazikian, H. Neilson, M. Oldaker, M. Okabayashi, C. K. Phillips, N. Pomphrey, J. Schmidt, S. Scott, P. Sichta, W. Tang, R. Woolley, L. Zakharov, M. Zarnstorff, S. Zweben

CEA, Cadarache - G. Giruzzi, G.T.Hoang

CompX, Inc.- R. Harvey

CNR, Padova - P. Martin

Columbia University - M. Mauel, G. Navratil, A. Sen

Culham Laboratory - G. Gimlett, T. Hender, G. McArdle, W. Morris

ENEA, Frascati - A. Cardinali

Fusion Physics and Technology - F. Levinton

General Atomics Corporation - M. Chu, T. Jensen, R. LaHaye, R. Pinsker

ITER, Joint Central Team - W. Nevins, D. Post

Johns Hopkins University - M. Finkenthal, D. Stutman

JET-Joint Undertaking - A. Santagiustina, P. Savrukhin*
*(also Russian Research Center, Kurchatov Institute, Moscow)

Korea Advanced Institute of Science and Technology - D.-Y. Lee

Lawrence Livermore National Laboratory - C. W. Domier, N. C. Luhmann
(also University of California, Davis)

Lodestar Research Corporation - D. D'Ippolito, J. Myra

Los Alamos National Laboratory - W. Reass, G. Wurden

Massachusetts Institute of Technology - A. Bers, J. Freidberg, J. Kesner, A. Ram, J. Ramos

Oak Ridge National Laboratory - T. Bigelow, C. Bush, G. Hanson, R. Maingi, S. Milora, P. Mioduszewski, C. C. Tsai

Russian Research Center, Kurchatov Institute, Moscow - P. Savrukhin
(also JET-Joint Undertaking)

University of California, Davis - C. W. Domier, N. C. Luhmann
(also Lawrence Livermore National Laboratory)

University of California, Los Angeles - L. Schmitz
(also University of California, San Diego)

University of California, San Diego - J. Boedo, R. Conn, S. Luckhardt, L. Schmitz*
*(also University of California, Los Angeles)

University of Maryland - D. Boyd, F. Skiff

University of Texas - R. Fitzpatrick

University of Wisconsin - R. Fonck, S. Prager

Section 1: Introduction

1.1 - Role of MHD Instabilities

Ideal and resistive magnetohydrodynamic (MHD) instabilities are responsible for the saturation of β (the ratio of the plasma pressure to the pressure of the confining magnetic field) or in causing high-β disruptions. The role of ideal MHD instabilities in determining β-limits has been recognized for a long time. The empirical scaling law proposed by Troyon et al.[1] suggests that, $\beta_{max} = C_T\ I\ /\ (\ a\ B)$ where C_T is a constant in the range, $2.5 \leq C_T \leq 3.5$, and I represents the plasma current in Mega-amps, a the minor radius measured in meters, and B is the toroidal field at the mid-point measured in Tesla. This expression has long been recognized to be approximate, as it does not include more detailed profile information. Variations in the profile can make C_T have values in the range $1 \leq C_T \leq 5$. Even though this expression was obtained using stability to the n=1 external kink mode as the defining limit, it is now used as a means of expressing the achievable β in an experiment, even when the external kink is not implicated in the experimental limit. We shall also refer to the achievable β in terms of C_T.

Experimentally the β-limit is observed either as a saturation and rollover of β, or as a disruption, see Fig. 1. These high-β disruptions are generally very rapid, 10-100 μs, and are a major concern for reactor relevant plasmas. They are believed to be caused by ideal external kink instabilities. Stabilization of these instabilities would raise the achievable β, but more importantly it would prevent or at the least mitigate the dangerous effects of a hard disruption. The saturation of β is a performance limiting phenomenon and does not have the dangerous side-effects of disruptions. However it represents a major obstacle to building an economically viable reactor, and may prevent ITER from achieving its goals.

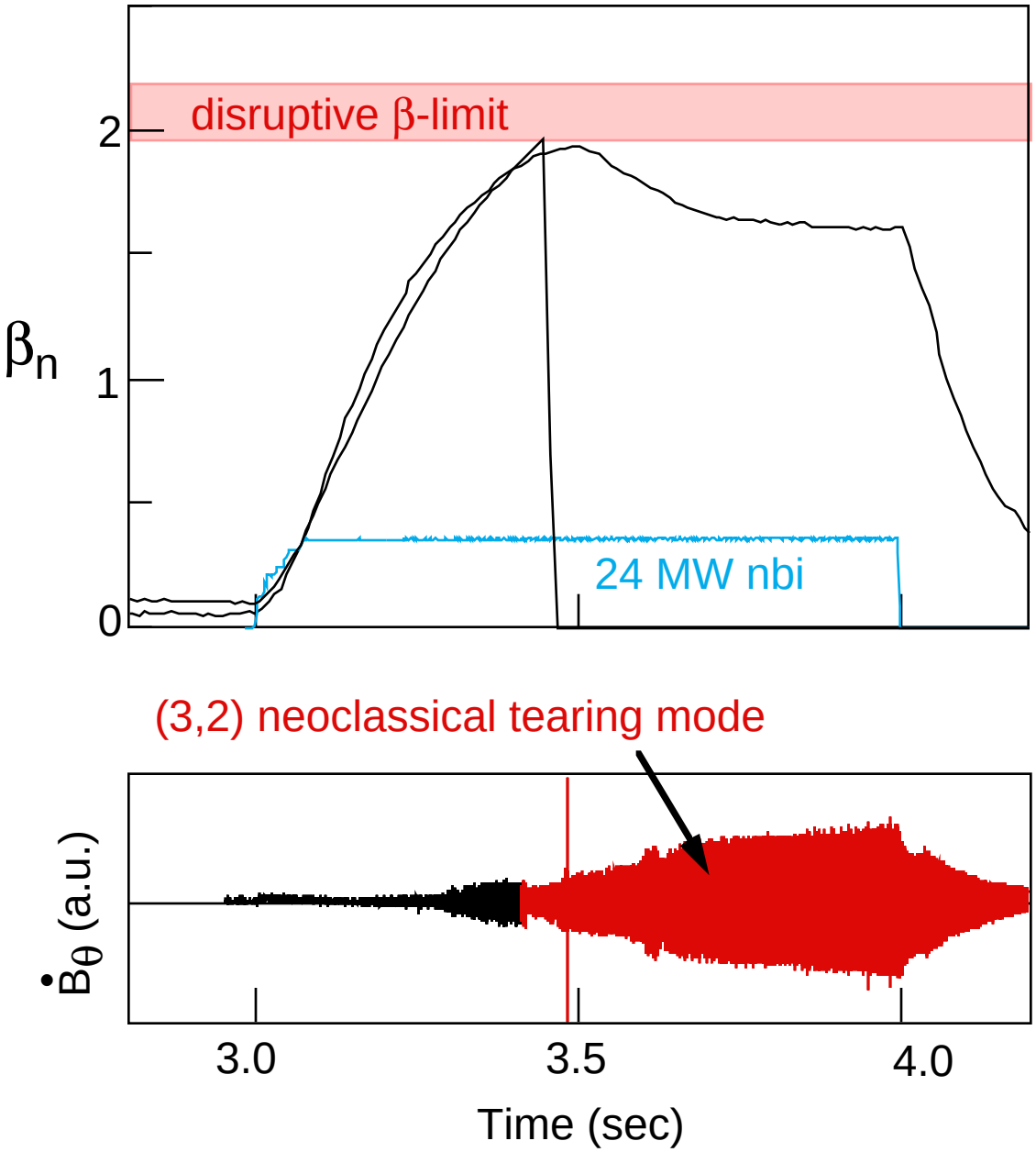

Fig. 1: Demonstration of disruption due to external kink mode and confinement degredation due to neoclassical tearing mode.

The external kink mode is driven by a combination of the free energy in the vacuum and the current drive and pressure drive terms in the plasma. Generally the current drive for the external mode can be minimized by carefully adjusting the shear, q´ , near the plasma edge. A typical example of an external mode is shown in Fig. 2. It shows the strong poloidal mode coupling to internal modes. Even though the instability is dominated by the 5/1 the eigenfunction has significant contributions from the 4/1, 3/1, 2/1 and even the 1/1. However stabilizing the 5/1 is

sufficient to stabilize the instability. This example had q_{axis} = 1.03. When q_{axis} is less than unity, the internal kink plays an important role. Stability to the internal kink depends on the details of q′ as well as the pressure gradient inside the q=1 surface. Peaked pressure profiles are particularly susceptible to strong internal kinks. In this situation the internal kink, a mode with toroidal and poloidal mode numbers m = n = 1, is dominant even though it is coupled to higher m poloidal mode numbers. In fact for most conventional tokamak scenarios, the most likely form of the limiting kink instability shows this coupling, see Fig. 3. It should be noted however that even though the m=1 mode appears to be dominant, the free boundary plays a critical role in driving the instability. Hence stabilizing the external components alone will stabilize the instability.

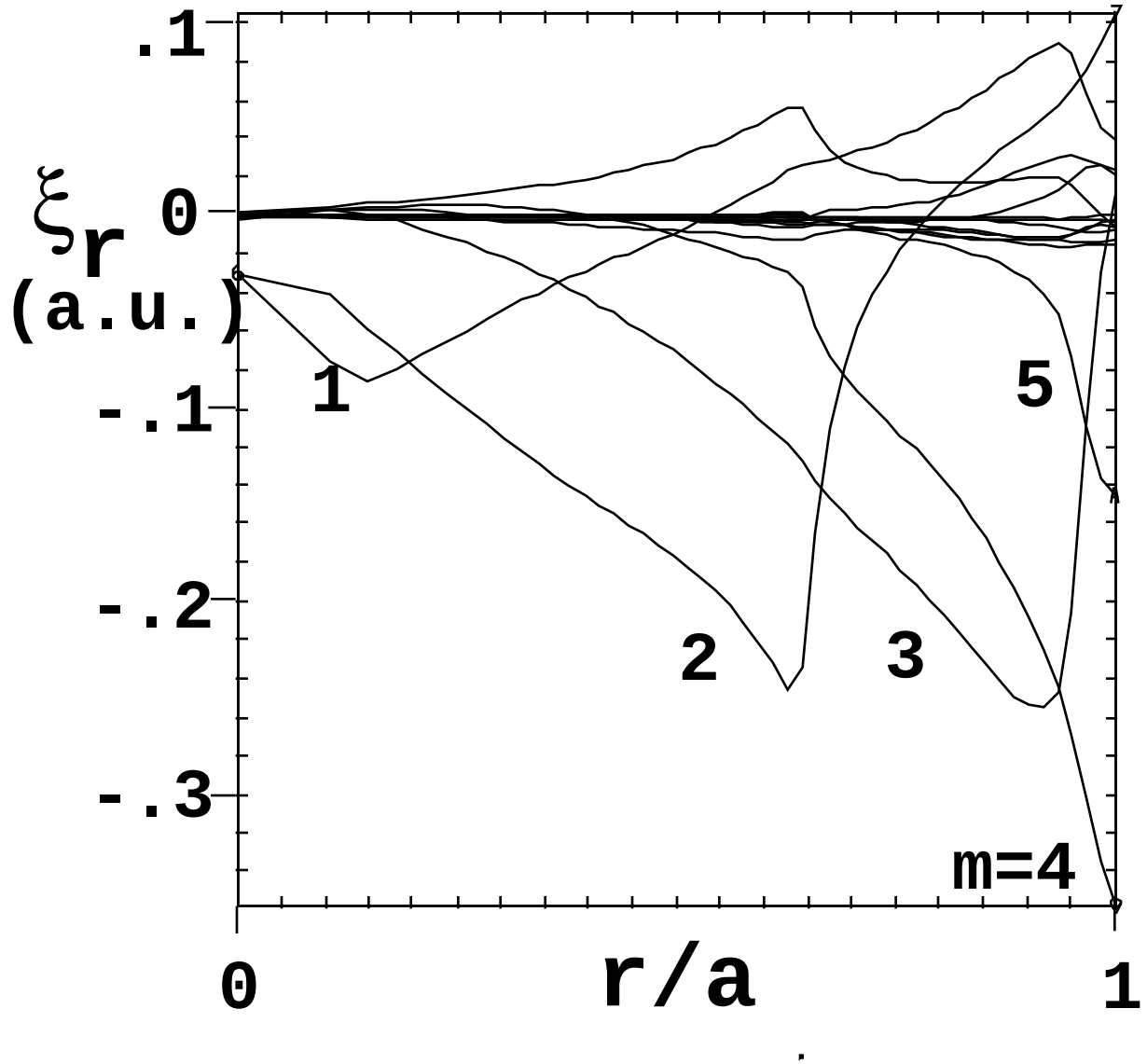

Fig. 2: Mode structure showing external kink instability.

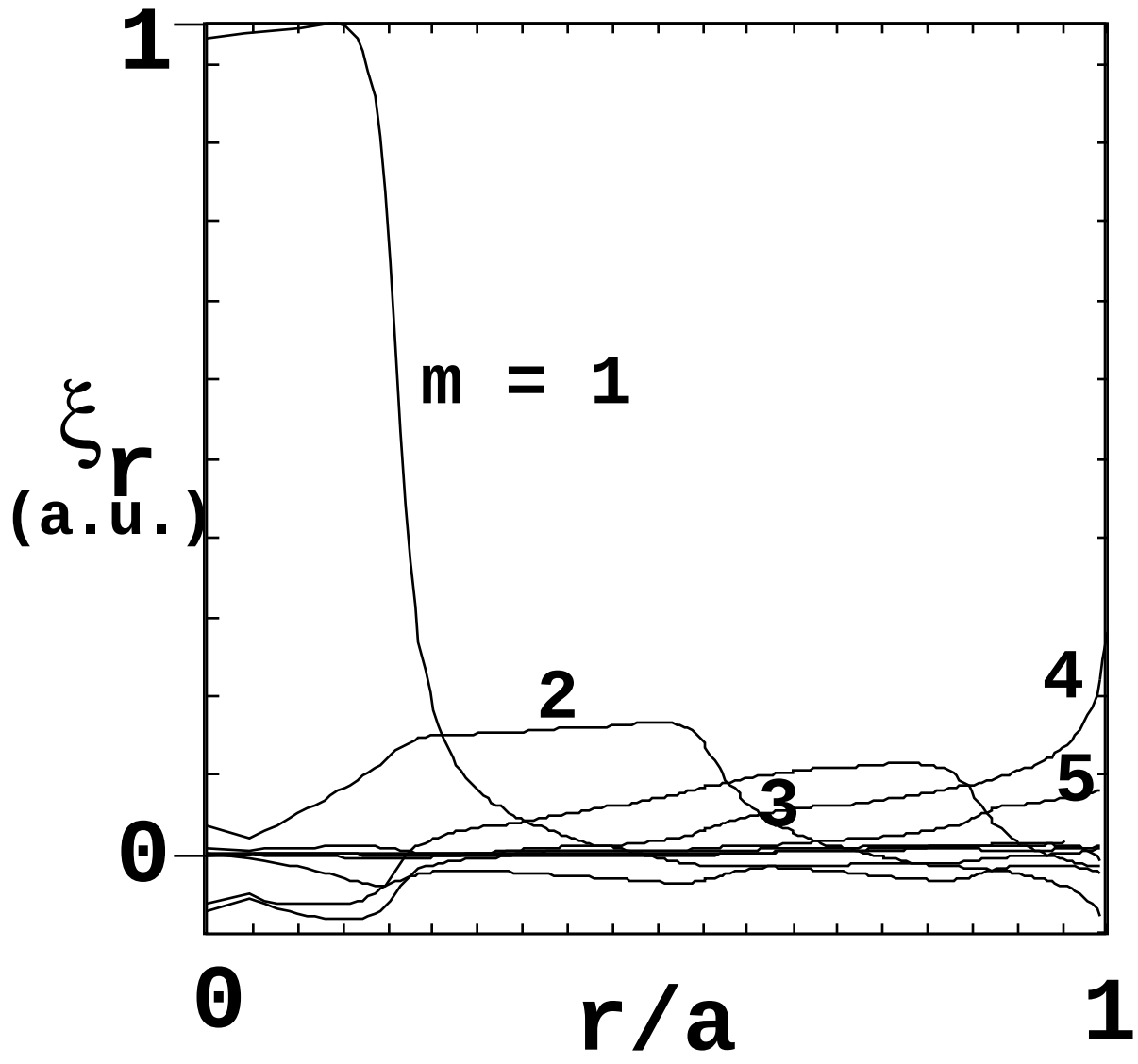

Fig. 3: Mode structure showing strong internal kink instability.

Stabilization of the external kink is easily achieved by placing an ideal conducting wall close to the plasma edge. The wall modifies the boundary condition on the perturbed radial field and forces it to zero. This effectively reduces the vacuum free energy available for the instability to grow. Wall stabilization leads to enhanced β-limits. In reality the wall in an experiment will have finite receptivity and will not cover the entire poloidal cross-section of the plasma. In this situation we expect that the ideal kink will not be completely stabilized and will be observed as a resistive wall mode.[2] Complete stabilization requires additional active elements. The elements of an active feedback system are discussed in detail in Sections 4 and 5.

The primary cause for β saturation, the other major MHD phenomenon, are tearing modes, either the conventional resistive tearing modes, or the neo-classical bootstrap current driven tearing modes. Both these modes are manifested as islands with a well defined helicity matching the rational surfaces where they are located. The most dangerous of these is the m=2/n=1, (2/1) mode located at the q=2 surface. Over the years efforts have been made to stabilize the resistive 2/1 modes with partial success. However the value of stabilizing the mode lies in providing safe access to higher β, which in turn requires stabilzing the ideal kink mode. The proposed experiment is unique in trying to stabilize both modes simultaneously.

The tearing mode is driven by a combination of the current gradients, boundary conditions and resistivity. The neo-classical version depends on the local pressure driven bootstrap current and requires a finite seed perturbation to grow. Stabilization may be accomplished by either modifying the current density within the island or by changing the boundary conditions to restrict the allowed perturbation. Both methods will be attempted in FSX details are presented in Section 5.

Pressure	Monotonic-q		Reverse Shear
	$q_{axis} < 1$	$q_{axis} \geq 1$	$q_{axis} > 1$ $q_{min} > 1$
Peaked	small 1/1	moderate 4/1 + 3/1 + 2/1 + 1/1	moderate 2/1
Broad	moderate 1/1 + 4/1	higher 4/1 + 3/1 + 2/1	largest 4/1 + 3/1 + 2/1

Table 1: The role of the pressure and q profiles in determining the potential for improvement of β by kink mode stabilization and the dominant mode numbers for q_{edge}~4.

It is important to recognize the role of the pressure and current profiles and their relationship to the MHD instabilities. As indicated earlier the value of q_{axis} relative to unity is crucial in determining the role of the 1/1 mode. We can define three classes of q profiles, $q_{axis} < 1$, $q_{axis} > 1$, and reversed shear profiles. The last of these gives access to the advanced operating mode, characterized by high β and high bootstrap currents. The pressure profile is generally characterized by the ratio of the peak to the average value. Here we will use a broader definition and discuss peaked and broad pressure profiles. Table 3.1 describes the main mode characteristics and the prospects for β enhancement in these different regimes. The values shown here are approximate and specific computations must be made including the details of the profiles. Nevertheless the table

indicates the plasma profiles where wall stabilization has the biggest impact and the relative importance of the different poloidal modes. It is clear from this table that experiments with broad pressure profiles and q >1 are most favorable for demonstrating performance improvement due to kink mode stabilization. This highlights the importance of having some measure of profile control. This will be possible if the PBX-M facility is used for these experiments, since it already has a lower hybrid system for current profile control and an ion Bernstein wave system for pressure profile control (see Sec. 3.5.1)

References

[1] F. Troyon et al., Plasma Phys. and Cont. Fusion **26**, 209 (1984).
[2] A. Bondeson and D. J. Ward, Phys. Rev. Lett. **72**, 2709 (1994).

1.2 Background and Motivation

1.2.1 Plasma Science

All the magnetic plasma confinement facilities, e.g., the tokamak, reversed field pinch, spherical torus, stellerator, etc. have problems related to one of the many MHD instabilities. The control of macroscopic coherent MHD instabilities requires further elucidation of the physics mechanisms that underlie them, so advances in plasma science will be a clear consequence of the feedback stabilization initiative.

As the leading magnetic confinement device, the tokamak concept has been pushed towards maximum performance to realize the goal of creating an efficient fusion reactor. The three largest tokamak machines in the world (TFTR in the US, JET in Europe and JT-60U in Japan) are all showing stability limitations in their highest performance regimes (Li-aided supershot, VH-mode, high-β_{pol} hot-ion mode, reversed-shear mode, etc.), including disruptions due to some type of MHD instability. Even in more modest plasma regimes, plasmas are often degraded by the existence of internal or external MHD modes. Plasma science will be advanced by the deeper understanding of these regimes which will result from the development of feedback stabilization schemes.

1.2.2 Innovation

Feedback stabilization or control of MHD has been a driver for innovation in fusion science and technology. For example, a novel feedback stabilization scheme using measurements of the eddy currents in conducting plates has been used in PBX-M to stabilize the vertical instability. Many experiments in small takamaks have also shown very promising results on the stabilization of internal MHD modes. On the HBT-EP tokamak (Columbia University), scientists have

demonstrated that adding a conducting shell can effectively suppress the edge modes and therefore increase the plasma performance. Also, in the DITE tokamak, utilizing a few external saddle coils, plasma physicists at Culham England have demonstrated the feasibility of stabilizing the m/n=2/1 tearing mode. Using local electron cyclotron wave heating and current drive, the JIPP-T11 group has shown that the sawtooth (m/n=1/1) mode can be suppressed.

However, the experimental results in small tokamaks may not be directly applicable to large takamak plasmas due to large differences in plasma parameters, and this motivates the development of further innovative feedback control concepts. For example, in TFTR, the tearing modes during supershots become pressure-gradient driven (i. e., bootstrap current driven neoclassical tearing modes). Since these modes (n=2,3) are located in the core region, feedback stabilization using external coils becomes very inefficient. Internal profile control using RF, plus a sophisticated smart coil system are required. This external plus internal feedback stabilization methodology is the main motivation of the feedback stabilization initiative, and a dedicated facility is needed and being proposed to determine its feasibility for large fusion devices like ITER.

1.2.3. Burning Plasma Physics

Burning plasma features such as steady-state operation and a high alpha particle population will likely enhance many MHD modes, including the resistive wall mode and the alpha-driven TAE/KBM. It will be critical to develop feedback technologies that are applicable to MHD stabilization in new thermonuclear plasma regimes such as those anticipated in ITER.

A specific example of an ITER relevant issue is the resistive wall mode. Since a close fitting conducting shell and external feedback coils are not practical in a reactor, a more powerful and carefully designed feedback system (such as Fitzpatrick's smart sensor and "fake-rotation" coil systems[1]) needs to be demonstrated. Implementation of this type of feedback system is one of the main experimental goals in the design of a dedicated feedback stabilization facility.

Table 1 summarizes the main MHD modes observed in present tokamaks (and other toroidal) devices. Also listed are the physical driving mechanism, their effects on plasma performance, potential effects on a fusion reactor, existing stabilizing schemes, and existing feedback experiments. The FSX goals and the tools that will be used to achieve the goals are also listed.

Reference

[1] R. Fitzpatrick and T. H. Jensen, Phys. Fluids **3**, 2641 (1996).

Table 1.

MHD mode	**mode #, frequency growth rate**	**driving mechanism**	**observed effects**	**effects on ITER**	**stabiliza-tion method**	**existing feedback experi-ments**	**feedback experiment goals and tools**
vertical instability	n=0, f=0 $\gamma \approx 1/t_A$	shaping field	termination	termination	conducting plates	elongated machines	passive shell (PBX-M)
external kink	n=1, f=0, $\gamma \approx 1/\tau_A$	∇J	disruption, lose H-mode	distuption, lose H-mode	cond. wall, high edge q'	HBT-EP PBX-M	passive shell (PBX-M)
resistive wall mode	n=1 f<kHz $\gamma \approx 1/\tau_{wall}$	∇J	mode-locking, disuption	mode-locking, disruption	active coil feedback, rotation		**goal:** smart shell & IBW active coils
classical tearing mode	n=1,2 f~10kHz γ^{-1}~10-100ms	∇J	performance degradation, disruption	low ignition margin, disruption	saddle coils, RF heating & CD	DITE (coil) Compass (ECCD)	**goal:** active coils, RF
neoclassical tearing	n=1,2,3,4, f<50 kHz, $\gamma^{-1} \approx$10-100ms	∇P	same as classical tearing	same as above	same as above	Compass ECCD DIII-D ECH	**goal** active coils, RF
sawteeth	n=1/m=1 f≈1-10kHz	q<1	reduce performance	α-driven sawteeth	local CD	JIPP-T11 (ECCD)	**goal:** RF active coils,
double-tearing in RS	n=1,m=2,3 f≈1-10kHz $\gamma \approx \omega^*_e$	qmin<2 or 3	off-axis swteeth, RS disruption		RF heating and CD		**goal:** RF
ELMs	??	edge ∇P?	reduce beta	low-β ELMy H-mode	edge IBW vel.ocity shear		**goal:** IBW
ideal/kinetic ballooning	high n f~100kHz $\gamma \approx 1/\tau_{Ap}$,	∇P	disruptions, alpha-loss	?	profile control		**goal:** RF profile ontrol
fishbone	n=1/m=1 f≈1-10kHz	fast ions	reduce performance	a-driven fishbone	local RF heating		**goal**: RF profile control
TAE	any n, f≈$f_A/2$	fast ions	fast ion loss	expel alphas			??

1.3 Opportunities for Alternate Concepts

Feedback stabilization is even more imperative for the reversed field pinch (RFP) than tokamaks. In the RFP, the ideal kink modes are unstable in the zero beta limit, and grow in the resistive wall time scale. Even with a perfectly conducting wall, the resistive tearing modes are marginally unstable, resulting in enhanced transport, and with a resistive wall, they grow to cause discharge termination.

Nonetheless, the RFP shares many similarities with tokamaks in terms of MHD instabilities and their feedback stabilization. All feedback physics understanding and technologies achieved in a high-β tokamak will be generically applicable to the RFP configuration. For instance, feedback stabilization of the resistive wall modes arising from ideal kink instabilities is expected to be the same except in mode number. The neoclassical tearing modes in tokamaks differ from the tearing modes in the RFP, but the feedback method will be the same whether local current drive or external coils are used to suppress the islands. In addition to these common features, we describe two specific experiments which can further contribute to the RFP program.

1.3.1 Feedback stabilization of nonlinearly coupled MHD modes

Unlike tokamaks, where MHD controls macroscopic stability and microturbulence controls transport, in RFPs, MHD controls both stability and transport. Both ideal and resistive MHD modes with $m=1$ and $n \approx 2R/a$ are marginally unstable in RFPs. These modes are internal, with resonant surfaces near the plasma center. Experiments [1] have demonstrated that nonlinear coupling between these modes via phase locking (see Fig. 4) is the essential process to sustain the field reversal configuration, i.e., the so-called dynamo process. The combination of large mode amplitudes – on the order of 1% of total magnetic field – and the proximity of neighboring resonant surfaces causes island overlapping, leading to formation of a stochastic region over the whole plasma volume, except within the very edge region. The resulting parallel convection along stochastic field lines is the dominant loss channel for both particle and electron energy confinement [2].

There are two logical ways to eliminate these instabilities: modification of the current profile to make the plasma stable to these modes, or to suppress them by external feedback coils. An initial test of the first method by pulsed edge poloidal current drive in MST [3] proved to be effective. A further test by radio frequency (RF) current drive is being planned as part of a national feedback stabilization initiative. The feedback method has been studied by numerical simulations [4] which showed that the feedback should eliminate the resistive wall effects. Initial feedback experiments

have been performed in HBTX-1C [5] for the external kink modes. However, no experimental test has been carried out to date for the internal modes.

Feedback stabilization of the internal MHD modes is complicated by the fact that the unstable modes are highly non-linearly coupled. Assuming that one mode could be effectively suppressed by external coils, other nearby modes would be expected to grow in its place [4]. An understanding of the physics mechanism of mode coupling is therefore highly desirable to further develop this method and to design a practical feedback system for the RFP. We point out that studies of feedback suppression of multiple modes simultaneously is a generic issue for RFPs, and even in tokamaks if one wants to operate them at or near the highest possible beta, which is clearly the ultimate objective.

We propose a two-step experiment to achieve the goal of feedback stabilization of nonlinearly coupled MHD modes. In the first step, a comprehensive physics understanding of nonlinear coupling is the objective. An elongated tokamak with a high beta or a tailored current profile can drive more than one mode unstable near the edge, providing an opportunity to study the physics of non-linear coupling in a controlled way, since the unstable mode structures are more likely concentrated on the outboard side.[6] The presence of only a few unstable modes is an important advantage in the study of the underlying physics, compared to the RFP case where many unstable modes often complicate the physics processes. For instance, if both (m=3, n=2) and (m=2, n=1) modes are coupled, then the (m=1, n=1) mode could be non-linearly unstable even though it is linearly stable. These modes can be measured by a combination of soft-X ray arrays, ECE detectors, and edge pick-up coils. Detailed measurements of the bi-spectra of these modes would shed light on the understanding of the nonlinear coupling physics.

The second step is to simultaneously stabilize a multiplicity of modes, which are nonlinearly coupled, by feedback using the knowledge acquired in the first step. The feedback can be applied to one mode first, then to two modes, and so on to investigate the extra complications which set in as one adds modes. The feedback technique can be a single method or any combination of what is described in Sections 4 and 5. Simultaneous suppression of multi-modes will eliminate not only stochastic regions, but also possibly occurrence of sawteeth, thus leading to a great improvement of confinement in the RFP.

1.3.2 Wall-locked mode control

Wall-locked modes occur in the RFP [7] much more frequently than in tokamaks, due to its sensitivity to the boundary conditions. The locked modes cause a high heat flux to impinge on

small regions of the wall or limiter, leading to impurity influx and a serious degradation of confinement. The majority of wall-locked modes in the RFP are triggered by field errors at the shell gaps or diagnostic ports. Error field suppression by feedback coils located at the shell gaps can eliminate the locked modes. However, the impulsive field errors associated with disruptive events, such as sawteeth, can cause the modes to lock to the wall. A more sophisticated system is necessary to help the modes to unlock.

Many new idea can be tested on a dedicated feedback stabilization facility, where a locked mode can be induced under certain conditions in tokamak operation. For example, the "smart" coils (Section 4.2) can be programmed in a way that they produce "fake" rotating field errors, to prevent the mode from locking to the wall, or spin up the plasma to unlock the mode. As another example, in the case of the presence of multi-modes which might nonlinearly couple to each other, one can spin up only one mode to observe the behavior of other modes, or simultaneously rotate several modes at different phases or rotation speeds. This could be used to investigate the strength of the coupling, related to the physics discussed in Section 4. If wall-locking occurs for multi-modes whose nonlinear couplings are strong, then what is locked to the wall may no longer be islands but may be a stochastic region. The transition from locking of the single-mode islands to locking of a whole stochastic region would be of great interest since RFPs are likely experiencing both cases.

References

[1] J. Sarff, et al., Phys. Fluids B 5, 2540 (1993).
[2] G. Fiksel, et al., Phys. Rev. Lett. 72, 1028 (1994); M. Stoneking, et al., Phys. Rev. Lett. 73, 549 (1994)
[3] J. Sarff, et al., Phys. Rev. Lett. 72, 3670 (1994).
[4] E.J. Zita. et al., Nucl. Fusion 32, 1941 (1992).
[5] B. Alper, Phys. Fluids B 2, 1338 (1990).
[6] S. Sesnic, et al., Nucl. Fusion 34, 1365 (1994).
[7] A. Almagri, et al., Phys. Fluids B 4, 4080 (1992).

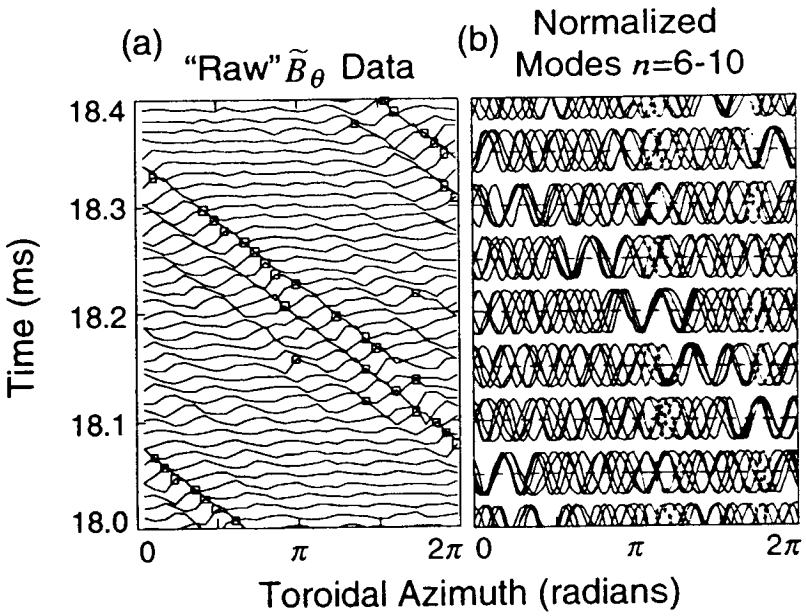

Fig. 4: An example of nonlinearly coupled MHD modes (via phase locking) observed in MST RFP device (from Ref. 1). (a) Spatially localized rotating "bump" in poloidal field fluctuations. (b) Phase alignment between the dominant modes at the location of the “bump.”

Section 2: Background and History of Work

2.1 Introduction

For the development of feedback stabilization schemes, we require high performance regimes which are initially unstable to a variety of modes (possibly coupled through the shape and finite beta effects) of different geometrical structures and time dependencies. Ideal external kink modes and their resistive counterparts, tearing modes, are the most essential instabilities which limit respectively the peak and long term plasma performance. Their feedback stabilization is crucial for further increasing tokamak performance.

In this section, we present overview of stability of the kink and tearing modes as well as different kinds of possible feedback stabilizations based on control of magnetic fields, application of a ponderomotive force (by neutral beams and radio frequency waves), the local current drive near the resonant surface, and control of the halo currents in the scrape off layer.

2.1.1. External kink modes

When the plasma pressure increases, the external kink modes first become unstable if there is no stabilizing wall outside the plasma. In conventional tokamaks, this instability leads to the absolute (hard) beta limit, i. e., $\beta_0 \equiv \beta_{\text{no wall}}$. The presence of the ideal (virtual) wall would stabilize the plasma over an extended range of the plasma pressure, and thus would result in a higher beta limit, i. e., $\beta_W \equiv \beta_{\text{with wall}} > \beta_{\text{no wall}}$.

In the range $\beta_0 < \beta < \beta_W$, with a resistive wall within the radius of a virtual ideal wall, the plasma still remains unstable (assuming no rotation), but the growth rate of the instability is reduced from that of MHD fast growth to a significantly lower value determined by the resistive penetration time of the wall.[1]

In the simplified case of a plasma with a circular cross section and only one unstable mode this residual growth rate (γ)of the external mode can be written in terms of the resistive penetration time of the wall (τ_W) and the radius (r_{iW}) of the virtual ideal wall, marginally stabilizing the plasma according to the expression

$$\gamma\tau_w = \frac{2m}{(\frac{r_{iw}}{r_{rw}})^{2m} - 1}, \tau_w \equiv \mu_o \sigma \delta r_{rw}, r_{iw} > r_{rw}, \qquad 1.1$$

where m is the poloidal mode wave number, r_{rw} is the radius of the resistive wall, σ is the wall conductivity, and δ is the thickness of the wall. Because of reduced growth rate, the appropriate feedback system can completely suppress the instability.

According to Eq.(1.1), feedback stabilization can be effective only when $r_{rw} > r_{iw}$. Implicitly, the radius r_{iw} depends on the current and pressure profiles inside the plasma and on the shape of the plasma and geometry of the wall. Eq.(1.1) shows that when r_{iw} is reduced (e. g., due to an increase in the plasma pressure) and approaches r_{rw}, the growth rate of the mode increases to infinity. In fact, for $r_{iw} > r_{rw}$, the mode becomes violently unstable with a the fast MHD growth rate, and according to Eq. 1.1, cannot be stabilized by feedback.

Thus, concerning external modes, the best that can be expected for a feedback system is that in combination with a resistive wall, the feedback system can create the equivalent of an ideal wall at the same position. Such a feedback system can stabilize the plasma for $\beta < \beta_w$.

In Eq. 1.1, it was assumed that the resistive wall has no gaps. A real resistive wall, with the presence of both toroidal and poloidal gaps, is less effective for stabilization. It still can reduce the growth rate of an instability, but in a narrower range of the plasma beta. Essentially, a wall with gaps has a larger effective distance (or radius $r_{rw,eff}$) from the plasma, or $r_{rw,eff} > r_{rw}$.[2] The second negative effect is that gaps expand the spatial harmonic spectrum of the magnetic field applied to the plasma, and make its time behavior very complicated.

On the other hand, gaps in the resistive wall allow for control of the slowly growing tearing modes by the feedback system. In the presence of gaps and with an appropriately optimized signal, a feedback system can be more stabilizing for the tearing modes than an ideal external wall.

2.1.2 Tearing modes

Tearing modes have a resonant surface inside the plasma. They produce magnetic islands inside the plasma and deteriorate the confinement. Growing magnetic islands can lead to mode locking and disruptions a lower level of β than the limit imposed by the external modes. These modes have been extensively studied theoretically and and were the object of feedback stabilization on several tokamaks.[3,4,5]

Even at low beta, interaction of the tearing modes with the externally applied magnetic fields have a significant dependence on many nonideal effects near the mode resonant surface, including plasma motion relative to the magnetic island, viscosity, diamagnetic drifts, etc. Nonideal effects make the

interaction of the island with external magnetic fields complicated, but on the other hand, allow mode stabilization even with nonrotating external fields.[6,7]

At low beta, the stability of the tearing modes depends on the plasma current profile and the boundary conditions. At low beta, for typical tokamak conditions, the stability can be easily provided for all tearing modes with m>2. The m=2 mode imposes some restrictions on the current profiles and may lead to disruptions if the current channel shrinks (i. e., due to plasma boundary cooling). Feedback stabilization at low beta has been successful in suppressing the m=1 disruption precursor, and allowed an increase in the density limit up to 20%.[5]

At finite beta, there is a significant destabilization due to the bootstrap current.[8,9] Theoretically, all tearing modes should be unstable at finite beta and lead to saturated islands. Partial (but insufficient) stabilization occurs due to the Glasser-Green-Johnson (GGJ) effect.[10]

While at low beta tearing modes were studied comprehensively, and understanding of the bootstrap current driven tearing modes at finite beta is one of the challenges forfeedback stabilization in high beta plasmas.

In general, the stability of the tearing mode is described by the Δ' parameter, which determines the time evolution of the magnetic island,[11] i. e.,

$$0.8\tau_\eta \frac{d}{dt}\frac{W}{r_s} = r_s\Delta', \tau_\eta = \frac{\mu_0 r_s^{\,2}}{\eta}, \qquad 1.2$$

where W is the island width, τ_η is the plasma resistive time, and r_S is the radius of the resonant magnetic surface. It is important to point out several contributions into Δ', specifically coming from the plasma global current distribution Δ'_0, quasilinear current redistribution Δ'_W, feedback system Δ'_{fb}, possible local active current drive Δ'_{CD}, bootstrap current Delta'_{neo}, GGJ effect Δ'_{GGJ}, and the polarization drift.

At finite beta for small magnetic islands, the most significant effect comes from the bootstrap current, i. e.,

$$\Delta'_{neo} = 3.17 k_2 \beta_{pe} \sqrt{\frac{r_s}{R}} \frac{L_s}{L_{Te}} \frac{W}{W^2 + W_e^{\,2}},\ k_2 = 1.17, \qquad 1.3$$

where β_{pe} is the local poloidal beta $2\mu_0 p/B_p^2$, $L_s \equiv q/q'$ and $L_{Te} \equiv T_e'/T_e$ are the scale lengths of the safety factor and electron temperature, and W_e is a characteristic island width determined by the ratio of the perpendicular and parallel transport.

For $W<W_e$, the neoclassical term can be small compared to other contributions, and becomes dominant when W approaches W_e. Thus, W_e determines the threshold for excitation of tearing modes. Theoretically, W_e may be very small ($\cong$0.1 cm),[12,13] which makes the bootstrap current contribution large for small islands. In TFTR experiments,[14] excitation of the mode typically starts at W$\cong$1cm, which is several times larger than what theory estimates. This discrepancy is one of the important issues in the further study of neoclassical tearing modes.

The GGJ contribution[15] depends on the total pressure gradient

$$\Delta'_{GGJ} \cong 3.7266 \frac{2\mu_0 p' r_s}{B_s^2 s^2 / 4}\left(q^2 - 1\right)\frac{1}{W}, s \equiv \frac{q' r_s}{q}, \qquad 1.4$$

and stabilizes small islands. The GGJ effect plays a role in determining the threshold for mode excitation,[13] and may be important in regimes with $T_i > T_e$.

The contribution from local current drive depends on its localization and positioning with respect to the resonant surface

$$\Delta'_{CD} \cong +\frac{\mu_0 R\delta j}{B_0 q' h_l} - \frac{\mu_0 R\delta j}{B_0 q' h_r}, h_r \equiv r_r - r_s, h_l \equiv r_l - r_s, \qquad 1.5$$

where δj is the value of the CD current density, and h_l and h_r are the distances (with the proper sign) between the resonant surface and the left r_l and right r_r boundaries of the current drive region.

The contribution from the electromagnetic feedback system can be evaluated based on the linear theory of tearing modes in terms of solutions of the Euler equation outside the resonant surface

$$\Delta'_{fb} = -g\left(\frac{\psi'_{ext}}{\psi_{ext}} - \frac{\psi'_{pl}}{\psi_{pl}}\right)_{rs+\varepsilon}, g \equiv \frac{\psi_{ext}}{\psi_s} \propto \frac{I_{fb}}{\psi_s}, \qquad 1.6$$

where g is the gain factor, ψ_{ext} is the helical flux from the feedback coils with currents I_{fb}, ψ_{pl} is the helical flux outside the plasma from the plasma deformation (i. e., the linear solution which vanishes at $r \rightarrow \infty$), and ψ_S is the perturbation of the helical flux at the resonant magnetic surface

$$\psi_s = \frac{B_{pol}}{16} \frac{r_s q_s'}{q'} W^2, \qquad 1.7$$

which is equivalent to the detected signal used for feedback.

Use of the vacuum approximation for perturbations of the magnetic field gives

$$\psi_{ext} \cong \frac{\mu_0 r 2_{fo} I_{fb}}{2} \frac{r^m}{r_{fb}^m}, r_s \Delta'_{fb} = -\frac{m}{2} \frac{\mu_0 r_{fb}^2 I_{fb}}{\psi_s} \left(1 + \frac{r_s^{2m}}{r_{fb}^{2m}} \right), \qquad 1.8$$

where r_{fb} is the distance of feedback coils from the plasma center.

Figure 1 shows plots of two groups of terms in the RHS of the mode evolution equation (1.2), one which is dependent on the island size W and another which is not.

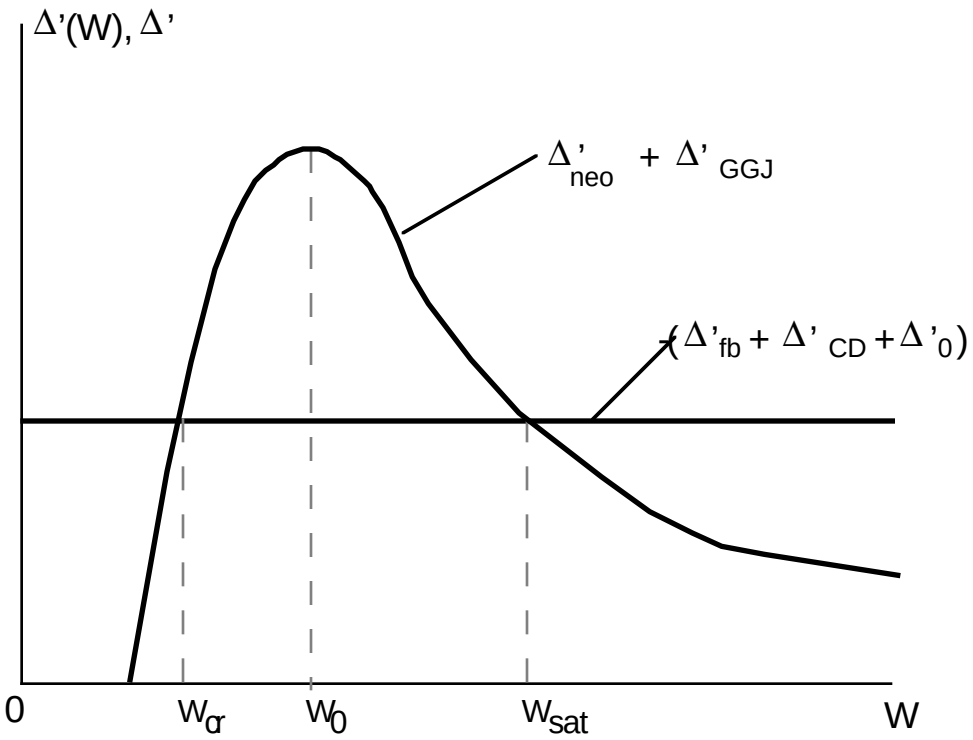

Fig. 1: Mode evolution with and without dependence on island size (W).

Here, W_{cr} is a threshold island width, W_{sat} is the saturation island width, and W_0 is a characteristic island width for the local plasma effects. The mode is excited when the initial perturbation exceeds W_{cr}.

A feedback system can control the intersection of the two curves on Fig. 1 through the value of Δ'_{fb} as well as be used to study the saturation level W_{sat} and the threshold W_{cr} of excitation. At present, the theory of tearing modes only qualitatively predicts the dependence of the Δ' on the island size, while there are appearent descrepancies between the theory and experiment in the values of W_{cr} and W_0.

Thus, use of feedback in a high beta experiment can provide unique information for further understanding the tearing modes and limits they impose on high beta tokamaks.

Suppression of neoclassical tearing modes requires a much higher Δ'_{fb} contribution (or equivalently, a higher gain factor) and the possibility of the phase flip instability exists in the presence of big saturated islands.[16] Because of this possible caveat, the best resolution achievable in the detection the perturbation is of high priority. Furthermore, if the detectable level

of W would be lower than the threshold value W_{cr}, a feedback system can completely stabilize the tearing modes.

References

[1] S.W. Haney and J.P. Freidberg, Phys. Fluids **B 1**, 1637.

[2] R. Fitzpatrick, Phys. Plasmas **1**, 2931, (1994).

[3] K. Bol et al., Plasma Physics and Controlled Nuclear Fusion Research, Tokyo, 1974 (International Atomic Energy Agency, Vienna, 1975), **Vol. 1**, p. 83.

[4] V.V. Arsenin et al., Plasma Physics and Controlled Nuclear Fusion Research, Innsbruck, 1978 (International Atomic Energy Agency, Vienna, 1979), **Vol. 1**, p. 233.

[5] A.W. Morris et al., Phys. Rev. letters **64**, 1254 (1990).

[6] F. Karger, H. Wobig, and S. Corti, Plasma Physics and Controlled Nuclear Fusion Research, Tokyo, 1974 (International Atomic Energy Agency, Vienna, 1975), **Vol. 1**, p. 207.

[7] T.C. Hender et al., Nucl. Fusion **1**, 2091 (1992).

[8] J. D. Callen et al., in Plasma Physics and Controlled Nuclear Fusion Research, Kyoto, 1986 (International Atomic Energy Agency, Vienna, 1987), **Vol. 2**, p. 157.

[9] R. Carrera, R.D. Hazeltine, and M. Kotchenreuther, Phys. Fluids **29**, 899 (1986).

[10] A.H. Glasser, J.M. Green, and J.L. Johnson, Phys. Fluids **18**, 875 (1976).

[11] P.H. Rutherford, Phys. Fluids **16**, 1903 (1973).

[12] R. Fitzpatrick, Phys. Plasmas **2**, 825 (1995).

[13] N.N. Gorelenkov et al., Phys. Plasmas **3**, 3379 (1996).

[14] Z. Chang et al., Phys. Rev. Letters **74**, 4663 (1995).

[15] M. Kotschenretuer, R.D. Hazeltine, and P. J. Morrison, Phys. Fluids **28**, 294 (1985).

[16] E. Lazzaro and M.F.F. Nave, Phys. Fluids **31**, 1623 (1988).

2.2. Critical Discussion of the Literature

Role of the feedback techniques in *controlled* nuclear fusion research.

Various feedback control techniques have been extensively used in controlled nuclear fusion research from the very beginning of the program. Through the years they provided tremendous improvement in plasma parameters and reliability in the operation of experimental facilities.

Feedback control systems have become even more important at the present stage of the fusion research, where the main effort of the fusion community is to design an economically-feasible and environmentally-safe tokamak reactor. Moreover, application of feedback techniques is even more crucial in the present extensive experimental analysis of various alternative systems (reversed field pinches, spheromaks, etc.) with extremely complicated magnetic configurations and plasma scenarios.

At the present stage of the tokamak research, the reliable attainment of good confinement in a reactor-grade plasma is limited, in particular, by a variety of the plasma perturbations (see Sections 1.1 and 2.1). In order to overcome the instabilities, and improve plasma operation close to the stability limits for a longer time, several feedback control systems must be installed and effectively studied in the experiments.

These experiments differ mainly in the various strategies of the feedback control and utilization of various control techniques and parameters. **Four strategies** for feedback control systems are used in order to improve the effectiveness of the tokamak reactor:

- a) Identification of potentially unstable plasma conditions and **avoidance** of operation in the regimes with low stability limits.
- b) Identification of the plasma perturbations and control (**stabilization**) of the dominant modes.
- c) **Soft termination** of the plasma discharge.
- d) Amelioration of the instability and **recovering** from the possible disruptions.

The first two strategies were considered as the primarily ones in previous experiments because they provided performance improvement, and allowed record plasma parameters to be reached. The disruption mitigation strategies are approaching the same level of importance at the present stage of the research, where the goal is improved effectiveness for a reactor.

Feedback schemes based on an avoidance strategy is a standard technique commonly used in magnetic confinement devices. They range from simple feedback for gas fueling and current

control to elaborate state-of-the-art plasma shaping systems (e. g., the Plasma Position and Current Control system in JET [1] or the vertical position control system in PBX-M [2]).

Stabilization techniques were extensively studied in many experiments. It was demonstrated that the control systems allowed dominant perturbations (m=2,n=1 m=1,n=1, etc. modes) to be stabilized, and this resulted in considerable improvement in the plasma parameters (see reviews in References 3,4, and 5). However, most of ththis work involved so-called "open loop" loop schemes without feedback adjustment of the system. To date, studies of feedback control have been made with the application of external stabilizing resonant magnetic perturbations (RMP) in the tokamaks DITE [6], TO-1 [7], and ATC [8], and modulated ECRH/CD in Compass-D [9] and JFT-2M [10] (see below). More experiments are thus urgently required for optimization of the strategy and design of feedback stabilization systems for reactor applications.

The problem of mitigating disruptions, which were considered in early experiments as a simply a nuisance, has arisen as a primarily concern in large tokamaks (e. g., TFTR, JET, JT-60U). This is due to their extremely strong potential for significant plasma perturbations and plasma-wall interactions. Such consequences will be even more serious in future reactors if no sufficient feedback systems are designed. At present, methods of the disruption amelioration include the controlled ramping down of the plasma current and magnetic field in a preprogrammed, way when some plasma perturbations exceed the threshold for soft discharge termination by pellet injection,[1] ergodisation of the magnetic surfaces by external currents (Tore Supra), [12] and application of electron cyclotron resonance heating (ECRH) to reheat the plasma (T-10).[13] One of the main problems in the studies to date, however, is the lack of feedback experiments in this area.

Experimental studies of the modes control in tokamaks.

Control of plasma perturbations has been extensively studied in many experiments on tokamaks. Such studies have been generally based on the separate application of various control techniques, including resonant magnetic perturbations (RMP) and systems providing non-inductive current drive (i. e., ECRH/CD, LHCD, and FWCD), local plasma heating (i. e., NBI, RF, and ECRH), and momentum transfer (i. e., NBI and IBW).

Experiments with the Resonant Magnetic Perturbations

Experiments with resonant magnetic perturbations were initiated in 1973-1975 on ATC [8] and Pulsator,[14] and were later continued on many tokamaks (see Table 1).

Table 1

Machine	R/a (cm)	aspect ratio	k	SHAPE of the windings	place	control scheme	dominant harmonics of the perturbed field
TBR	30/8	3.8	-	helical windings 2/1 3/1 4/1	OUT	DC	3/1 2/1
TOSCA	30/8	3.8	-	4 saddle coils ($\Delta\varphi=180^{o}$)	OUT	DC	1/1 3/2 2/2
TORIUT-4	30/12	2.5	-	helical windings 3/1 2/1	OUT IN	DC	2/1 egodisation
HT-6B	45/12	3.8	-	helical windings ($\Delta\varphi=180^{o}$)	OUT	DC	2/1
Compass-C	50/20	2.5	-	poloidal field shaping system	OUT	DC	2/1(1mT at 20cm) 3/2 1/1 3/1
Tokoloshe	52/24	2.2	-	helical windings 2/1 3/1 1/1 ($\Delta\varphi=180^{o}$)	OUT	DC	2/1 1/1 3/1
Compass-D	56/20	2.6	1.6	poloidal field shaping system (3000 combinations)	OUT	DC, AC	2/1, 3,1
TO-1	60/18	3.3	-	helical windings 2/1($\Delta\varphi=180^{o}$)	IN	DC,AC, FB	2/1
PULSATOR-I	70/12	5.83	-	helical 2/1,1/1 ($\Delta\theta=270°$)	IN OUT	DC	2/1 1/1 4/2
CLEO	90/13	6.9	-	4 Saddle Coils	OUT	DC	2/1(1mT at 13cm) 1/1, 3/2
ATC	90/20	4.5	-	4 Saddle Coils		DC,AC, FB	2/1

HBT-EP	92/15	6.1	-	Saddle Coils ($\Delta\varphi<6^o$)	OUT IN	DC,AC, FB	2/1
JIPP-TIIU	91/24	3.8	-	2 helical 3/1 ($\Delta\varphi=30^o$)		DC	3/2 3/1 ergodisation
T-7	100/30	3.3	-	2 Saddle Coils ($\Delta\varphi=10^o$)	OUT	DC	2/1(2.5mT at 30cm)
DITE	119/23	5.2		8 Saddle Coils	IN	DC,AC, FB	2/1(0.1mT at 20cm)
JFT2M	130/30	4.5	-	8 Saddle Coils	IN	DC,AC	2/1, 1/1
PPPL high-β feedback experiment	145/45	4.5	1.6	active & passive coils	IN	DC,AC, FB	2/1
DIIID	168/70	2.4	1.4	1 Saddle Coil 6 Saddle Coils	OUT	DC	n=1 FB error field correction
Tore-Supra	240/75		-	6 Saddle Coils ($\Delta\theta=120°$, $\Delta\varphi<11°$)			16 <m<22, n=6
JET	296/99	2.4-3	1.5 - 1.7	8 Saddle Coils	IN	DC,AC, FB	2/1(0.75mT at 70cm)

Experiments with RMP (open loop) demonstrated:

- Suppression (stabilization) of the 2/1, 3/1, and 1/1 modes and sawteeth (see [14-
- 17] and refences therein]
- Delay of the mode locking with a rotating AC field (JET [18] initial experiments)
- 15-20% increase of density limit (DITE [6], Compass-C [16])
- Prevention of the fast plasma disruption at density limit (Tore-Supra [12])
- Verification of the dynamic model for locked and rotating MHD modes, and trigger conditions for disruptions under specific experimental conditions (see [19] and references therein).

Most of the experiments listed in Table 1 were made on small tokamaks with plasma parameters far from reactor conditions. This complicates extrapolation of the results to larger machines. Initial experiments with the reactor-relevant plasmas (e. g., JET [20] and DIIID [21]) provided important

results, but they also demonstrated that control techniques cannot be effectively tested and optimized on such large-scale tokamaks with tight schedule of the experiments, extremely high cost of operation, and the damaging consequences of the possible disruptions.

Feedback stabilization has been studied on several smaller plasma devices [6-8], but these results also have not yet been extended to major tokamaks (e. g., JET and DIII-D), due in part to the necessary investment in expensive feedback hardware and by the conflict of such studies with other important facility missions competing for very limited run time for experiments.

A very successful campaign of feedback stabilization experiments was carried out on the DITE facility.[6] The feedback was done using a set of eight saddle coils using phase controlled feedback. In these experiments, a (2,1) tearing mode was stabilized and the density limit was raised by 10-20%. However, the experiments were carried out in ohmically heated plasmas, and the bootstrap current contributions to stability were minor. Typical DITE parameters were R_0=1.19 m, r_p=0.23 m, I_p = 70 - 125 kA, and B_t= 1.0 - 2.0 T. Experiments similar to those carried out on DITE are in progress on HBT-EP.[22] The experience gained on these smaller experiments should prove invaluable in initiating the next phase of feedback stabilization experiments on a high beta feedback experiment.

Experiments on ACT, TO-1, and DITE indicated the complexity of the non-linear dynamics of the MHD perturbations, often leading to the loss of control system stability. Control of the modes by magnetic feedback is also complicated due to direct detection of the external field by the magnetic pickup coils used for measurements of the internal magnetic perturbations. In order to provide stabilization of the MHD modes in a wide range of the plasma parameters, control systems require on-line processing of the feedback signals and adaptation of the control algorithms. Such adaptation of the control system can be provided by a digital controller (see for example Ref. 23). This improves stability of the control technique, but contributes additional non-linearity to the system dynamics. The non-linear characteristics of the control system and non-linear dynamic features of the MHD modes (generally not well defined) complicate assessment of the control techniques. Under such conditions, evaluation of the feedback parameters in the initial stages of the experiment often leads to loss of system stability with the subsequent abrupt growth of the magnetic perturbations and plasma disruptions. Therefore, optimization of the initial stages of the experiment with magnetic feedback becomes quite important in order to minimize the possibility of such disruptions.[24]

A number of experiments have been carried out with static resonant fields. These include experiments on COMPASS,[25] JET,[18] and DIII-D.[21] Studies of the susceptibility of tokamak plasmas to modes excited by static resonant fields have provided important information on scaling to larger machines. The present understanding of these effects suggests that very stringent restrictions on the error fields in ITER are necessary to avoid excitation of MHD modes. Initial experiments on JET allowed the measurement and partial compensation for the intrinsic error field under some specific conditions.[18] More experiments are urgently required in this area to improve predictions of error field effects in future reactors. The external coil set in a future high beta feedback experiment can be used to provide additional documentation on this important topic.

Control of the MHD instabilities with non-inductive current drive (LHCD, ECCD) and plasma heating (ECRH).

Application of the current drive and plasma heating for suppression of the MHD perturbations is based on an extensively developed theory of the tearing modes (see Section 2.1 and Section 5) as well as the analysis of numerous experiments.[26-38] Several mechanisms for mode suppression were considered in the experimental and theoretical studies (Table 2). Realization of the different ways for m=2,n=1 mode control is based on a variety of plasma parameters (including current density, shear, and transport coefficients) and on the scheme of heating and current drive used in the particular experiments.

Among the more commonly used techniques is the continuous application of power in the electron cyclotron (EC) frequency range. Stabilization of the m=2,n=1 mode was observed when the radio frequency (RF) power was on the order of the ohmic power. Initial experiments involving the stabilization of MHD activity with the use of lower hybrid current drive (LHCD) were made in ASDEX-U [39] and PBX-M.[40] These experiments indicated that LHCD can be also considered as a technique for feedback control in future experiments. Dedicated LHCD experiments are required to permit a systematic comparison between the electron cyclotron current drive (ECCD) and ECRH techniques.

Continuous (unmodulated) application of ECRH/ECCD and LHCD was also used for the suppression of the internal m=1,n=1 mode and the stabilization of sawteeth. It was demonstrated that one can change the amplitude, period, and crash time of the sawteeth in a controllable manner by adjusting the input power and plasma parameters.[41]

Application of modulated co-current drive or plasma heating in the O-point of the island is theoretically a more effective technique compared with continuous heating or current drive. While

initial experiments at Compass-D [9] and JFT-2M [10] indicated the possibility of feedback control of the 2,1 mode, they have also shown that more dedicated experiments are required for reliable mode stabilization.

Future high beta feedback experiments can use modulated LHCD and ECRH/CD for local current feedback control of MHD. Both RF sources can also be used for feedback control through local heating. The proposed applications of such methods in a high beta feedback stabilization device is described in Section 5. (See also detailed descriptions of the ECRH and current drive techniques the reviews in References 42 and 43.)

Mechanism of the tearing mode stabilization	Technique	Experimental background
Local increase of the non-inductive current inside the magnetic island (around O-point)	Modulated ECCD	COMPASS-D [9,29] 60 GHz, $2\omega_{ce}$, 13^{o} 20-100% reduction of the m=2,n=1 island
Local decrease of the resistivity by heating of the magnetic island (O-point);	Modulated ECRH	JFT2M [10]
Modification of the equilibrium current density/pressure profile	Continuous ECRH, ECCD LHCD	T-10 [26,34,37] 140 GHz, $2\omega_{ce}$, 11^{o} Compass-D [30] TFR [31] JFT2M [32] 60 GHz TEXT [33] WT-3 [35] 56 GHz DIIID [38] ASDEX-U [39]
Braking of coupling of the tearing modes with various helicities by modifying equilibrium current density profile	Continuous ECRH	T-10 [28] m=2,n=1 & m=1,n=1
Prevention of the mode-locking by maintaining of fast plasma rotation due to large pressure gradient at the plasma edge	Continuous ECRH	T-10 [36] n=1
Control of the savteeth	Continuous ECRH, ECCD, LHCD	many tokamaks (see references in [41])

Table 2

Conclusions

Feedback control of the plasma stabilities is a subject of primary importance for modern experiments in order to achieve economically-viable operation of a tokamak reactor. Previous studies demonstrated the possibility in principle of feedback techniques needed to control various plasma instabilities. More experiments are urgently required for optimized design and testing of control techniques for future tokamak reactors.

References

[1] M.Keilhaker, Plasma Phys. and Contr. Fusion, 37 (1995) A1.
M.Garribba et al., SOFT XVI, Karlsrue, 1994.

[2] M.Okabayashi, Nucl.Fusion, 36 (1996) 1167.

[3] A.W.Morris, Plasma Phys. and Contr. Fusion, 34 (1992) 1871.

[4] T.N.Todd, Nucl. Fusion, 32 (1992) 1071

[5] F.C.Schuller Plasma Phys. and Contr. Fusion, 37 (1995) A135

[6] W. Morris et al., Phys. Rev. Lett. 64 (1990) 1254.

[7] V. V. Arsenin, L. I. Artemenkov, N. V. Ivanov et al., in Plasma Physics and Controlled Nuclear Fusion Research 1978 (Proc. 7th Int. Conf. Innsbruck, 1978), Vol. 1 IAEA, Vienna (1979) 233 and Yu. V. Gvozdkov, N. V. Ivanov, A. m. Kakurin, Fiz. Plazmy 6 (1980) 234 [Sov. J. Plasma Phys. 6 (1980) 130].

[8] K. Bol et al., in Plasma Physics and Controlled Nuclear Fusion Research 1976 (Proc. 6th Int. Conf. Tokyo, 1975), Vol. 1, IAEA, Vienna (1975) 83.

[9] G.J McArdle, A.W.Edwards,B.Lloyd,A.W.Morris,P.R.Simpson, and G.A.Whitehurst, "Instability control with Modulated ECRH" in Proceedings of the EC-9 Workshop, 271-283 (Borrego Springs, California, January, 1995).

[10] K Hoshino, H Aikawa, Y Asahi et al., 15th IAEA, Seville Spain, IAEA-CN-60/A-5-II-3 and Hoshino K et.al. AIP Conf.Proc. 289 (1994) 149.

[11] V.Yu.Sergeev et al., In Proc. of the 22nd Eur. Conf. on Contr. Fusion and Plasma Phys, 1995, Bournemouth, V19C, P.IV, p.57.

[12] J.C.Vallet et al., Phys.Rev.Lett, 67 (1991) 2662.

[13] P.V.Savrukhin et al., In Proc. of the 20th Eur. Conf. on Contr. Fusion and Plasma Phys, 1993, Lisboa, V17C, P.1, p.259

[14] F.Karger, H. Wobig, and S. Corti, Plasma Physics and Controlled Nuclear Fusion Research, Tokyo, 1974 (International Atomic Energy Agency, Vienna, 1975), Vol. 1, p. 207.

[15] K.McGuire, D.Robinson, In Proc. of the 9th Eur. Conf. on Contr. Fusion and Plasma Phys, 1979, Oxford, EPS 1980, p93

[16] A.W.Morris et al., Phys Fluids, 4 (1992) 413.

[17] A.A.Bagdasarov et al., Plasma Physics and Controlled Nuclear Fusion Research, Baltimore, 1982 (International Atomic Energy Agency, Vienna, 1983), Vol. 3, p. 281.
[18] P.Savrukhin, S. AliArshad, D. J. Campbell et al., In Proc. of the 23th Eur. Conf. on Contr. Fusion and Plasma Phys, 1996, Kiev.
[19] R.Fitzpatrick, Nuclear Fusion33 (1993).1049
[20] A.Santagiustina et al., In Proc. of the 22th Eur. Conf. on Contr. Fusion and Plasma Phys, 1995, Bourenouth, V19C, P.IV, p.461.
[21] R.LaHaye et al., Phys.Fluids B, 4 (1992) 2098.
[22] M. Mauel , E. Eisner, A. Garofalo et al., in Eddy-current Characterization and plasma rotation control in wall-stabilized tokamak discharges, 16th IAEA Fusion Energy Conference, Montréal, Canada (Oct 7-11,1996) paper IAEA-CN-64/AP1-19.
[23] G.D'Antona, et al, IEEE Transactions on Nuclear Science, 43 (1996) 207.
[24] P.Savrukhin et al., IEEE Transactions on Nuclear Science, 43 (1996) 238 and P.Savrukhin et al., JET Report JET-R(95)06, 1996.
[25] T.C. Hender et al., Nucl. Fusion 1, 2091 (1992).
[26] Borshegovskij,A.A., Popov,I.A., Stepanenko,M.M., in Proc. of 12th EPS Conference on Plasma Physics and Controlled Fusion (Budapest, 1985) V9F, P.1, p.307. and Alikaev,V.V. et al., Proc. of the 10th Int. Conf. on Controled Fusion and Plasma Phys, (IAEA, Vienna,1984), London, v1, p.419.
[27] Morris,A.W., IAEA-TECDOC-604, 1990, p.1.,
[28] Savrukhin,P.V., Lyadina,E.S., Martinov,D. et al., Nucl. Fusion, 34 (1994) 317.
[29] Morris,A.W.,Fitzpatrick,R.,Hender,T.C.,O'Brien,M.R., in Proc. of 19th EPS Conference on Plasma Physics and Controlled Fusion (Innsbtuk, 1992) P.1, p.423
[30] Morris,A.W., Proc. of the 15th Int. Conf. on Contr. Fusion and Plasma Phys, (IAEA, Vienna,1994), Seville, A2-IV-1.
[31] TFR Group and FOM ECRH Group, Nucl. Fusion 28 (1988) 1995
[32] Hoshino,K. et al., Phys.Rev.Lett., 69 (1992) 2208
[33] Sing,D.C. et al., Phys Fluids B, 5 (1993) 3239
[34] Kislov,D.A. et al., in Nucl.Fusion 37 (1997) to be published.
[35] Terumichi,Y. et al., Proc. of the 15th Int. Conf. on Contr. Fusion and Plasma Phys, (IAEA, Vienna,1994), V.II, p.189.
[36] Ivanov,N.V., in Proc. of the 22th EPS Conference on Plasma Physics and Controlled Fusion (Bournemouth, 1995) V.19C, P.III, p.77.
[37] Esipchuk,Yu.V., Plasma Phys. and Contr. Fusion, 37 (1995) A267.
[38] DIIID Team, Proc. of the 15th Int. Conf. on Contr. Fusion and Plasma Phys, Seville (IAEA, Vienna,1994), V.I, p.83.

[39] H.Zohm et al., Plasma Phys. and Contr. Fusion, 33 (1991) 1423.

[40] S. Bernabei et al., Phys. Fluids B, 5 (1993) 2562.

[41] Savrukhin,P.V. et al., Plasma Phys. and Contr. Fusion, 33 (1991) 1347.

[42] Hsuan,H.,Fredrickson,E. in Proceedings of the EC-9 Workshop, (Borrego Springs, California, January, 1995) 285. and H. Hsuan et al., Plasma Physics and Controlled Fusion Research 26, 265 (1984).

[43] V.Erckmann et al., Plasma Phys. and Contr. Fusion, 36 (1994) 1869.

Section 3: Feedback Stabilization Experiment

Section 3.1 - Introduction and Motivation

To make further significant progress in feedback stabilization, it must be approached in a systematic and dedicated manner in high performance plasmas. The Princeton Plasma Physics Laboratory (PPPL) is developing a proposal to fill this need through a new collaborative national facility, called the Feedback Stabilization Experiment (FSX). The mission of the FSX device would be to study MHD mode suppression and feedback control in high beta plasmas. It would provide a cost effective means of obtaining valuable and relevant results for tokamaks and alternate magnetic confinement concepts, such as reversed-field pinches, spheromaks, and spherical torus experiments.

Supporting objectives are to:

- Optimize plasma performance through active feedback control of the external and internal MHD activity in a high temperature plasma.
- Achieve this optimization using techniques of “Smart” or “Fake Rotating” Shells, Resonant magnetic perturbations, Lower Hybrid modulation, IBW ponderomotive, NBI modulation and Scrapeoff-layer current modulation.
- Demonstrate the feasibility of a high beta advanced tokamak configuration utilizing the techniques of MHD feedback stabilization and obtain an understanding of the limitations of our ability to control that MHD activity.

The FSX machine would thus enable the development and evaluation of feedback control techniques for ideal and resistive MHD modes, applicable both to tokamaks and to alternate concepts. This proposed facility will both be unique in the world program, and complementary to other U.S. tokamak and alternate concept activities.

3.2 Broader Context of Work Done, Relationship to Other Projects, and Opportunities

The FSX will be dedicated to the study and design optimization of the feedback control systems required for future tokamak reactors. New feedback strategies to be explored in FSX project will be based on the simultaneous application of integrated control logic with novel control techniques (actuators) and an advanced set of the plasma diagnostics (transducers). The experiments are particularly important because they provide unique information on plasma dynamics under the reactor-relevant plasma conditions (see below).

Integrated plasma control

Reliable operation in regimes with improved plasma performance, and sustaining such advanced conditions for extended periods of time, requires the simultaneous application of various control strategies. As an advance beyond the previous experiments, the FSX control system is intended to provide an Integrated Plasma Control Strategy (IPCS). The main task of such integrated control is to identify safe areas of plasma operation close to stability boundaries, stabilize or delay plasma perturbations, and provide a "soft" termination of the plasma due to disruptions or recovery of tokamak operation after such events (Fig. 1).

The integrated control strategy is based on the design of a dynamic model of the complete feedback control system, which provides algorithms for integrated stability control in a future reactor. The dynamic model consists of multi-layer identifiers of the dominant perturbations, based on a combination of neural networks and logical switches. Logical switches are based on the experimentally-determined thresholds of the instabilities (e. g., empirical scalings) and on theoretical models describing the conditions under which various plasma instabilities occur. Prevention of unstable configurations is provided by control of the equilibrium magnetic fields, correction of error fields, application of the auxiliary heating and current drive (see below), tailoring of plasma-wall interactions, and appropriate fueling of the plasma discharge.

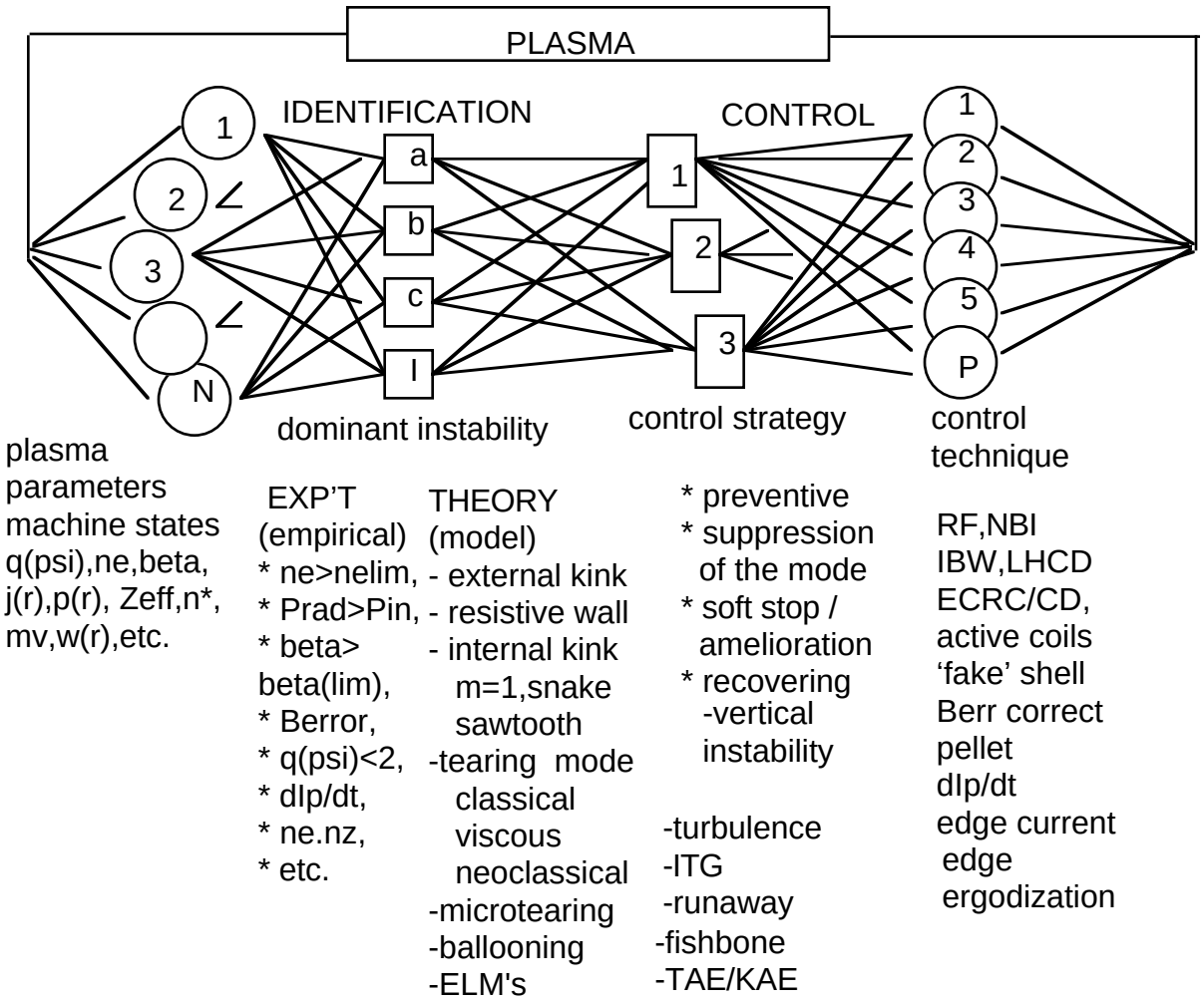

Fig. 1 Schematic view of the Integrated Plasma Control logic.

Varieties of instabilities in tokamaks under reactor-relevant conditions.

The magnetically-confined plasma required for an economically-feasible reactor is characterized by extremely high plasma parameters. Attainment of such conditions is possible only in large-scale experiments (i. e., JET, TFTR, and JT60-U). Unfortunately, testing of feedback systems under the appropriate conditions is an exhausting task (see above). However, detailed studies of the plasma perturbations in the large-scale experiments have indicated that the dominant instabilities reflect many physical mechanisms that are similar to the ones observed in medium-size machines. Therefore, the experimental study and clarification of the physical mechanisms of these instabilities can be the primary task of a medium-size tokamak. The FSX device (using the facilities already available on PBX-M) is a unique installation for allowing the study of reactor-relevant instabilities (neoclassical tearing modes, resistive wall modes, etc. as described elsewhere in this document) in a reactor-relevant plasma configuration (i. e., D-shaped plasma, high pressure, poloidal divertor,

and thick conducting shell). The FSX thus provides a unique opportunity for dedicated experiments with feedback control of reactor-relevant instabilities at a minimum cost of operation.

Feedback techniques in FSX and their application to a tokamak reactor

In order to provide control over a variety of the plasma instabilities, FSX is equipped with a unique set of the control techniques (see Table 1). The detailed description of the techniques is presented in other sections of the text.The most important feature is the possibility of simultaneously applying the novel 'fake' rotating coils, modulated LHCD and NBI, and a comprehensive set of active coils to introduce Resonant Magnetic Perturbations (RMP's). The FSX is designed to test the new synergistic effect of simultaneously using LHCD and IBW heating, and several techniques for control of the plasma edge (segmented biasing divertor, edge ergodisation, etc.). Possible installation and testing of ECRH/ECCD (i. e., using the internal mode conversion technique), based on the novel gyrotrons designed for ITER, makes FSX a unique tokamak for the study and optimization of the feedback techniques urgently required for a reactor.

Table 1 Feedback techniques in FSX and their application to the reactor

control method	experimental background	FSX	DIII-D	ITER	mode	Alt.
main program		Feedback	Divertor	Feedback & Divertor		
RMP active coils	many tokamaks (see above)	many task 20 coils internal 2G at q=2 0-20kHz	6 coils external DC	+	IM NTM	RFP?
Conducting plates passive shell	PBX-M HBT-EP	40		+	VDE EM	RFP
fake rotation coils and sensors				+	EM RWM	RFP: - MST - HBT X-1C
NBI 50keV	many tokamaks	7.0MW 0.3 sec	12MW?	+	EM IM	
modulated NBI	70-100%test	3.6 MW 0.3 sec		+	IM EM	
LHCD	ASDEX-U	2,0 MW 0.7 sec 4.6GHz		+	EM	
IBW	TFTR, ASDEX-U C-Mod	4MW 1.0 sec 40-80MHZ		+	EM	
LHCD+IBW synergy	JET PBX-M			+	IM	

pellet: fueling					DISR	
pellet soft stop				+	DISR	
vertical pos.control	PBX-M			+	VDE	
edge curent modulation- HALO Current				+	VDE	
edge ergodisation	TEXT ToreSupra			+	EM	
electrostatic shell biassing				+	EM	
negative edge current inject.				+	EM	
segmented divertor biassing			planned on DIIID	+	EM	
ECRH ECCD (project)	many tokamaks (see above)	0.2-0.6MW required		+	IM NTM SAW	

(IM- internal mode, NTM- neoclassical tearing mode, SAW- sawteeth, VDE- vertical displacemnt event, EM- external mode, DISR- disruption, RWM- resistive wall mode)

FSX diagnostics (transducers).

Previous experiments have indicated that the design of feedback systems is crucially dependent on the available set of transducers. Moreover, identification of the dynamics of the feedback system and an understanding of the physical mechanisms of the mode control require a comprehensive set of the plasma diagnostics for measurement of the plasma temperature, density, rotation, plasma current, etc. Such a set is uniquely provided on the medium-size FSX project by the advanced PBX-M diagnostic systems, including 2-D soft x-ray imaging, MSE, CHERS, Mirnov coil arrays, ECE, reflectometry, etc. (see Section 6). In order to improve plasma control, several new techniques will be incorporated in the study (e. g., “smart” sensors and 2-D hard x-ray detectors).

Table 2 Representative FSX diagnostics.

diagnostic	experimental background	FSX	DIII-D	ITER	mode
smart sensors	-	+		+	RWM
3D-SXR	2-D	+		+(-)	IM
2D hard x-ray	1-D	+		+(-)	run-away
Mirnov	+	+	+	+	IM,EM
ECE	+	+			Te
CHERS	+	+		+(-)	Ti,Vt
MSE	+	+		+(-)	j(r)

Supplementary experiments on FSX

The FSX will be a flexible tokamak that provides wide possibilities for the study of various physical effects, including plasma stability and confinement, plasma-wall interactions, dynamic heat transport, and plasma fueling.

In addition to feedback studies, the application of the extensive system of active coils (for RMP studies) will provide the unique possibility of evaluating the physical mechanisms underlying tearing modes (neoclassical tearing modes), measuring the 2-D structure of the plasma current perturbations across a magnetic island, evaluating plasma parameters not measured directly in other tokamak experiments (e. g., viscosity), etc. (see Table 3).

Installation of a modulated NBI, LHCD, and ECRH/ECCD capability will also provide a versatile tool for the analysis of the dynamics of heat transport (perturbative analysis), and non-inductive initiation and ramp-up of the discharge.

Design of the feedback system in FSX will permit considerable contributions to the effectiveness of future tokamak reactors and control theory in general, with numerous applications to various aspects of science and technology.

Table 3 Possible experiments with the RMP in tokamaks

1	Physical Mechanisms of the tearing mode	a) coupling of internal tearing modes - different helicities of the modes, - effect on (of) sawteeth, - effect on fishbones, - effect on ELMs b) analysis of the tearing mode growth and rotation (flip instability)	Unambiguous identification of the tearing modes in large tokamaks. Prediction of the tearing mode dynamics.
2	Assessment of plasma parameters	a) estimation of the tearing modestability parameters at different resonance surfaces from analysis of driven tearing modes, b) evaluation of 'viscosity' profile and its dependence on the plasma parameters, c) evaluation of the softness of the stability threshold (analysis of the tearing mode growth with approach to stable limits of operation).	Estimation of difficult to measure plasma parameters ('viscosity', current density). Recommendations for safe limits of operation.
3	Disruption amelioration	a) slowing down of the plasma decay during disruptions, b) control of dynamic of plasma perturbations during disruptions, c) evaluation of trigger conditions of disruptions; dependence on amplitude and spectrum of the external field.	Minimization of damaging consequences of disruptions. Physical mechanisms of disruptions.
4	Error field compensation	a) prevention of n=1 mode locking b) determination of trigger condition of the n=1 mode, c) plasma rotation control.	Assessment of optimal target plasma for NBI. Improvement of stable operation of the plasma.
5	Effect on modes in current ramp phase	a) repetitive control of m=6, 5, ... modes	Improvement of plasma operation
6	Effect on energy and particle confinement	a) tailoring of rotation profile by initiating and control of magnetic islands at different rational surfaces, b)ergodisation of the plasma edge by generation of a wide spectrum of harmonics of perturbations, c) studies of three-wave coupling and its role on confinement d) resonance diffusion of plasma species with specified energies	Improvement of energy and particle confinement
7	Impurity control by generation of 'helical' divertor	a) initiating of static magnetic islands(s) at the plasma edge b) power deposition sweeping	Optimized deposition of the loss power.

8	Design and operation of fast on-line adaptive digital control system	a) on line estimation of the tearing mode parameters (amplitude and angular speed), data filtering,	Design of control networks for future experiments
9	TAE- mode stability	a) excitation of toroidal Alfvén Eigenmodes. b) Measurement of damping rates	Evaluate stability of TAE modes under wide range of plasma conditions
10	Suppression of the tearing modes (open loop)	a)analysis of tearing mode dynamic with simultaneous application of static and rotating fields b) mode suppression by external field with periodic suppression action with reversing of the phase of the external field c)chaotic movement	Improvement of plasma operation. Control of disruptions
11	Evaluation of the plasma stability regions (tranquility factor identification) (closed loop)	a)forced destabilisation and suppression of the magnetic perturbations b) soft stop with low tranquility	Improvement of the plasma operation. Prevention of disruption

Conclusions

Detailed studies on earlier tokamak experiments and analysis of the requirements for an economically-feasible fusion tokamak reactor have indicated that the design and optimization of feedback control systems are primarily tasks in modern fusion studies.

Unique possibilities for advanced feedback studies in FSX are provided by:

- incorporation of a reactor-relevant control strategy (i. e., integrated plasma control) including avoidance and stabilization of instabilities, and soft termination of the discharge and recovery after a disruption;

- reliable identification and control of the reactor-relevant instabilities, including the neoclassical tearing mode, resistive wall mode, external kink mode, etc., in reactor-relevant plasma configurations and plasma parameters (e. g., poloidal divertor, D-shape, conducting shell, high β_n,>3, $\tau_E/\tau_{ITER89P}$=2.5-3.0).

- application of a number of novel control techniques urgently required for reactor design (e. g., passive shell, 'fake rotating' coils, advanced RMP systems, LHCD, IBW, modulated NBI, electrostatic biasing, segmented divertor, ECRH/CD, etc.). While some of the feedback techniques are being explored on other machines, the strength of FSX will be that it provides

the capability for direct comparison of each of these techniques on the same device. This will allow a detailed evaluation of the efficacy of each technique under controlled conditions.

- incorporation of advanced diagnostics systems (i. e., those that exist on PBX-M) with novel sets of transducers (e. g., 'smart' coils, 3-D soft x-ray imaging, 2-D hard x-ray imaging).

Unlike other facilities, where feedback stabilization experiments necessarily compete for run-time with other experiments more central to their missions, feedback experiments will have highest priority on FSX.

In addition to the feedback control of instabilities, the FSX project will provide a versatile tool for addressing a broad spectrum of challenging problems, ranging from basic plasma physics to control theory with numerous applications in science and technology.

3.3 Baseline Parameters, Geometry, and Performance

The major parameters of the FSX configuration are given in Table 1. Assuming a performance equivalent to at least 2.0 x ITER89-P (see Sec. 3.3.4), the power delivered by the heating and current drive systems will enable FSX to achieve normalized beta values, β_N in the range of 2-3% m-T/MA for a plasma current of 0.66MA, and toroidal field values in the range of 1.1-2.5 T.

The plasma volume in the FSX vacuum chamber is maximized by operating as a Double Null (DN), closed divertor, Dee-Shaped configuration. The major radius is R = 1.47m, minor radius a = 0.45 m (i.e., Aspect Ratio A = 3.5), elongation κ_{95} =1.54, and triangularity δ_{95} = 0.54, which results in a plasma volume of V = 9.5 m^3. A close-fitting poloidally-segmented conducting shell surrounds the plasma (Fig. 1), which serves as a passive stabilizer for the vertical n=0 instability, and as a stabilizing cage for the external n $\geq$ 1 kink instability. A detailed description of the conducting shell is given in Section 4.

The FSX configuration contrasts with the PBX-M configuration (see Sec. 6). In PBX-M, a "pusher" coil is used to indent the plasma at the inboard midplane. The plasma is a large aspect ratio (A=5.5), bean-shaped configuration with a major radius of R = 1.65m,

Figure 1. (See Figure Folder)

midplane minor radius a = 0.30m, and elongation κ = 2.1. The PBX-M plasma volume is 7.2 m^3, approximately 25% smaller than the proposed FSX device.

3.3.1 Reference Discharge Scenarios

The projected performance of FSX plasmas is shown in Figures 2 and 3. We assume various levels of auxiliary power delivered to a 0.66MA FSX plasma and calculate normalized beta, β_N, as a function of toroidal field. Predictions based on H x τ_E(89-P) with H = 2 and H=3 are shown. For the largest attainable toroidal field values in FSX, i. e., B_T = 2.5T, and H-factor of 2.0, the transport scaling predicts β_N = 2.0. If the toroidal field is lowered to 1.1T, the same confinement scaling predicts β_N = 3.5. As the toroidal field is varied, the safety factor evaluated at the 95% flux surface, q_{95}, varies between 3.2 and 5.6. The poloidal beta exceeds unity for the given range of B_T. Figure 3 shows the projected performance for plasmas with I_p = 1.0MA.

3.3.2 Pressure-Driven Resistive Wall Modes (RWM's)

In order to demonstrate the efficacy of active feedback stabilization in FSX, it is necessary to establish plasma conditions that reliably excite instabilities of a chosen type. To generate pressure-driven resistive wall modes (RWM's) the following conditions must be met:

(C1) An external kink must be unstable for normalized beta values that are sufficiently higher than β_N^{∞} with magnetic boundary conditions imposed at infinity.

(C2) The external kink must be stable for $\beta_N < \beta_N^{w}$, where $\beta_N^{w} > \beta_N^{\infty}$ is the beta limit with "ideal" magnetic boundary conditions imposed at the location of the FSX passive plates. In such a case, pressure-driven RWM's will exist for β_N in the range $\beta_N^{w} < \beta_N < \beta_N^{\infty}$. With no active feedback, the β-limit will be observed to be $\beta_N^{crit} = \beta_N^{\infty}$. A successful suppression of the RWM by active feedback will raise the β-limit to $\beta_N^{crit} = \beta_N^{w}$. For a convincing demonstration of feedback stabilization, it is desirable:

(C3) That the improvement in the β-limit achieved by the active feedback system should be substantial, and the achieved limit should be significant. Thus, target plasma profiles should give $\beta_N^{w} / \beta_N^{\infty} >$ or $\approx$ 1.5, with $\beta_N^{w} \geq$ 3.0.

In Figures 2 and 3, the operating space for RWM feedback stabilization experiments is shown as the cross-hatched region with B_T = 1.5T. This is a region which corresponds

Figure 2. (See Figure Folder)

Figure 3. (See Figure Folder)

to $q_{95} < 4$, sufficiently low to avoid shear stabilization of the external kinks. We see from the figures that the auxiliary power delivered to the plasma for these levels of toroidal field is sufficient to achieve sufficiently high β_N.

The stability of a baseline FSX configuration suitable for RWM feedback stabilization experiments is shown in Fig. 4. The figure shows a plot of the normalized β-limit for external kink modes with n = 1, 2, and 3, as a function of the ratio, b/a, of the separation distance between an ideal conducting wall and the plasma boundary, and the midplane minor radius, a, of the plasma. The plasma configuration corresponds to $B_T = 1.5T$ with I_p=1.0MA, with profiles of pressure and current shown in Fig. 5. The PEST equilibrium and stability code is used for the calculations, and the conducting wall is assumed to be conformal with the plasma boundary. With the conducting wall at infinity, the β-limit is $\beta_N^{\infty} = 2.1$. As the ideal conducting wall is brought in from infinity, the β-limit is increased. With $b/a < \text{or} \approx 0.2$, the β-limit for the n=1 external kinks exceeds that due to n=∞ ballooning modes, $\beta_N^{\text{balloon}} = 3.4$. Since the actual location of the FSX conducting plates corresponds to $b/a \approx 0.2$, we see that the demonstratable improvement in the β-limit due to an external intervention system, which serves to make the FSX conducting plates act as if they are ideal, is the ratio of β_N^{∞} to $\beta_N^{\text{balloon}} = 1.6$. It follows from the criteria discussed in previous paragraphs, that this baseline configuration is suitable for studying the efficacy of active feedback stabilization of resistive wall modes.

As mentioned previously, a necessary condition for the existence of resistive wall modes in FSX at a given β, is the requirement that if ideal conductor boundary conditions are applied at the location of the *actual* conducting plates in FSX, the external kink modes should be stable. In Fig. 1, an outboard midplane gap is seen between the conducting plates in the upper and lower half planes, representing access for neutral beam ports and RF antennas. It is well-known that eddy currents generated in the outboard midplane region of an ideal conducting shell that completely surrounds the plasma are particularly effective in stabilizing external kink modes.[1] Furthermore, if an outboard midplane gap is made too large, the external kink mode is destabilized. It is important, therefore, to demonstrate that the midplane gap shown in Fig. 1 is not "too large." For this purpose, we have run the PEST stability code using a "crescent shaped" ideal conducting wall to simulate outboard midplane gaps, to verify that the poloidal coverage by conducting plates is robustly sufficient in FSX to stabilize the external kink modes of interest to the feedback stabilization of RWM experiments.

Figure 4. (See Figure Folder)

Figure 5. (See Figure Folder)

Figure 6 shows a plot of the β-limit for n=1 external kink modes as the outboard midplane gap angle, θ is varied about the actual angular gap, θ_A of the conducting plates in FSX. It is seen that, for the profiles considered, the outboard gap can be made 50% larger without causing the β-limit to decrease beyond $\beta^N = 2.8$. We conclude that the proposed poloidal coverage of the plasma by conducting plates in FSX is ample to fulfill the feedback stabilization mission.

3.3.3 Neoclassical Tearing Modes

Conditions favourable to the excitation of neoclassical tearing modes require $\beta_{pol} > \text{or} \approx 1$ (see Sec. 2.1.2). From Figures 2 and 3, the auxiliary power delivered to the plasma is sufficient to achieve $\beta_{pol} > 1$ for the full range of toroidal fields. $1.0T < B_T < 2.5T$. Stabilization methods for tearing modes are of two types:

(T1) Stabilization by profile control methods such as ECE, and

(T2) Stabilization by active intervention of magnetic fields.

Type (T1) stabilization experiments require operating with $B_T > \text{or} \approx 1.5T$, while Type (T2) stabilization has no such restriction. However, if the dominant resonant surface on which the instability grows is at small q, such as is the case for the m/n = 2/1 tearing mode, stabilization by external magnetic feedback coils will favor operation at low B_T so that the q=2 surface is not too deep within the plasma core.

Figure 6. (See Figure Folder)

Table 1: Major Parameters of 1.5T Baseline FSX

Toroidal Field, B_T	1.5 (1.1 - 2.5)	T
Plasma Current, I_p	0.66	MA
Major Radius, R	1.47	m
Minor Radius, a	0.45	m
Aspect Ratio	3.5	
Elongation, κ_{95}	1.54	
Triangularity, δ_{95}	0.54	
Edge Safety Factor, q_{95}	(3.2 - 5.6)	
Configuration	Double Null Poloidal Divertor	
Pulse Length	3	sec
Heating and Current Drive:		
NB	7	MW
LH	1.2	MW
EC	(planned)	
IBW	2 (4 MW source of power)	MW

Reference

[1] D.J. Ward, Phys. Plasmas **3** (1996) 3653.

3.3.4 Confinement and Transport

The physics mission of FSX is to study feedback stabilization of MHD activity and so the essential consideration for energy confinement in FSX is only that it be good enough to reach beta values that challenge MHD limits, i.e. β_t and β_n should be MHD-limited and not confinement limited. Based on previous experience in the PBX-M facility and DIII-D (whose B_t and R_o are comparable to FSX), there is ample energy confinement to reach the β-thresholds for various MHD instabilities with the available 6-8 MW of auxiliary heating in FSX.

As will be described below, the combined perpendicular- and parallel-beam configuration on FSX provides an important capability to control the toroidal velocity and velocity shear. Control of the toroidal velocity will provide essential data on the effect of mode rotation frequency on proposed MHD feedback-control schemes. The ability to vary the velocity shear will provide a useful tool for studying the effect of velocity shear and E-field shear on local transport, which is emerging as an important issue for extrapolating confinement results in present-day tokamaks to ITER.

A useful benchmark for estimating τ_E in FSX is the power-law regression expression developed for plasmas in the L-mode regime,

$$\tau_E(89\text{-}P) = 0.048\, M^{0.5}\, I_p^{0.85}\, R^{1.2}\, a^{0.3}\, \kappa^{0.5}\, n_{e20}^{0.1}\, B_t^{0.2}\, P^{-0.5}.$$

Here $\tau_E(89\text{-}P)$ is the confinement time in seconds, M is the average hydrogenic isotopic mass, Ip is the plasma current in MA, R is the major radius in meters, a is the minor radius in meters, k is the elongation, is the line-averaged density in units of 10^{20} m^{-3}, B_t is the toroidal field in Tesla, and P is the total heating power in MW. The available heating power in FSX (6-8 MW) exceeds the power threshold for H-mode transitions (1.5-3 MW in PBX-M [1]) and so FSX should operate routinely in the H-mode regime with confinement times substantially in excess of that predicted by $\tau_E(89\text{-}P)$. Figure 1 plots the ratio of actual τ_E to the L-mode value (i.e. $\tau_E(89\text{-}P)$) obtained in PBX-M H-mode plasmas as a function of β_n. Energy confinement times in excess of 2.5 times $\tau_E(89\text{-}P)$ were routinely achieved in PBX-M even at high normalized beta.

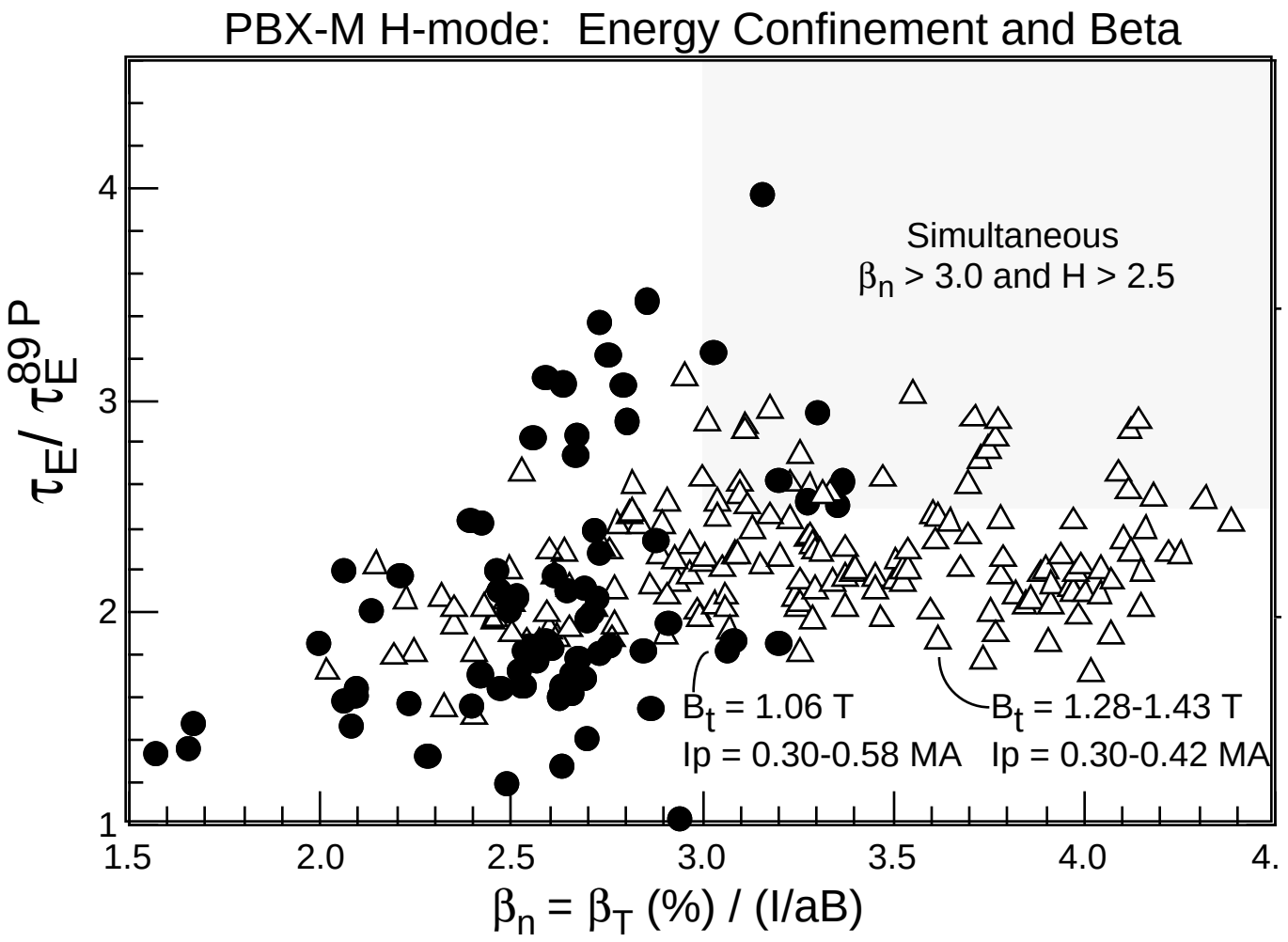

Fig. 1. Energy confinement times realized in PBX-M normalized to the ITER-89P scaling relation as a function of normalized beta.

The PBX-M dataset shown in Fig. 1 spans the expected range of toroidal field for FSX, but the maximum FSX plasma current (0.66-0.80 MA) is somewhat higher than in PBX-M (0.30-0.58 MA). Fortunately there is no evidence in the PBX-M database suggesting that the H-mode confinement multiplier, $H = \tau_E / \tau_E(89\text{-}P)$, deteriorates with Ip. In addition, high H-factors have been achieved in the DIII-D tokamak - again at high β_n - in a plasma configuration (R_o, B_t, κ) comparable to FSX, but at plasma currents substantially *in excess* of the proposed FSX operating point. In both PBX-M and DIII-D many of these impressive confinement results were sustained only transiently, with MHD eventually

spoiling the performance. FSX will study whether feedback stabilization mechanisms can control the MHD and thereby prolong the duration of high confinement and β_n.

	DIII-D NCS[2]	DIII-D VH[3]	DIII-D H-mode[4]	PBX-M H-mode[5]	FSX
R (m)	1.67	1.68	1.66	1.65	1.54
a (m)	0.61	0.62	0.62	0.28	0.45
κ	2.15	2.0	2.1	1.7	1.87
δ	0.9	0.86	0.32	0.70	???
indentation				0.18	
Vol (m^3)	22			4.5	
Bt (T)	2.15	2.1	>1.9	1.35	1.12
Ip (MA)	2.25	1.6		0.34	0.66
q95	4.2			4.7	
Pinj (MW)	17.8	8		4.3	8
β (%)	6.7	3.6		4.5	
β_n	4.0	2.9	3.0	5	
τ_E (ms)	400	340		34	70
H(ITER-89P)	4.5	3.7	2.7	2.4	2.5*
Neo (1019 m-3)	10	7.1		5.6	
nebar		6.5		4.3	4
T_{io}	18	5.6		4.5	
T_{eo}	7.5	6.0		2.1	
Z_{eff}	2.0			2.9	
Configuration	87977 DN	75121 DN		260678 bean	SN,DN

* The H-factor assumed for FSX is 2.5.

Table 1. Comparison of confinement achieved in various confinement regimes of DIII-D, PBX-M, and FSX.

References

[1] F. Ryter et al., Nucl. Fusion **36** (1996) 1217.

[2] E. Lazarus et al., Phys. Rev. Lett **77** 2714 (1996) and DIII-D team, paper F1-CN-64-O1-6, "DIII-D Tokamak Concept Improvement Research", Sixteenth IAEA Fusion Energy Conference, Montreal, Canada, 7-11 October, 1996.

[3] C. M. Greenfield et al., Plasma Phys. Control. Fusion **35** (1993) page B263 and T. H. Osborne et al., Nuclear Fusion **35** (1995) p. 23.

[4] E. A. Lazarus et al., IAEA1994, Vol. 1., p 609. "The role of shaping in achieving high performance in DIII-D".

[5] B. LeBlanc et al., Nuclear Fusion **33** (1993) 1645.

3.4 - Runaway Studies on FSX

ITER Physics Issues

Runaways are a major concern for ITER because of the damage they could do to first-wall components, and their identification has been identified as a high priority task (ITER 1.1.4). This activity has several elements that can be addressed uniquely on FSX.

1) Benchmarking of codes for ITER disruption modeling with ITER-like geometry.

The Tokamak Simulation Code (TSC) has already been used in developing high-beta scenarios for highly-shaped PBX-M plasmas, and it has been extensively benchmarked against current profile modification experiments with lower hybrid current drive in PBX-M. The TSC can be used to benchmark the transition of the FSX equilibrium from a thermal to a runaway plasma with a conducting wall and ITER-like geometry. In particular, the highly-conducting wall of FSX slows down the time scale of vertical displacement events (VDE's) such that $\tau_{\text{thermal collapse}} < \tau_{\text{current decay}} < \tau_{\text{VDE}}$.

In ITER, the VDE is similarly separated from the current decay, this is a condition that can be investigated only on a thick-shelled device, unlike DIII-D. The duration of the runaway electron period may provide the opportunities for various control techniques to ameliorate their effects, including the deposition of runaways on sacrificial targets. Other tools that can be developed to control runaway plasmas through "soft termination" are gas injection, negative loop voltage, and pellets.

After the VDE terminates the plasma current, the halo current buildup could be affected by runaway electron bombardment. If runway electrons dominate the plasma at time of the VDE, as is anticipated in ITER, the resultant halo event could be completely different from that in DIII-D and C-MOD, where $\tau_{\text{current decay}} \approx \tau_{\text{VDE}}$.

2) Testing of the "avalanche" model and study of tail instabilities.

Lower hybrid current drive has been used successfully to generate "seed" runaway electrons. Their spatial and temporal evolution can be measured with hard X-ray and infrared cameras because of the unique tangential access available on FSX, and velocity-space instabilities in runaway plasma can be studied.

The power deposition of runaways in the MeV range can be investigated with carbon targets. Runaway generation and loss can also be affected by error fields and "killer pellets," and these can also be examined.

Diagnostics

The FSX facility already has a set of diagnostics that can be readily applied to runaway studies. These include a grating polychromator for vertical electron cyclotron emission ("X" and "O" mode) measurements, a tangential 2-D hard X-ray camera, and IR cameras that can be located on tangentially-viewing windows to image target surfaces and the runaway beam. Other diagnostics that can take advantage of hardware available at PPPL include soft X-ray "spectrometry" k-shell emission, ω_{pi} (lower hybrid frequency) detectors, "edge" Thomson scattering (for T_e and n_e profiles), and spectrometers for post-disruption Z_{eff} measurements.

Section 3.5 - Status of the Facility

The FSX facility proposes to take advantage of unique capabilities at PPPL, including hardware that already exists in the Princeton Beta Experiment-Modification (PBX-M). These include the following unique features (Fig. 1):

- Close-fitting, highly conducting shell.
- Lower hybrid current drive (LHCD) system with programmable phase shifters.
- Ion Bernstein wave (IBW) antennas.

They are complemented by capabilities critical for high-performance plasmas, such as:

- High-power NBI in both tangential and perpendicular directions .
- Unique and specialized diagnostics, including multichannel motional Stark effect polarimetry with a dedicated neutral probe beam for current profile measurements and two-dimensional hard X-ray imaging system.
- m=1 divertor biasing.

Within the PBX-M vacuum vessel, an extensive magnetic field coil set permits flexible plasma shaping, and the capability of electrically-biasing the conducting shell segments permits modfication of edge plasma flows. Earlier experiments have shown that the shell slows down the motion of MHD modes so lower frequency control systems can be used to stabilize them. The flexible shaping capability can be used to study the growth rate of these modes, since it is affected by the separation between the shell and the plasma.

The feedback stabilization mission of FSX requires a sophisticated plasma control system and specialized diagnostics. A new digital plasma control system has been acquired to replace the PBX-M analog shape and position control subsystem and additional computer power will be needed to implement feedback control schemes. The basic diagnostic set permits profile measurements of the electron temperature and density, ion temperature and toroidal velocity, and current density. MHD mode identification is possible with arrays of magnetic pickup coils and soft X-ray diode detectors, and additional electron cyclotron emission diagnostics are planned to augment this capability.

H-mode: Divertor and limiter H-modes achieved with good confinement enhancement above L-mode ($\tau_E/\tau_E^{ITER89P} \approx 2$ - 3) on PBX-M with the neutral beam heating system available for FSX (Fig. 2). The H-mode power threshold was also reduced by up to 25% with limiter biasing, also available for FSX.

Figure 1: PBX-M features available for FSX. (See Figure Folder)

Figure 2: Confinement enhancement above L-mode achieved in PBX-M). (See Figure Folder)

CH-mode: The enhanced core high confinement (CH) mode was discovered on PBX-M with the the IBW system available for FSX.

Reversed shear: The stabilization of low--n modes is particularly important for raising β_N in enhanced reversed shear plasmas. Figure 3 shows β_N values for plasmas with (a) shear-reversed and (b) monotonic q profiles for instabilities with various low toroidal mode numbers. In the reversed shear case, the n = 1 mode limits β_N to 2 if there is no wall. However, the stabilizing effect of a conducting shell located 1.3 times the plasma minor radius raises β_N by a factor of 2.5.

Current profile modification was achieved in PBX-M plasmas by combining the lower hybrid current drive (LHCD) and neutral beam injection (NBI) systems available for FSX.[1] Emission profiles from a soft X-ray diode array showed a steady decrease in MHD activity when LHCD power was applied. From the precursors of the sawtooth oscillations, the q = 1 surface decreased steadily in time, and it disappeared 200 ms after the start of LHCD. Equilibria reconstructed with internal magnetic field measurements from the motional Stark effect diagnostic indicated that q(0) increased from about 0.9 in the Ohmically-heated target plasma to 1.15 after about 300 kW of LHCD was applied for 250 ms. When a comparable power level of NBI was added for 200 ms, q(0) remained above unity.

The Lower Hybrid Simulation/Tokamak Simulation Code (TSC/LSC)[2] was benchmarked by using it to simulate the LHCD results on PBX-M. The program assumes an axisymmetric toroidal geometry, and it uses ray tracing to determine the lower hybrid wave propagation. The influence of the local electric field on the electron velocity distribution function is neglected in the calculation of the absorbed radio frequency power. Wave-particle interactions are computed only in a direction parallel to the magnetic field, but two-dimensional effects of the DC electric field (E_{DC}) on the current are included from fits to separate Fokker-Planck calculations.[3] The resonant electron slowing-down time is considered to be much less than either the diffusion time or the acceleration time in the E_{DC}.

Profiles of the bremsstrahlung emission from the fast electrons generated during LHCD showed that although their radial diffusion time was much longer than their slowing down time, they still had a finite diffusion coefficient in the range of 0.5 to 2 m^2/s.[4] For this reason, a current diffusion model was implemented in TSC/LSC.[5] If a diffusion

coefficient within the range of measurement (D_{LH} = 0.6 m^2/s) is used, the calculated q(0) rises to slightly above 1.1 and stays near this value as observed experimentally (Figure 3a).

If the same diffusion coefficient is assumed, but the LHCD power is increased to 900 kW, TSC/LSC predicts a q(0) of 1.8 and a shear reversal in the q profile (Figure 3b). On FSX, 1.2 MW of LHCD power will be available, and localized noninductive currents up to 400 kA can be driven with the mode conversion system. Therefore, obtaining reversed shear plasmas should not be a problem, and the noninductive means by which it can be achieved in FSX is unique in the U. S. fusion program.

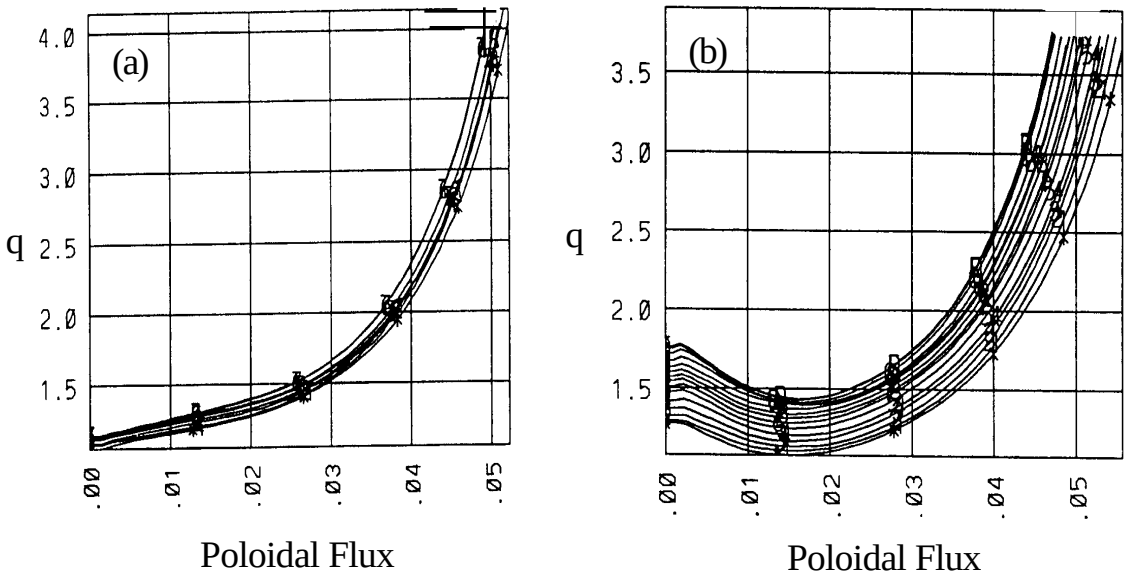

Fig. 3. Time evolution of q profiles from TSC/LSC assuming (a) P_{LH} = 300 kW and (b) P_{LH} = 900 kW. The traces represent the time evolution of the q profile during the application of LHCD power.

References

1. Bernabei, S. et al., *Physics of Fluids B* **5**, 2562 (1993).
2. Ignat, D. W. et al., *Nuclear Fusion* **34**, 837 (1994).
3. Karney, C. F. F. and Fisch, N. J., *Physics of Fluids* **29**, 180 (1986).
4. Jones, S. et al., *Plasma Physics and Controlled Fusion* **35**, 1003 (1993).
5. Ignat, D. W. et al., *Nuclear Fusion* **36**, 1733 (1994).

Section 3.5.1 - Plasma heating and current drive

The FSX facility will use a combination of existing PBX-M capabilities and new hardware additions to implement feedback stabilization schemes. The new systems will be discussed later in Sec. 6.

Lower Hybrid Current Drive

Up to 1.2 megawatts of radio frequency (RF) power can be supplied by a lower hybrid waveguide. Lower hybrid current drive (LHCD) for stability studies can be utilized in two scenarios which will be discussed in section

The PBX-M LHCD system, which is available for FSX, is unique and well suited for possible feedback experiments. Its parameters are given in the following table.

frequency	4.6 GHz
source power	2 MW
pulse length	0.5 sec (extendable up to 0.7 sec)
complete control of the phase	
dinamic phase change	≈ 250 μsec
modulation	> 100 kHz

Ion Cyclotron Range of Frequencies

For experiments in the ion cyclotron range of frequencies (ICRF), PBX-M facility has two ion Bernstein wave (IBW) antennas that can provide up to two megawatts of RF power. These are intended to control MHD modes in FSX by applying a ponderomotive force to the plasma.

The parameters for the ICRF capability that is available for FSX are given in the following table.

frequency	40 - 80 MHz
source power	4 MW
pulse length	1 sec
launchers	2 loop antennas
	1 folded waveguide (ORNL)

Neutral Beam Injection

There are two perpendicular neutral beamlines on PBX-M that are capable of injecting up to 3.6 MW. In FSX, these will be modulated to input radial momentum with the appropriate phase to suppress MHD modes.

Two tangential beamlines are also available for injection of an additional 3.4 MW. The ability to control the plasma rotation by varying the mix of high-power neutral beams is an attractive feature of FSX. The tangential beamlines can be oriented for perpendicular injection as they were on PDX, or the perpendicular beamlines can be moved to a counter-tangential configuration for “balanced” injection as on TFTR.

The parameters for the neutral beam system that is available for FSX are summarized in the following table.

Injected power	3.4 MW (two tangential beamlines)
	3.6 MW (two perpendicular beamlines)
Beam species	deuterium or hydrogen
Pulse length	0.5 sec

Plasma Rotation

The neutral beam system currently installed on FSX consists of two beamlines which inject nearly perpendicular (9^o from perpendicular) and two more which inject more tangentially (36^o from perpendicular). Currently, all beam sources are oriented to inject in the same direction as the plasma current. As would expected from the factor-of-four difference in deposited beam torque, the "parallel' beamlines drove significantly higher toroidal rotation speed in PBX-M than did the 'perpendicular' beams. In H-mode plasmas [1] the central rotation speed achieved with 2-parallel beams was $3.0 \cdot 10^5$ m/s, while only $1.0 \cdot 10^5$ m/s was achieved with the 2-perpendicular beams. In both cases there was a substantial rotation edge 'pedestal' which differed by less than a factor of two between the parallel and perpendicular beams. Between the edge and center the velocity varied roughly linearly with radius, with a velocity gradient which was a factor of nine larger with parallel beams compared to perpendicular beams. The rotation speed achieved with all four beamlines injecting simultaneously was slightly larger than that achieved with only the two parallel beams, consistent with the small additional torque contributed by the perpendicular beams.

With the present FSX beam geometry, the experimenter has considerable control over the toroidal rotation speed (and hence MHD mode frequency), though selection of parallel or perpendicular beams, up to a power level of ~3 MW. This capability will be useful for studies of effects of velocity shear on local transport, which cannot be addressed in other U.S. tokamak facilities. It may also be useful for studies of the effect of mode frequency on MHD growth rates and on MHD feedback-stabilization schemes, but the scope of these studies will be limited by the beta which can be achived with 3 MW of auxiliary heating. At

a higher power level of ~4.5 MW some control (factor ~2) of the toroidal velocity will be possible by selecting 2 perpendicular plus 1-parallel, versus 1-perpendicular plus 2-parallel, beam sources. At the highest power level which necessarily requires all of the beam sources injecting simultaneously, some range of toroidal rotation speed could be explored depending on the plasma density and momentum confinement time, but thes variations in rotation speed will be correlated with other changes in plasma parameters, and cannot be independently controlled by the experimenter.

A possible modest-cost upgrade for FSX involves moving one of the parallel beamlines so that it points in the direction counter to the plasma current. This upgrade would provide the capability to study MHD feedback stabilization in plasmas with negligible rotation speeds even up to the maximum heating power of 6-8 MW.

[1] N. Akasura et al., Nucl. Fusion **33** (1993) p. 1165.

Section 4 - Control of External Modes (Wall modes)

Introduction

Several external modes can be excited depending on the plasma periphery conditions and the hardware arrangement just outside the plasma surface. One of the most important external modes is the external kink mode and its modified branch, the resistive wall mode. The resistive wall modes are excited as a consequence of the finite resistivity of the passive stabilizing plates when the external kinks are stabilized by the conducting shell. The modes are relatively low frequency, with the growth rate being characterized by the inverse of the L/R decay time constant of the passive stabilizing shell (see Section 4.3.1). Several schemes have been proposed to stabilize this weakly-growing mode. Magnetically, this mode can stabilized if the helical flux leakage from the shell is compensated by active feedback coils mounted behind the passive plates (Fig. 1). For the non-magnetic approach, we have developed several schemes for stabilizing the resistive wall mode. One is the utilization of the ponderomotive force with IBW. The FSX facility has two ion Bernstein wave (IBW) antennas that can provide up to two megawatts of radio frequency power. These are intended to control MHD modes by applying a ponderomotive force to the plasma. A second approach is to use neutral beam modulation. There are two perpendicular neutral beamlines that are capable of injecting up to 3.6 MW. In FSX, these NBI sources will be modulated to input radial momentum with the appropriate phase to suppress edge MHD modes and resistive wall modes. Other schemes are based on edge current/halo current modulations. A variety of techniques for edge plasma modification are also under consideration for MHD control. Currents that are a modest percentage of the total plasma current can be driven in the edge plasma “halo” or “scrapeoff” region to stabilize external modes.

Over several years, new theoretical analyses have been developed for these approaches, and our theoretical understanding has made excellent progress. These new theoretical advancements, combined with unique experimental tools and enhanced numerical simulation capabilities at PPPL, will allow a concerted exploration of feedback stabilization of tokamaks and alternates.

Fig. 1 - Section 4.1 (See Figure Folder)

4.1 Mode identification for external MHD

For definitive mode identification, it is important to monitor both internal and external mode structures. Here, we focus on resistive wall mode feedback stabilization, which is one of our main objectives in FSX. The magnetic information from outside the plasma surface is not sufficient alone to distinguish between edge localized modes, locked modes originating from the resistive tearing modes, and resistive wall modes branching out from external kink modes. This structure information must be processed for determining the mode characteristics. The feedback system should be activated only after the mode is definitively identified as either a resistive wall mode or a tearing mode. The external mode structure sensors used here are: (1) helical flux leakage sensors, (2) sensors to measure the eddy current pattern on the shell, and (3) Mirnov coils. The internal sensors are (1) vertical/horizontal soft x-ray arrays and (2) newly-planned ECE diagnostics.

(1) Magnetic sensors for the external mode structures

The main magnetic sensors for the external structure of modes are (a) helical flux leakage sensors (to measure the normal magnetic field component behind the passive shell), and (b) Rogowski coils for monitoring the eddy current on the passive shell.

(a) Helical flux leakage sensors

For resistive wall mode control, the key element is the helical magnetic flux leakage through the resistive shell. We plan to install a set of the flux leakage sensors just behind the passive stabilizer plates. The helical flux leakage sensor will consist of two identical rectangular flux loops aligned torodially at the same poloidal angle, as discussed in the Section 4. These two loops are connected in an “anti-series” manner to observe only the variation of poloidal magnetic flux along the toroidal direction, i. e., $\delta\psi_{helical} = \langle\delta\int BndS\rangle_{helical}$. A total of 20 leakage flux sensor loops will be installed to monitor the local flux change behind the passive shell.

(b) Eddy current measurements on the shell with Rogowski coils

Eddy current measurements with Rogowski coils have been serving as excellent sensors for global MHD activity.[1,2] In PBX-M, the “smart” shell approach for the control of the n = 0 vertical motion has been successful, utilizing the eddy

current monitor signal at the midplane.[2] The detected eddy current pattern was also used to observe the n = 1,2 helical MHD modes, and identify the resistive wall mode.[1] For the present experiment, two additional arrays in the gaps between plates (2) and (3) above and below the midplane in Fig. 1 will be added to the analysis. In addition, the eddy current path within the thick 2.5 cm aluminum passive plates themselves will be monitored by inserting a 1-m Rogowski coil onto the front plate surface through the passive plates. The minimum detectable current by the Rogowski coils in the actual experiment has been ≈ 200 A for low frequencies near the $R/L \approx 50 - 100\ s^{-1}$ range. At higher frequency (1-100 KHz), the detectable current is 30-50 A.

These 2-dimensional eddy current pattern measurements will serve as the major diagnostic to study the edge/halo current, and investigate MHD control with the plate biasing and segmented divertor biasing discussed in Sections 4.6 - 4.10. The halo current during the precursor/postcursor phase of disruptions will be studied by measuring these eddy currents as a part of the ITER R&D tasks. The thick aluminum PBX-M arrangement is extremely suitable to study the effect of the ITER highly-conducting first wall on MHD stability.

(2) Sensors for the internal mode structure

The internal structure will be monitored by the soft X-ray arrays and measurements of the electron cyclotron emission frequency spectrum. The PBX-M soft X-ray array monitoring the vertical profile has high sensitivity with an excellent signal-to-noise ratio, even near the plasma edge. It is possible to determine a magnetic island with a spatial resolution of 3 cm. The vertically-viewing soft X-ray array will be made operational to observe the two dimensional mode structure. A new ECE diagnostic is planned to provide mode structure information up to the near the plasma edge. This instrument will most likely be a grating polychromator.

References

[1] M. Okabayashi et al., Nuclear Fusion **36** (1996) 1167.

[2] R. Hatcher and M. Okabayashi, "Integrated Shell Approach to Vertical Position Control," Princeton Plasma Physics Laboratory Report PPPL-3089 (1995).

4.2 Feedback-signal processing and generation

The sensor signals for determining the internal and external mode structure discussed in Section 4.1 require extensive data processing to prepare the feedback actuator signals. The schematic of the process is shown in Fig. 1. Processing can be achieved with a digital system, since the growth time of the resistive wall mode is relatively slow, i. e., in the range of 1-5 ms according to the previous PBX-M results. The first step of the process is the processing of individual data signals. In the second step, the internal measurements will be correlated with global mode structures to aid in the identification of the modes.

(1) Individual data processing

The magnetic and non magnetic signals require data processing before the data are used for mode identification. For example, the $\delta\psi$ helical flux leakage-loop will require compensation due to other effects such as toroidal field, misalignment of loops, etc., although the geometrical arrangement (anti-series connection) itself minimizes the direct coupling to the axi-symmetric equilibrium and/or the plasma field. Non-magnetic signals will require both gain and DC component subtraction.

(2) Comparison of internal/external mode structure and mode identification

The decomposition of the leakage flux loop signals will provide toroidal n-values. The internal mode sensors will provide the internal mode structure, and determine whether the global characteristics are consistent with the resistive wall mode. The mode identification process will also provide the vertical positional status (n=0 vertical mode), enable the detection of locked modes related to the tearing mode, and establish the need for error field compensation. It is noted that the feedback system can provide simultaneously both n=1 feedback and the field error correction. Equilibrium data, such as beta, beta-p, li, κ, and "D-ness," are available from the other parallel processors, and will assist the choice of the adjustable parameters. Depending on the choice of the feedback logic, the error signals will be prepared from this data for either a "fake rotating shell" or an "intelligent shell."

Fig. 1 - Section 4.2 (See Figure Folder)

A new digital plasma control system has been acquired to replace the PBX-M analog shape and position control subsystem, and for the implementation of other feedback control schemes. Its data acquisition subsystem can handle up to 128 analog signals at a 10 kHz sample rate, and up to 32 analog signals at a 250 kHz sampling rate. The basic diagnostic set permits profile measurements of the electron temperature and density, ion temperature and toroidal velocity, and current density. MHD mode identification is, in principle, possible by using one of the parallel processors.

4.3 MHD Control Techniques with Magnetic Fields: Integrated shell

"Integrated shell" for feedback stabilization of the resistive wall mode

The characteristics of the resistive wall mode depend entirely on the passive shell performance. The passive shell should be located close enough to the plasma surface so that the external kink modes are modified into following the resistive wall mode branch. The growth rate is related to the stability margin from the ideal kinks and the proximity of the shell to the plasma surface. As discussed in Section 3.3, the present passive stabilizing plates should be able to stabilize the external kinks, with sufficient margin relative to the ideal kink onset conditions.

A summary of the predictions from theoretical studies of the partial passive shell are:

(1) A variety of current and pressure profiles are stable with a shell separation parameter of b/a = 0.2.

(2) The midplane gap for the shell to accommodate NBI and diagnostics does not change the stability properties significantly, provided the gap is ≤ 10% of the conformed shell surface circumference.

(3) Poloidal shell coverage over a one-poloidal wavelength outboard region is adequate for achieving stability.

4.3.1 The Resistive Shell Mode and Active Shell Stabilization

4.3.1.1 What is the definition of a resistive shell mode?

A resistive shell mode is a helical instability of a tokamak plasma which would ordinarily grow on a hydromagnetic time-scale (i.e., very rapidly), but in the presence of a conducting shell grows instead on the characteristic L/R time of the shell (i.e., fairly slowly. Of course, the growth-rate of the mode becomes zero if

the shell is perfectly conducting, since the L/R time becomes infinite in this limit. Thus, there are two criteria which a candidate mode must satisfy before it can be classified as a resistive shell mode. First, the mode must be unstable (preferably, very unstable) in the absence of a shell, and, second, the mode must be completely stable in the limit in which the shell behaves as an ideal conductor. Any mode which fails to satisfy either one of these criteria is *not* a resistive shell mode. In particular, an *unstable* mode which *oscillates* on a time-scale which is *much shorter* than the L/R time of the shell cannot be a resistive shell mode, because the shell essentially behaves like a perfect conductor as far as this mode is concerned.

4.3.1.2 What is the pertinent resistive time-scale of the shell?

For a uniform shell of radius r_w, thickness δ_w, and conductivity σ_w there are at least three different resistive time-scales: the skin time,

$$\tau_s = \mu_0 \sigma_w \delta_w^2, \tag{1}$$

the L/R time,

$$\tau_w = \mu_0 \sigma_w r_w \delta_w, \tag{2}$$

and the diffusion time,

$$\tau_d = \mu_0 \sigma_w r_w^2, \tag{3}$$

Assuming that the thickness of the shell is small compared to its radius (i.e., $\delta_w << r_w$), it follows that

$$\tau_s << \tau_w << \tau_d. \tag{4}$$

However, the *pertinent* time-scale is the L/R time: this is the growth time of the resistive shell mode, and is, therefore, the appropriate response time of any feedback system placed external to the shell.

In order to appreciate that τ_w is the pertinent time-scale, consider the m,n resistive shell mode in cylindrical geometry. The dispersion relation of this mode can be written

$$\Delta_w = \sqrt{\gamma \tau_d}\, \tanh\left(\sqrt{\gamma \tau_s}\right), \tag{5}$$

where Δ_w is the shell stability index (analogous to the conventional tearing stability index, except that the discontinuity in the radial derivative of the eigenfunction takes place at the radius of the shell).The above formula is valid provided that

$$|\gamma| \tau_d >> 1. \tag{6}$$

It is easily demonstrated that

$$\Delta_w = \frac{2|m|}{\left(r_c / r_w\right)^{2|m|} - 1}, \tag{7}$$

where r_c is the *critical radius*. For $r_w < r_c$, the resistive shell mode grows on a relatively slow resistive time-scale determined by the shell. As $r_w \rightarrow r_c$, the resistive shell mode converts into an ideal mode which grows on a relatively fast hydromagnetic time-scale determined by the plasma. For $r_w > r_c$, the shell has no effect whatsoever on the growth-rate of the m,n mode.

Suppose that $r_w > r_c$, so that the growth-rate of the mode is determined by the shell. Unless the radius of the shell almost coincides with the critical radius, Eq. (2.7) gives $\Delta_w \sim O(1)$, and Eq. (2.5) reduces to

$$\gamma\tau_w = \Delta_w. \tag{8}$$

Thus, the resistive shell mode grows on the L/R time of shell. Since this time-scale is much less than the skin time, the shell lies in the so-called *thin shell* limit (analogous to the so-called (*constant-* ψ limit in tearing mode theory). The constraint (2.6) is satisfied provided that $r_w \gg \delta_w$. Thus, as long as the thickness of the shell is small compared to its radius, the conventional thin shell analysis of the resistive shell mode is valid.

Suppose that r_w approaches r_c. In fact, let

$$r_c = r_w + d, \tag{9}$$

where $d \ll \delta_w$. It follows that $\Delta_w \cong r_w/d$. For $d \gg \delta_w$, Eq. 5 again reduces to Eq. 8. However, for $d \ll \delta_w$, Eq. 5 yields

$$\gamma\tau_s = \left(\frac{\delta_w}{d}\right)^2. \tag{10}$$

Note that, in this limit, the mode grows on the skin time, and, therefore, only penetrates a few skin depths into the shell (*i.e.*, the thin shell approximation breaks down). Thus, as the radius of the shell approaches the critical radius, the growth-rate of the resistive shell mode increases, but the thin shell approximation only breaks down when the shell lies within a few shell thicknesses of the critical radius. In other words, the thin shell approximation remains valid until the resistive shell mode is just about to convert into an ideal mode. Since it is clearly not sensible to attempt to feedback stabilize the resistive shell mode under these circumstances, it follows that in all cases which are at all amenable to feedback stabilization the resistive shell mode grows on the L/R time of the shell, and the thin shell approximation holds. This conclusion is valid as long as the thickness of the shell is small compared to its minor radius.

4.3.1.3 How does the intelligent shell feedback scheme work?

The intelligent shell [1] is a set of feedback controlled, current carrying conductors, external to the actual shell, which *mimics* the eddy current pattern of a stationary shell possessing a relatively long L/R time.

Suppose that the actual shell lies at radius r_v and has the L/R time τ_v, and the effective, or 'fake,' shell generated by the feedback coils lies at radius r_w and has the L/R time τ_w. As long as the fake shell lies *inside* the critical radius (*i.e.*, as long as $r_w < r_c$), the resistive shell mode *must* penetrate the fake shell in order to be unstable. This follows because if the mode does not penetrate the fake shell then this shell effectively acts like a perfect conductor, and *by definition* a resistive shell mode is stabilized by a perfectly conducting shell placed inside the critical radius.

The intelligent shell concept only works if the L/R time of the fake shell greatly exceeds that of the actual shell (*i.e.*, provided that $\tau_w >> \tau_v$). Now, the resistive shell mode can only penetrate the fake shell when $\gamma\tau_w \sim O(1)$. It immediately follows that $\gamma\tau_v << 1$. In this limit, the eddy currents excited in the actual shell are too feeble to affect the growth-rate of the mode. Thus, the actual shell effectively `disappears' from the problem, and its place is taken by the fake shell. This implies that the resistive shell mode grows on the L/R time of the fake shell. Strictly speaking, the feedback scheme does not stabilize the resistive shell mode. However, if the L/R time of the fake shell is made longer than the pulse length of the tokamak then, too all intents and purposes, the resistive shell mode is stabilized.

The L/R time of the fake shell is given by the product of the intrinsic L/R time of the feedback coil array which generates the fake shell and the gain in the feedback circuits. If, as seems probable for reasons of economy and practicality, the intelligent shell is implemented with a relatively *small* number of coils, then the intrinsic L/R time of the feedback coils is necessarily very small. This follows because there is hardly any metal in the coils (compared to an actual shell), and their fractional area coverage of the plasma is small. Under these circumstances, the critical gain in the feedback circuits needed to make the L/R time of the fake shell *longer* than the pulse length of the tokamak is bound to be *extremely large*. This is the main drawback of the intelligent shell scheme: high gain feedback circuits are hard to implement experimentally because they tend to suffer from instabilities associated with the non-ideal nature of real feedback amplifiers.

4.3.1.4 How does the fake rotating shell feedback scheme work?

The fake rotating shell [2] is a set of feedback controlled, current carrying conductors, external to the actual shell, which *mimic* the eddy current pattern of a poloidally *rotating* shell possessing a relatively short L/R time.

Suppose that the actual shell lies at radius r_v and has the L/R time τ_v, and the effective, or 'fake' shell generated by the feedback coils lies at radius r_w and has the L/R time τ_w. As long as the 'fake rotating shell' generated by the feedback coils lies inside the critical radius (*i.e.*, as long as $r_w < r_c$), the resistive shell mode *must* penetrate the fake shell in order to be unstable. Of course, the mode must simultaneously penetrate the actual shell.

A rotating shell acts rather like a *band-pass filter* for magnetic flux. If flux is Fourier analyzed according to its rotation frequency, then only those frequencies which lie in a band, centred on the rotation frequency of the shell, and of width one over the L/R time of the shell, can penetrate the shell. Suppose that the fake shell has the rotation frequency Ω_w. The range of rotation frequencies which can penetrate the fake shell is approximately

$$\Delta\omega_w \cong \Omega_w \pm \frac{1}{2\tau_w}. \qquad (11)$$

Of course, the actual shell is *non-rotating*. Thus, the range of rotation frequencies which canpenetrate the actual shell is approximately

$$\Delta\omega_v \cong \pm\frac{1}{2\tau_v}. \qquad (12)$$

The fake rotating shell scheme works by ensuring that the two ranges of frequencies given in Eqs.(4.1) and (4.2) *do not overlap*. This means that there is no rotation frequency at which magnetic flux can simultaneously penetrate both shells. In other words, at least one of the shells acts like a perfect conductor. Since both shells lie inside the critical radius, if either one of them acts like a perfect conductor then *by definition* the resistive shell mode is stabilized. In the fake rotating shell scheme the L/R time of the fake shell is the same as the intrinsic L/R time of the feedback coil array, and is, therefore, very small. In particular, the L/R time of the fake shell is much less than that of the actual shell (*i.e.*, $\tau_w << \tau_v$). This means that the resistive shell mode grows on the L/R time of the actual shell (*i.e.*, $\gamma\tau_v \sim O(1)$). Furthermore, it follows from Eqs. 11 and 12 that the fake shell is transparent to a

far wider range of frequencies than the actual shell. In fact, in this limit, the criterion that the two ranges of frequencies given above do not overlap reduces to

$$\Omega_w \geq \frac{1}{2\tau_w}. \qquad (13)$$

In other words, the rotation frequency of the fake shell needs to be greater than one over its L/R time.

The rotation frequency of the fake shell is approximately given by the product of one over the L/R time of the actual shell (i.e., the typical growth-rate of the resistive shell mode) and the gain in the feedback circuits. Now, the resistive shell mode is *completely stabilized if* the inequality (4.3) is satisfied. This means that stabilization occurs whenever the feedback gain exceeds a critical value which is approximately the ratio of the L/R times of the actual shell and the fake shell: *i.e.*, $G_c \sim \tau_v / \tau_w$. This critical gain is *far less* than that required in the intelligent shell scheme, where $G_c \sim \tau_p / \tau_w$. Here, τ_p is the pulse length of the discharge, which typically exceeds the L/R time of the shell τ_v by a factor of a thousand.

The fake rotating shell feedback stabilization scheme is, in many ways, very similar to the intelligent shell scheme. Both schemes used feedback controlled conductors to create the illusion of a second 'fake shell' exterior to the actual shell. The major difference is that in the former scheme feedback is used to make the fake shell appear to rotate, whereas in the latter scheme feedback is used merely to increase the L/R time of the fake shell. As mentioned above, the former scheme is capable of completely stabilizing the resistive shell mode at comparatively low values of the gain in the feedback circuits, whereas the latter scheme is only effective when the gain is extremely high. Since, generally speaking, low-gain feedback circuits are far easier to implement experimentally than extremely high-gain circuits, the fake rotating shell scheme appears to be the most promising of the two schemes.

References

[1] C.M. Bishop, Plasma Phys. Contrld. Nucl. Fusion **31**, 1179 (1989)

[2] R. Fitzpatrick and T.H. Jensen, Phys. Plasmas **3**, 2641 (1996)

4.3.2 Eddy Currents in the FSX Shell

1. The induced current on the conducting shell

It is now generally conceded that the external kink mode is a principal factor which limit the performance of tokamaks. This mode and its relatives such as the tearing, kink tearing and perhaps **TAE** modes which may have a finite surface magnetic perturbation can be affected by a conducting shell because the motion of the perturbation induces a shell current **K** which, by Lentz's law, tends to suppress the growth of the mode. Examination of the current pattern proves to be essential for economical use of the passive conducting material necessary for at least slowing down these potentially dangerous modes. It also provides valuable information for constructing a positive feedback system since such a system could ideally (but perhaps not practically) be effected by just enhancing the induced current pattern seen in the shell. The calculation of these currents can also provide quantitative information about the stresses generated in the tokamak vacuum vessels due to perturbations, or more violent disruption-like processes. An example of such a current pattern on a conforming shell at **0.5a** enclosing an **n=1** kink unstable plasma is shown in **Fig. 1**. There, the projection of the induced current is seen on the shell over one period in the unfolded $\mathbf{L}_\phi$ - $\mathbf{L}_\theta$ plane where the axes are both physical lengths and normalized to be unity. Top and side views are also shown in the figure. Even though the shell is placed equidistantly from the plasma the current is localized in the vicinity of the outer major radius side of the plasma because of the `bad curvature' effects on the kink mode there. The Fourier components, ξ_m, of the radial plasma displacement at the surface of the plasma which are responsible for the induced current are shown in the side bar. One sees immediately that the most effective locale for passive or active mode suppression is at the outer midplane. Unfortunately, present day devices have conventionally placed beam lines, diagnostics, etc., in his crucial region, thus creating a competition for valuable real estate there and imposing severe constraints on the design of an effective feedback system: the amount of passive material needed for slowing the mode is drastically reduced and the geometry of the coils necessary for an active system is severely compromised. It is therefore important to carefully assess the currents in the shell to design a system effective over a wide variety of discharges.

In order to categorize these patterns we have calculated them for a variety of envisioned FSX plasma configurations.[1] As we shall show, the patterns share

enough similarities over a wide range of configuration parameters so that it is possible to design a not too complicated intelligent feedback system. Several cases of such currents and some salient information are presented as follows:

Figure 1: Projection in the (Lf-Lq)plane of the induced current on a conforming shell at 0.5a due to an ustable n=1 kink mode. The coordinate axes are physical lengths and normalized to unit length. The top and side views of the outer and inner sides are also shown. (See Figure Folder)

1.1 Safety factor, $q(\psi_{edge}) = 4.9$

- Induced current for a self-consistent case, n=1. A kink unstable case with a conforming wall at **0.5**. The eddy current pattern is shown in Fig. 1. The top and side views of the outer and inner regions are also shown. The eigenfunction used for this is the self-consistent one for this wall position from the PEST-1 code.

- Current for the wall at 0.1a, n=1. *Using the same eigenfunction as the self-consistent case* of Fig. 1 we calculate the eddy current pattern on a wall at **0.1**. This makes it physically inconsistent. We show the result in **Fig. 2**. Note that the pattern is very similar to the self-consistent case of **Fig. 1**.

Figure 2: Projection in the L_ϕ - L_θ plane of the induced current on a conforming shell, *artificially placed at* **0.1a**, due to the unstable n=1 kink mode of **Fig. 1**. (See Figure Folder)

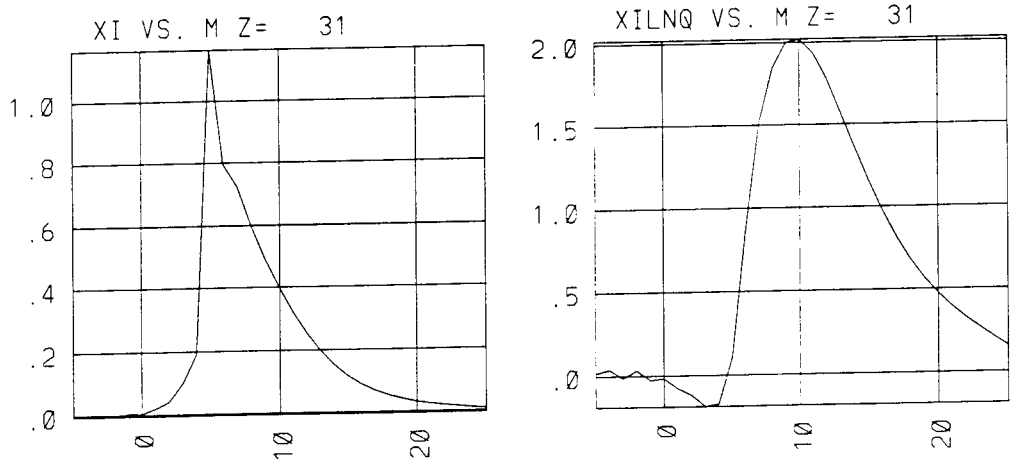

Figure 3: The Fourier harmonics, plotted as a function of **m**, of the radial displacement (left) of the perturbation at the plasma surface due to the **n=1** kink mode of Fig. 1. The curve in the figure on the right is proportional to the radial magnetic perturbation.

- **Surface perturbations, n=1**. The Fourier coefficients of the radial displacement and the normal magnetic field at the surface of the plasma which are responsible for the eddy currents of Fig. 1 are plotted as a function of **m** in Fig. 3 (left) [the displacement, ξ_m] and in Fig. 3 (right) [(m-nq) ξ_m]. The latter is proportional to the normal magnetic field perturbation.

- **Current for a self-consistent case, n=2**. The eddy current distribution for the unstable **n=2** mode of Fig. 1 is shown in Fig. 4 for the wall at **0.5**. The eigenfunction is self consistent for this wall position.

Figure 4: Projection in the **(L_ϕ-L_θ)** plane of the induced current on a conforming shell at **0.5a** due to the unstable **n=2** kink mode of the same equilibrium of Fig. 1. The coordinate axes are each normalized to unit length. The top and an outer side view are also shown. (See Figure Folder)

- Current for the wall at 0.1a, n=2. Note again the similarity of the current pattern of Fig. 5 with that of Fig. 4 even though the radial perturbation is inconsistently used from the case where the wall is at **0.5a**.

Figure 5: Projection in the **(L_ϕ-L_θ)** plane of the induced current on a conforming shell, *artificially placed* at **0.1a**, due to the unstable **n=2** kink mode of Fig. 1. (See Figure Folder)

- Surface perturbations, n=2. The corresponding surface perturbations are plotted in Fig. 6.

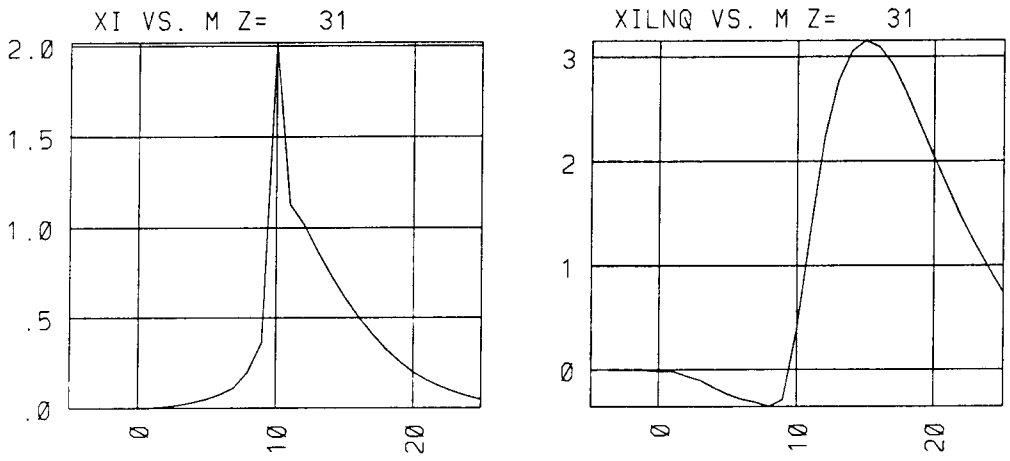

Figure 6: The Fourier harmonics, plotted as a function of **m**, of the radial displacement (left) of the perturbation at the plasma surface due to the **n=2** kink mode of Fig. 1. The curve in the figure on the right is proportional to the radial magnetic perturbation.

1.2 Safety factor, $q(\psi_{edge}) = 3.82$

The eddy current pattern seen in Fig. 7 for a case in which $\mathbf{q_{edge} = 3.82}$ and a wall at **0.5a** is also similar in gross features to the case above for $\mathbf{q(\psi_{edge}) = 4.9}$. In this case the **n=2** mode was stable.

Figure 7: Projection in the **(L_ϕ-L_θ)** plane of the induced current on a conforming shell at **0.5a** due to an unstable **n=1** kink mode for a case in which $\mathbf{q_{edge} = 3.82}$. The coordinate axes are physical length and each normalized to unit length. (See Figure Folder)

1.3 Safety factor, $q(\psi_{edge}) = 2.83$

Again, as seen in Fig. 8 for the **n=1** mode and Fig. 9 for the n=2 mode, the pattern is very similar to those above with the larger safety factors.

Figure 8: Projection in the **(L_ϕ-L_θ)** plane of the induced current on a conforming shell at **0.5a** due to an unstable **n=1** kink mode for a case in which q_{edge} = 2.83. The coordinate axes are each normalized to unit length. (See Figure Folder)

Figure 9: Projection in the **(L_ϕ-L_θ)** plane of the induced current on a conforming shell at **0.5a** due to an unstable **n=2** kink mode for the case in which $q_{edge} = 2.83$. The coordinate axes are each normalized to unit length.

2 The cylindrical Fourier response

In order to gain some insight as to why these patterns are so similar in their gross features and, apart from the **Heaviside**-like localization in the outer major radius region, why they seem to have seemingly low harmonic content, we turn to the cylindrical model.

In a cylinder with radius r = a, periodic length $2\pi/k$ and a conducting shell at r = b, the Fourier components of the magnetic scalar potential are given in terms of a response function, $\Re_m$, by:

$$\chi_m(r) = -Bm\frac{k}{m}\left(\frac{r}{a}\right)^{-m}\frac{1+(r/b)^{2m}}{1-(a/b)^{2m}} \tag{1}$$

$$\equiv \; - \; kB_mR_m \tag{2}$$

where

$$B_m \equiv \delta B_{rm}(a)\frac{a}{k} = \frac{a}{k}\mathbf{e}_r \bullet \nabla \times (\xi_m \times \mathbf{B}) \tag{3}$$

$$= \; i(B_\theta / a)(m \; - \; nq)\xi_{rm} \tag{4}$$

Since the unstable mode is almost rational at the plasma surface, note that factor of **(m- nq)** on the radial perturbed magnetic field, $\delta \mathbf{B_{rm}}$, Eq. (4)**,** reduces its Fourier harmonic but enhances the modes with higher **m**. As shown in Fig. 3 and Fig. 6, the Fourier spectrum of the radial displacement $\xi_\mathbf{r}$ peaks at the rational surface near the plasma edge but the Fourier spectrum of the radial magnetic field which is actually responsible for the induced current peaks at a much higher value of **m**, *i.e.*, in the vicinity of **m ~ 10** or higher. This is significant since the response function, $\Re_\mathbf{m}$, to the scalar potential falls off very rapidly with **m** as seen in Fig. 10. This is true even if the wall is very close to the plasma. Indeed, by setting **r=b** and letting

Figure 10: The Fourier harmonics of the response, $\Re_m$ at **r=b**, to the cylindrical plasma perturbation, normalized to the **m=1** component, plotted as a function of **m**. In the limit where **b/a = 1**, $\Re_m / \Re_{m=1} = m^{-2}$. This limiting curve almost overlaps that for **b/a = 1.1.** (See Figure Folder)

$$b / a = 1 + \varepsilon \tag{5}$$

one finds

$$R_m = \frac{1}{\varepsilon m^2} \tag{6}$$

so that

$$\frac{R_{m=1}}{R_{m=10}} = 100. \tag{7}$$

In the figure are the responses for cases in which the wall distances are **1.5a**, **1.1a** and **1.0a**, each normalized to its response for m=1. This rapid falling-off of the response of the scalar potential also occurs in general two-dimensional configurations. In Fig. 11 are shown the decrease of the responses at the shell for the **m=-1, 0, 1, 2, 7, 8, 9** and **10th** harmonics of the plasma surface perturbation of the unstable kink mode of **Fig. 1**. This observation is a factor responsible for the eddy current patterns being very similar for a variety of plasma discharges with a wide variation in plasma shapes, edge safety factors and wall distances. This facilitates the design of the feedback coils since only the lower harmonics need be addressed in the feedback circuits.

Figure 11: The decreasing two dimensional response, $\Re(\theta)$ at the shell for the **m=-1, 0, 1, 2, 7, 8, 9** and **10th** harmonics of the plasma perturbation for the unstable kink mode of the case described in Fig.1. (See Figure Folder)

The normal component of the magnetic field vanishes at the shell, and the skin current, **K**, gives the required discontinuity in the tangential field at the shell. The latter involves derivatives only within the surface and is given by:

$$\mathbf{K} = \hat{\mathbf{n}} \times \nabla\chi, \tag{8}$$

$$= -\mathrm{i}kB_m R_m \left[\frac{l}{r}\mathbf{e}_\phi + nk\mathbf{e}_\theta\right] e^{i(l\theta - n\phi)}, \tag{9}$$

evaluated at **r=b**.

Another way to perhaps understand the induced current is to imaginethat the current arises in order to cancel the normal component of the magnetic field due to the plasma perturbation which would exist in the shell if the shell were absent. This current density, $\Im_n$, would be given by taking the negative curl of this field:

$$\mathbf{J}_n = -\nabla \times \delta B_r \mathbf{e}_r \tag{10}$$

$$= \mathbf{e}_r \times \nabla \delta B_r \tag{11}$$

thus giving the same surface distribution as in Eq. (9). A similar observation holds in the two-dimensional case provided that the normal *covariant* component of the magnetic perturbation is used.

Reference

[1] M. S. Chance, "Vacuum Calculations in Azimuthally Symmetric Geometry," Princeton Plasma Physics Laboratory Report PPPL-3216, submitted to Physics of Fluids.

4.3.3 Hardware arrangement for "Integrated Shell"

Here, we will concentrate on the role of the feedback system in stabilizing the resistive wall modes. As discussed in section 4.3.1 and 4.3.2, the external kink mode modifies itself into the resistive wall mode during the resistive flux loss. If the lost helical flux is compensated by the feedback system without adding any unfavorable effects, the mode should be stabilized, or the growth should be reduced by an observable amount.

The "Integrated shell" is an integration scheme for resistive wall mode stabilization with a passive shell, active elements, sensors, and power supply units all controlled by an active control system. A diagram of the scheme is shown in Fig. 1.

The main feature is a "segmented coil set" helically stretched over 360 degrees in the toroidal direction as parallel as possible to the predicted wall eddy current flow. The total assembly consists of ten units surrounding the entire passive shell uniformly in the toroidal and poloidal directions at the outboard region. These active coils are located just behind the passive shell. The main function of these unit is to maintain the predicted helical flux pattern with minimal additional perturbations when the mode is excited.

These two schemes have been proposed: one is the "fake rotating" shell and the second is the "smart" shell approach. These two approaches use different combinations of input signals. The fake rotating shell uses the helical flux loss sensors to apply feedback with the proper toroidal phase shift. The "smart shell" utilizes the eddy current pattern on the shell as the primary sensor. The proof of the principle experiment for the "smart" shell was carried out for an n = 0 vertical position control using shell eddy currents in PBX-M.[1,2] The logic scheme was to minimize the asymmetric eddy current pattern, without using the actual plasma motion, this method has been working extremely well in PBX-M high-β studies .

Passive shell geometry

The PBX-M passive plates were designed to stabilize the external kinks and n = 0 vertical motion under a strongly unfavorable magnetic decay curvature index ($n \approx -2.5$), like the bean-shaped configuration. As reported in Ref. 1, kink modes were

Fig. 1 Integrated shell scheme for resistive wall mode stabilization. One set of active coils is lined up along the eddy current flow pattern. One unit stretches toroidally over 360 degrees. The two power supply systems energize the midplane coil section and the section at the off-midplane independently. Total of 10 units covers uniformly the domain of the outboard plane.

stabilized and modified to enter the resistive shell regime. For the proposed feedback stabilization experiment, the portion of the passive plates at the outboard side for the kink stabilization are kept intact.

The modification is made only to the plates which function for the n = 0 stabilization, located near the separatrix and the inboard side. The new arrangement of the passive shell is shown in Fig. 1 in Sec. 4.1. It is to be noted that the n=1 stability domain also serves as n=0 stabilizing domain by allowing the asymmetric current flow through the midplane jumpers (discussed later)

The passive plates are isolated from the vacuum vessel in order to eliminate the residual halo current through the vacuum vessel. This electrical isolation of the passive shell eliminates the complication of the eddy current path through the vessel. Therefore, the helical n=1,2 eddy components on the shell should reflect simply the reaction of the passive shell due to kink-associated phenomena.

The characteristic L/R time of the passive shell for the for n=1 mode is ≈20 ms, assuming that the induced current is uniformly distributed in the plates (thin shell approximation) as used in the SPARK analysis. The skin characteristic time is comparable to this thin-shell approximation L/R time.

To capture the helical flux produced by an MHD mode, the upper/lower outboard plates are electrically connected with jumpers located at 10 locations with equally spaced in the toroidal direction. These electrical jumpers allow the helical current to flow from the upper to lower plates or vice versa; otherwise the helical flux at the midplane will be lost. In the proposed arrangement, the number of connections will be reduced to 5 from the present 10 to accommodate the active coils. The stability properties may be reduced. However, theoretical analysis (in Section 2.1) of the gap width dependence on the stability suggests that this modification should be tolerable for an n = 1 kink stability. In addition to the midplane area, electrical jumpers exist between passive plates (2) and (3) as shown Fig. 1 in Sec. 4.1 The Rogowski coils located on these electrical jumpers serve as the diagnostics which aid in characterizing the eddy current patterns.

Fig. 2 The actual coil location shown in comparison with the eddy current pattern for n = 1 and n =2. The solid line represents the toroidal location of the maximum and minimum eddy current in the poloidal components, which is discussed in Sec. 4.3.1 (See Figure Folder)

Fig. 3 (See Figure Folder)

Fig. 4 (See Figure Folder)

Active coil geometry: partial helical configuration

In the high-β exploration experiments (Ref. 1, 3), the radial location of the plasma surface, rw, was adjusted to be within the kink stable radius rc (rw < rc), so that the kink modes are stable with the ideal shell. With the helical flux loss due to the finite resistance of the shell, the resistive wall mode, a modified ideal kink, was excited within the growth time of a fraction of the L/R time. The function of the active coil in the feedback system is to compensate the helical flux loss in a two-dimensional manner and to sustain the external kink mode-induced flux pattern as closely as possible until the mode is stabilized.

We have chosen a geometry with 5 segmented coils helically stretched over 360 degrees as one unit. A total of 10 such units uniformly cover the passive plates (Fig. 1). Each unit will be energized with the same phase relative to the other units. The helical arrangement for the active coils was chosen by noting that unwanted magnetic field patterns could excite unfavorable modes, such as "error-filed induced" locking modes, since the frequency is extremely low for such modes.

To allow for stabilization of both n = 1, and 2 modes, an eight subsection segmentation in the toroidal direction is adequate. However, the present hardware arrangement inside the vacuum vessel has been designed for a 20 TF coil geometry, so we have chosen a segmentation with a 10-fold toroidal symmetry in a quasi-helical manner.

The location of each coil relative to the eddy pattern is optimized to the eddy pattern for n =1 an 2 with 3 < qedge < 4. There is some concern for the loss of flexibility from choosing one helicity. However, the eddy current pattern, as discussed in Section 4.3.2, is relatively insensitive to the edge q, so a fixed coil set can cover the conditions of present interest.

The actual coil shape and location was determined by the availability of the space behind the passive plates and the engineering consideration of complex assembly process in the spatially tight area. Figure 2 shows the active coil location for n =1 and 2 cases and the connection required to form one helical unit corresponding to the one shown with dark area. The tilt angle of the current distribution is similar at the midplane for both cases. However, the results show large differences away from the horizontal plane. The optimized combination uses different off-midplane

coils. The quasi-helical coils are separated into two upper and lower segments so that there is the flexibility to choose different off-alignment combinations if it is necessary to accommodate extremely different eddy patterns related to qedge < 3 or qedge > 5. Figure 3 shows the active coil coverage domain related to the helical flux predicted by the resistive wall mode onset. The active coils will cover the dominant area of eddy current excitation.

An example of a feedback scheme is shown for the fake rotating shell (Fig. 4). In this case, the helical flux leakage sensor at one location will be used to provide the phase shift for the power supply in the adjacent segment and as a consequence, the fake rotation is introduced by the feedback scheme. The advantage of using this scheme is that the phase shift is from the direct measurement rather than from phase shifts in the control process. Secondly, the flux signal itself is free from coupling to the equilibrium magnetic field. Otherwise, complicated flux compensation would be required.

Power supplies

Estimates for the required power supply systems and their frequency response has been formulated by several groups assuming a minimum detectable magnetic field with a simple geometry.[4,5] This provides very modest power level and low frequencies. Here, we have estimated the power and required frequency based on the experimental observations in the PBX-M high–β studies.[1]

In the PBX-M high ß kink experiments, the eddy current just before the thermal collapse was 1 ≈3 kA for 200 - 500 kA discharges. Based on these PBX-M observations, and scaling up to the higher plasma current (possibly up to 1 MA), it would be reasonable to predict the current level ≈ 6 kA. Of course, the finite feedback gain should reduce the required current substantially. However, we have chosen the current of 6 kA as the design value. The 6 kA is equivalent to 30 gauss, when the current flow uniformly. Detailed calculations are in progress using the PPPL SPARK code. The L/R time for the n = 1 and 2 modes is approximately 20-30 ms for the thin-shell assumption.

The present theoretical effort, as discussed in Section 3.4.1, predicts the required characteristics frequency for the feedback is a fraction (1/3 - 1/4) of the L/R time. In addition, the experimentally observed growth time in PBX-M was ≈ 1- 5 ms (

corresponding to an angular frequency of w ≈ 1000 - 200 rad/s). We have chosen a frequency of w ≈ 700 rad/s as the upper limit. It is also assumed that the tolerable phase shift in the power supply unit is ≈ 9 degrees, which is 36 degrees divided by four, or from considering the 36 degree coverage of one of the unit segments.

References

[1] M. Okabayashi et al., "Role of the stabilizing shell in high β, low-q disruption in PBX-M, Nuclear Fusion **36** (1996)1167

[2] R. Hatcher and M. Okabayashi, "Integrated Shell Approach to vertical position control" PPPL-3089 (1995)

[3] R. Bell et al., Phys. Fluids B 2 (1990) 1271

[4] R. Fitzpatrick, in workshop on "Feedback Stabilization of MHD Instabilities" Dec., 11-13, 1996 at PPPL

[5] T. Jensen, in workshop on "Feedback Stabilization of MHD Instabilities" Dec. 11-13, 1996 at PPPL

4.4 MHD Control Techniques with Force on Plasma: IBW Pondermotive Force

4.4.1 Ponderomotive Feedback Stabilization of the External Kink and Resistive Wall Modes in FSX*

An RF feedback system would have several potential advantages over a magnetic coil-based system, including a faster response time and the absence of magnetic interference with the detectors. One possibility for such a system is to use modulated ion Bernstein wave (IBW) antennas to do ponderomotive feedback stabilization.

The ponderomotive force (PF) is a nonlinear force exerted on a charged particle or fluid element by a spatially decaying rf electric field. In magnetic mirror experiments during the 1980's ponderomotive stabilization of MHD modes was demonstrated on several devices.[1-3] Subsequent theoretical work showed good agreement with the experimental results.[4-5] Further theoretical investigations extended ponderomotive stabilization to external kinks and resistive wall modes in a tokamak using feedback modulation.[6] There have as yet been no experiments investigating ponderomotive stabilization in a tokamak. Such experiments may be performed in FSX using the existing IBW antennas, with little or no investment in additional hardware.

Although ponderomotive stabilization has not been pursued in tokamaks, there is evidence from PBX-M (see Fig. 1), and more recently from TFTR, that the ponderomotive force associated with a slow wave antenna of the type used in direct-launch IBW experiments affects the edge plasma. (Please note the distinction between *directly-launched* ion Bernstein waves, such as are discussed in this Section, and *mode converted* ion Bernstein waves, as discussed in the previous Section. In the latter technique fast waves are launched and converted to IBW at a mode conversion surface within the plasma.)

Previous work on PF stabilization has shown that MHD stability is influenced by the perturbed ponderomotive force $\delta\mathbf{F}\ \exp(-i\omega t)$ exerted on a fluid element by a radiofrequency (RF) field $\mathbf{E}_{RF}\ \exp(-i\omega_{RF}t)$, where ω and ω_{RF} are the MHD and RF frequencies. The relevant term for the MHD normal-mode equation is given by [4-6]

$$\delta \mathbf{F} = \sum_{\mu} \left[\delta\varepsilon_{\mu} \nabla \left(\frac{|E_{\mu}|^2}{16\pi} \right) - \left(\frac{\delta |E_{\mu}|^2}{16\pi} \right) \nabla\varepsilon_{\mu} \right] .$$

Here $\delta\mathbf{F}$ is that part of the perturbed force which survives the projection operation $\mathbf{b} \cdot \nabla \times$ with $\mathbf{b} = \mathbf{B}/|B|$, $\delta\varepsilon_{\mu} = -\xi \cdot \nabla\varepsilon_{\mu}$, ξ is the perturbed plasma displacement, and ε_{μ} is the plasma dielectric tensor in its diagonal basis. The RF electric field $\mathbf{E}_{RF} = \sum_{\mu} E_{\mu} e_{\mu}$ is summed over three independent wave polarizations: left- and right-circular and parallel to $\mathbf{B}$ (μ = L, R, ||). The ponderomotive force $\delta\mathbf{F}$ can modify the growth rate of an MHD mode, such as an external kink, by simply "pushing" on the plasma and forcing the instability to do work. If these "pushes" are appropriately phased with respect to the kink mode and of sufficient amplitude, then the instability becomes energetically unfavorable and the kink can be stabilized.[6]

The first term in $\delta\mathbf{F}$ is the "direct" ponderomotive force, which is the fluid analog of the usual single-particle ponderomotive force (proportional to the gradient of the ponderomotive potential). The second term involves $\delta|E_{\mu}|^2$, a modulation of the RF intensity on the MHD time scale, which can occur in two ways. In the first case, $\delta|E_{\mu}|^2$ results from the beating of the RF field with the low frequency perturbation and results in the so-called sideband term.[4-5] This term can be significant for fast wave antennas but is small for slow wave launchers. In the second case, which is relevant to feedback, an order unity modulation $\delta|E_{\mu}|^2$ can be "forced" by modulating the RF power to the IBW antenna. The modulated PF term is expected to dominate over the direct PF term by the factor $L_{RF}/\xi_d >> 1$, where $L_{RF} \approx \delta_e = c/\omega_{pe}$ is the radial scale length of the evanescent SW near field, $\xi_d = R\, Q_d/B$, and ξ_d, Q_d are the detection thresholds for the radial components of the plasma displacement and perturbed magnetic field $\mathbf{Q} = \nabla \times (\xi \times B)$, respectively. For typical parameters, the modulated PF term is expected to be a factor of 5 - 10 larger than the direct PF term and it also has the advantage that it does not depend on the sign of the RF field gradient, allowing the use of a larger class of RF waves for stabilization.

It can be readily seen that for a slow wave ($E_{||}$) RF launcher, such as a direct launch IBW antenna, the ponderomotive force in the edge plasma is dominated by the electron contribution because $\varepsilon_{||}/\varepsilon_{\perp}$ is proportional to the ratio of the ion to the electron mass. Within an electron skin depth of the plasma edge the parallel electric

field is large, given approximately by the antenna voltage/antenna length, and the electron ponderomotive force can be substantial, as shown by the ponderomotive density depletion near the antenna in Fig. 1.

In Ref., [6] two types of feedback models were considered: a "local response" system, in which each antenna responds to the total amplitude of the perturbed displacement at its location (summed over all modes), and a "Fourier mode response" system, in which each antenna responds to the amplitude of a targeted Fourier mode at its location. An example of a marginal stability diagram for the "local response" feedback system is shown in Fig. 2, which is taken from Ref. [6]. The required value of a normalized PF coupling parameter Γ to obtain marginal stability is plotted vs nq for three cases: (a) parameters similar to the existing FSX IBW antenna system with the conducting wall taken to infinity; (b) the same antenna parameters with the conducting wall at its nominal position on FSX; and (c) the theoretically-optimal "continuum" case of an infinite number of pointlike antennas with perfect feedback and complete coverage of the plasma surface area . This figure shows that two equally-spaced antennas in the poloidal direction ($N_{A\theta}$ = 2), with each covering a modest fraction of the poloidal area (angular half-width θ_w = 0.25), can provide stabilization. It is remarkable that an antenna system that covers only a small fraction of the plasma surface area requires only twice the PF (or rf power) required in the optimal continuum case.

Estimates of the IBW power requirements for stabilization of the external kink can be obtained from the value of Γ. Scaling formulas and estimates for kink stabilization in FSX using the two existing IBW antennas have already been published.[6] Depending on the current profile assumptions, these range from 0.8 MW for a diffuse current profile to 3.2 MW for a flat profile. However, note that these estimates assumed that a propagating ion Bernstein wave was launched as a result of the antenna excitation; in fact, if a launch of the Bernstein wave could be avoided (and if other sources of edge power dissipation, such as sheath effects, could be suppressed) then the power requirements would be negligible. This is because, in principle, edge ponderomotive stabilization requires only reactive, not dissipative, power flow. Evanescent edge electric fields (the reactive antenna near fields) are sufficient to provide stabilization.

At this time the principal uncertainty in the estimate of the power requirements for external kink stabilization is the strength of coupling of the edge ponderomotive force to the MHD mode. The radial overlap integral involving the evanescent slow wave intensity and the MHD mode amplitude is difficult to estimate from theory. The first phase of the ponderomotive stabilization experiment on FSX will therefore involve "MHD spectroscopy" to determine the coupling between the antenna and the MHD modes. The antennas will be amplitude modulated and the frequency of modulation will be varied across the MHD range. The plasma will be monitored via Mirnov coils for a "resonant" response. An analysis of the plasma response will yield the ponderomotive coupling to the external kink. The power requirements for these experiments are modest (a few kW of RF power should be sufficient). The "carrier" (radio) frequency will then be varied over the range $\omega < \Omega_i$ to $\omega \sim 1\text{-}5\ \Omega_i$. Unless a substantial reduction in power requirements can be had by choosing an alternate frequency, the high power kink stabilization experiments will be pursued at either 25-30 MHz or 40-80 MHz (the available high power RF source frequencies at PPPL). However, if launch of a propagating wave can be avoided at low frequency then a reduction in power requirements of an order of magnitude or more is possible. In this case use of an inexpensive low frequency source such as is currently installed on CDX-U will be considered.

If the initial experiments show good coupling of the PF to external MHD modes, feedback stabilization experiments will then be pursued on FSX. In these experiments the FSX mode detection and feedback systems will be used to control the frequency and amplitude of modulation of the RF power. Near 100% modulation of the RF sources at frequencies in excess of 100 kHz has already been demonstrated on TFTR; virtually all RF amplifiers are capable of similar feats. These experiments would test the feasibility of PF feedback stabilization, benchmark the theoretical scalings,[6] and allow extrapolation to larger tokamaks.

* D. A. D'Ippolito[1],*et al.*,
[1]Lodestar Research Corp., 2400 Central Ave., P-5 Boulder, CO 80301.

References

[1] J. R. Ferron, N. Hershkowitz, R. A. Breun, S. N. Golovato, and R. Goulding, Phys. Rev. Lett. **51**, 1955 (1983).
[2] Y. Yasaka and R. Itatani, Nucl. Fusion **24**, 445 (1984); **25**, 29 (1985).

[3] S. Golovato, K. Brau, J. Casey, J. Coleman et al., *Proceedings of the Seventh Topical Conference on Radio Frequency Power in Plasmas,* AIP Conf. Proc. 159, Kissimmee, FL, 1987 (American Institute of Physics, Woodbury, NY, 1988), p. 254.

[4] D. A. D'Ippolito and J. R. Myra, Phys. Fluids **29**, 2594 (1986).

[5] J. R. Myra, D. A. D'Ippolito and G. L. Francis, Phys. Fluids **30**, 148 (1987).

[6] D. A. D'Ippolito, J. R. Myra, S. C. Jardin, M. S. Chance, and E. J. Valeo, Phys. Plasmas **2**, 3429 (1995).

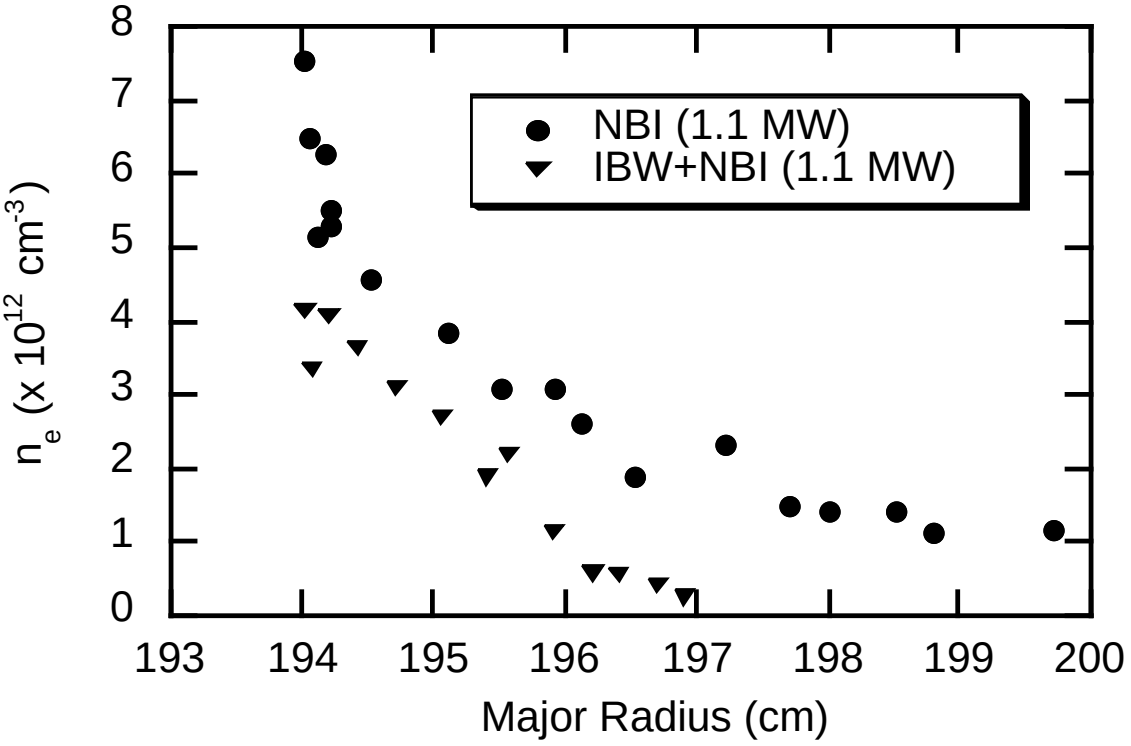

Figure 1. Edge density modification during IBW has been observed in PBX-M. Data from the UCLA fast probe.

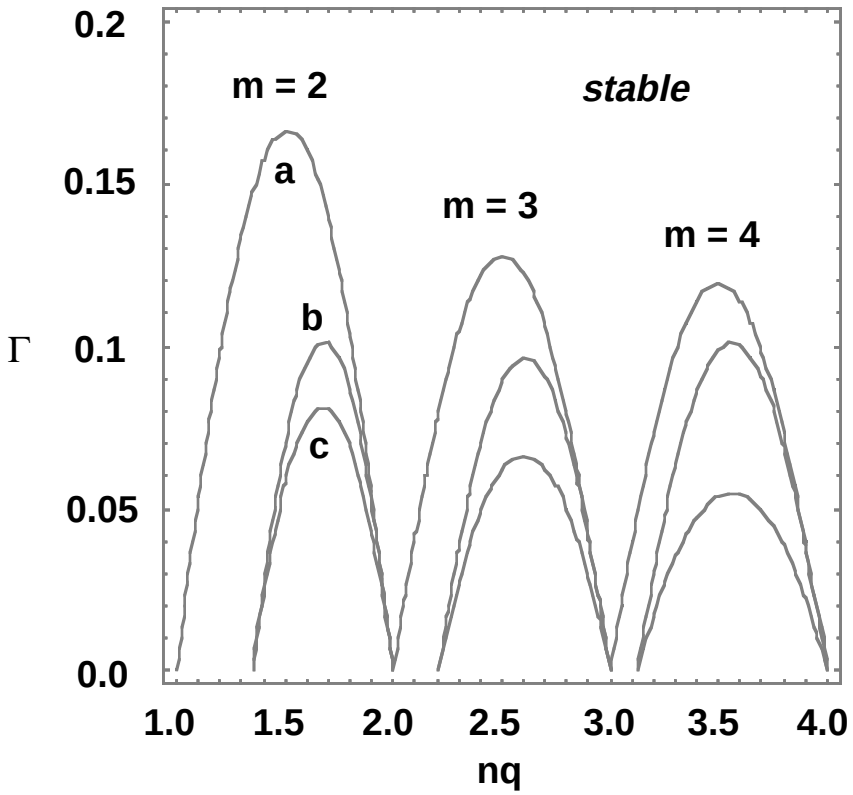

Fig. 2 Plots of the marginal stability figure of merit G versus nq for the local response feedback system and the parameters: (a) $N_{A\theta} = 2$, $\theta_W = 0.25$ and $w \rightarrow \infty$; (b) $N_{Aq} = 2$, $q_W = 0.25$ and $w = 1.3$; (c) $N_{A\theta} \rightarrow \infty$, $q_W \rightarrow 0$, and $w = 1.3$. Here $N_{A\theta}$ is the number of equally-spaced antennas in the poloidal direction, q_W is the angular half-width of each antenna in radians, and w is the wall position/plasma radius. The plasma is stable to the indicated mode above each curve.

4.4.2 IBW Antennae and Advanced ORNL Folded Waveguide (FWG)*

The FSX, directly launched, 2 MW IBW system operates in the frequency range from 40 to 80 Mhz using two antennae. The transmission lines to the antennae systems are improved to facilitate high power operation. A port is available for the installation of a duct and gate valve for an advanced ORNL Folded Waveguide (FWG) [1,2]. The FWG is a low electric field, all metal coupler that will permit the application of higher IBW powers (ITER application). Varying the shorting plate of the FWG changes the k-parallel vector applied to the plasma. A 90^0 rotation of the FWG from its IBW orientation relative to the vertical permits Fast Wave heating . The duct and gate valve interface will permit convenient and rapid configuration changes without venting the vessel. Fig. 1 is an elevation view of the ORNL FWG installed on FSX. Fig. 2 shows a schematic of the transmission line antenna and FWG connections. The RF switch shown in Fig. 2 will allow convenient conversions from IBW operation using either the two antennas, the FWG, or a combination of one antenna and the FWG for comparing respective characteristics during similar plasma conditions.

* T. S. Bigelow[1], S. Milora[1], *et al.*,
[1] Oak Ridge National Laboratory, Oak Rige TN.

References

[1] T. S. Bigelow, *et al.*, Proceedings of 11th Topical Conference on Radio Frequency Power in Plasmas, Palm Springs, CA, May 1995.
[2] C. H. Fogelman, *et al.*, in Proceedings of 16th IEEEE/NPSS Symposium on Fusion Engineering, Champaign, Illinois, Sept. 30- Oct. 5, 1995, V2, 964-967.

FIG. 1. ORNL FWG in Section 4 See Figure Folder

FIG. 2. FSX IBW System in Section 4 See Figure Folder

4.5 Neutral Beam Modulation*+

1. Feedback Stabilization of Disruptive Instabilities Using Modulated Neutral Beam Injection*

In the overview of MHD stability issues given above (5.1), it is noted that a substantial body of experimental and theoretical work has implicated the non-linear evolution of low *m,n* tearing modes and/or external kink modes as significant contributors to disruptive instabilities in tokamaks. In particular, in many scenarios, a *m=2, n=1* MHD mode (resistive or ideal) in the core plasma, often accompanied by higher *m,n* modes like *m=3, n=2* is the dominant instigator of a major disruption. These core instabilities can exhibit rapidly changing mode structures and frequencies/growth rates that can vary over a wide dynamic range. This dynamic behavior could reduce the effectiveness of stabilization techniques based solely on fixed suppressor geometries outside the plasma boundary which are optimized for a particular mode regime. In addition, as a reactor size increases, it may be difficult to achieve sufficient coupling to core modes using stabilization techniques based on driving near-surface currents. In an initiative to avoid these difficulties, a novel scheme is proposed by A. K. Sen of Columbia University for the control of major disruptions in tokamaks using a modulated neutral beam suppressor.[1] This suppressor will be in a feedback loop to supply radial momentum input to the plasma with appropriate amplitude and phase to suppress MHD modes.[1] Simple theoretical models predict modest levels of radially injected neutral beam energy, current, and power for tokamaks and other toroidal devices, and extrapolation to reactor scales appears to be practical.[1]

An injected neutral beam imparts density, current, and momentum to the target plasma. Since the dominant dynamics of these instabilities is believed to be radial kinking under **J** x **B** forces, it is proposed to investigate the extent to which radial neutral beam injection can impart sufficient localized radial momentum to promote mode stabilization.[1] A schematic feedback system is shown in Fig.1, where the feedback loop consists of candidate sensors, such as Mirnov loops and soft X-ray diodes, fast digital control computers and a modulated neutral beam to impart localized radial momentum to a target mode. Let us, for example, consider a heuristic model of the linearized ideal MHD equations for a low (*m,n*) ideal kink (current driven) and kink-ballooning (pressure driven) mode with the inclusion of a radial momentum term M_r from a modulated neutral beam:

$$\rho \frac{\partial^2 \xi}{\partial t^2} = \mathbf{F}(\xi) + \mathbf{e}_r M_r \qquad (1)$$

where $M_r = m_i (\sigma_e + \sigma_i + \sigma_x) N_o V_b^2 n_b$, and ξ, ρ, m_i, σ_e, σ_i, σ_x, N_o, V_b^2, n_b are the perturbed plasma displacement, mass density, ion mass, electron and ion impact ionization and charge exchange cross sections, equilibrium plasma density, beam velocity and feedback modulated beam density, respectively. $\mathbf{F}(\xi)$ is the usual MHD force operator which contains both current and pressure drives. The simple feedback law:

$$\frac{n_b}{N_0} = G\left(\frac{\xi_r}{a_o}\right) \qquad (2)$$

gives the feedback stabilization criterion in terms a constant feedback gain G when phase compensation is performed for the positional phase difference between the mode detector and the suppressor beam. A detailed calculation [1] for low *m,n* kink modes gives:

$$G = -|G| = \frac{-\gamma_o^2 \, a_o}{(\sigma_e + \sigma_i + \sigma_x) N_o V_b^2} \qquad (3)$$

Here we will consider γ_o to be the experimentally observed growth rate γ_o ~10^3 to 10^4 sec^{-1}, which may represent external kink/ballooning modes modulated by diamagnetic and wall effects (i.e., wall modes). Using Eq. (2), we find

$$\left|\frac{n_b}{N_o}\right| = G_{actual}\left(\frac{\xi_r}{a_o}\right) \sim \frac{G}{C_o}\left(\frac{\xi_r}{a_o}\right) \qquad (4)$$

where C_o is the geometrical coupling coefficient between the localized suppressor beam and the mode of interest. If B_{po} and B_p are the equilibrium and fluctuation poloidal fields, the modulated beam density imparted by the suppressor beam is approximately:

$$\left|\frac{n_b}{N_o}\right| \sim \frac{G}{C_o}\left(\frac{B_p}{B_{po}}\right) \qquad (5)$$

For good coupling to the relevant MHD modes, we must choose the beam energy for radial injection such that the penetration depth is roughly between the q =1 and q =2 surfaces. In the case of FSX , for ~ 20 keV H^o injection (derated to 50 keV),

$|G| \sim 8.4 \times 10^{-6}$, and $C_o \sim 4 \times 10^{-4}$ (in this example, using only the center of the power density profile), gives $|n_b| \sim 2 \times 10^{9}$, for a minimum detectable level of $B_p/B_{po} \sim 10^{-3}$. Hence, the required injected beam current at the mode is $I_b \sim 16.8$ A at the injected power of $P_b \sim 336$ kW. This required power is only about 50% of the power available from one FSX, 50 keV H^o neutral beam injection system derated to 20 keV. For 40 keV D^0 injection, the corresponding numbers are $|G| \sim 3 \times 10^{-6}$, $C_o \sim 4 \times 10^{-4}$, $|n_b| \sim 3.75 \times 10^{9}$, $I_b \sim 8.4$ A, and $P_b \sim 336$ kW. This represents about 30% of the power available from one 50 keV (deraded to 40 keV) D^0 neutral beam injection system. Improved beam coupling to the mode and improved B_p/B_{po} detectability level further reduces the estimated power required for early mode suppression. The required neutral beam modulation frequencies are expected to be in the range of experimentally observed real frequencies of 0.5 to 20 kHz. FSX neutral beam power modulation in the range of 5-10 kHz is technically feasible.

4.5.2. Available Neutral Beam Hardware

The four PBX-M Neutral Beam Injection systems can provide 7 MW, of 50 keV, D^o injection, or 5.3 MW, 50 keV, H^o injection. The energy of the beams can be derated to optimize deposition at the radial location of the target modes. The focused, circular grid, ORNL-style ion sources provide a broad perveance characteristic (conducive to beam modulation) with a focal length of 440 cm. Pulse lengths of 300 msec up to full power are routine; 500 msec pulse lengths have been demonstrated at powers up to 4 MW D^o, and higher powers can be expected to be achieved. Injection pulse lengths longer than 500 msec would require significant beamline upgrades proposed by ORNL. Two beamlines are oriented for perpendicular injection, and are more than adequate for the experiment proposed above. Two other beamlines are oriented for tangential injection. This configuration allows perpendicular and tangential injection experiments under the same plasma conditions. The tangential beamlines can be reoriented to more radial injection at a cost of about $125K and 5 weeks time per beamline.

These neutral beam injection systems are fully automated via a dedicated MicroVax neutral beam computer system. This computer control, in addition to programmed injection, includes filament, arc, and high voltage conditioning. Although these conditioning and injection operations have been performed in a steady state manner, the available hardware options will permit power modulation in the range of 5-10

kHz at relatively little additional cost. The options for beam power modulation are modulating either the acceleration grid high voltage, the arc power, or the decel grid high voltage. C.C. Tsai of ORNL has suggested, based on unpublished data, that modulating the decel grid voltage may allow injected power modulations up to 70-100% at possibly higher rates.[2] It is proposed that PPPL and ORNL perform collaborative measurements to compare the respective merits of the three techniques. This can be done readily using the existing neutral beam computer system for control and diagnostics.

* A. K. Sen, Columbia Uniersity, New York, NY 10027
+ C.C. Tsai[1], S. Milora[1], H. W. Kugel[2]
[1]Oak Ridge National Laboratory, Oak Ridge, TN
[2] Princeton Plasma Physics Laboratory, Princeton, NJ.

References

1. A. K. Sen, "Feedback Control of major Disruptions in Tokamaks", Phys. Rev. Lett. **76** (8), 1252 (1996).
2. C. C. Tsai, IEEE Conference on Plasma Science, Troy, NY, 1977, Paper 4B2 (unpublished), and Private Communication, Oak Ridge National Laboratory, November, 1996.

FIG.1 in Section 4 Final Figure Folder

4.6. MHD Control Techniques with Edge Currents: Halo Currents

Overview

Active control of plasma boundries using edge currents has been demonstrated in numerous experiments to produce edge conditions favorable to MHD stability, non-inductive current drive, fueling control, impurity and helium exhaust from the core plasma, reduced divertor heat loading, and access to enhanced performance regimes [1]. There has been, however, no routine operational use of feedback stabilization to achieve and maintain favorable edge conditions for high performance plasmas. This is due in part to the complexity of controling simultaneously edge density, edge profiles of density and pressure, edge radial transport, edge potential and radial electric field, and scrape-off layer particle and heat flow, independent of intrinsic core plasma parameters.

The stabilization of the plasma edge boundary is a neglected and next-step need that can be addressed immediately by making use of the unique site-credits and hardware capabilities available to FSX. In this Section and following four Sections, we propose FSX research to explore and evaluate five innovative methods for edge control and feedback stabilization. All of these proposed investigations can make immediate use of the available FSX electrically isolated and biasable passive shell and floating divertors as electrodes for applying edge biasing under feedback control in concert with the core stabilization techniques discussed above.

References

[1] Refer to papers in the "Proceedings of the IAEA Technical Committee Meeting on Tokamak Biasing", Montreal, Canada, 8-10 September, 1992 (IAEA, Vienna, Austria, 1993), and references therein.

4.6.1 Halo Current Control*

Tokamak reactor designs that utilize elongated plasma cross-section shapes require high-power feedback systems to keep the plasma column positionally stable [1]. The conventional design for these feedback systems uses either a dedicated pair of axisymmetric poloidal field coils with up/down asymmetric currents or some combination of the equilibrium shaping coils. The feedback electrical currents in these coils are driven by applying a voltage proportional to a linear combination of the plasma vertical displacement and itís time derivative. These poloidal field coils must be located behind the first wall and blanket assemblies in order to avoid excessive neutron capture and heating. The large power required for this system and the associated inductive heating of the cryogenic magnet assemblies cause design problems which set an upper-limit on the practical plasma elongation attainable.

In this Section, we propose an alternate method [2] for stabilizing the vertical instability utilizing biased electrodes in the vacuum vessel. The electrodes drive a force-free current in the plasma halo, and this current creates a field which acts to stabilize the plasma, resulting in a system with minimal coupling to the cold-structure, and hence reduced recirculating power requirements.

In recent work [2], we have investigated the principle of halo-current feedback by way of a two-dimensional MHD simulation. A tokamak plasma of essentially the ITER [3] shape was used but with a simplified vacuum vessel geometrical shape in an effort to be more generic. The actual results should be relatively insensitive to the shape of the plasma or the vacuum vessel. Fig. 1 shows the idealized configuration. The upper right corner of the vessel has a voltage difference proportional to the plasma vertical displacement. The volume inside the vessel is divided into 3 regions according poloidal magnetic flux. A high temperature plasma region existing for all magnetic flux values Y interior to the limiting flux surface Ψ_{lim}, *i.e.* for $\Psi_{lim} > \Psi > \Psi_0$, where Ψ_0 is the value of Ψ at the magnetic axis. The region outside the last closed flux surface is divided into two regions, the halo region with temperature T_H occupying the flux region with $\Psi_H > \Psi > \Psi_{lim}$, and the vacuum region with $\Psi > \Psi_H$. The halo region width (W_H) is defined as $W_H = (\Psi_H - \Psi_{lim})/(\Psi_{lim} - \Psi_0)$. Fig. 2 shows the stabilized poloidal current streamlines at a fixed time for two different halo feedback calculations with halo width $W_H = 0.4$ (Fig. 2a) and $W_H = 0.01$ (Fig. 2b). The other parameters for these runs were $T_H = 20$

eV, a = 266 cm, E_{MAX} = 40 V/m and T_V = 0.1 eV. Streamlines deep inside the plasma region are not shown.

These results indicate that within the confines of our computational model, it is possible to control the axisymmetric instability in non-circular tokamak plasmas by applying a voltage difference, proportional to the plasma vertical displacement, between poloidally separated electrodes in the vacuum vessel. This voltage drives a poloidal current through the vacuum vessel and the plasma halo.

As the current carrying electrons leave the vessel at the electrodes and enter the plasma, they pick up a toroidal component to align with the primarily toroidal magnetic field in the plasma. The toroidal component of the driven plasma halo current provides a radial magnetic field at the plasma such as to restore the plasma vertical position.

We can use this simple picture to estimate how much current in the halo would be needed to restore a typical displacement of the plasma. The radial component of the external magnetic field near the plasma magnetic axis is of order

$$B_R \approx \frac{\mu_0 I_P}{2\pi R}\left(\frac{Z}{R}\right)|n| \qquad (1)$$

where I_P is the plasma current, R is the major radius, Z is the vertical displacement and n is the external magnetic field index,

$$n \equiv -\frac{R}{B_z}\frac{\partial B_z}{\partial R}$$

The radial magnetic field at the magnetic axis produced by a halo current at the plasma edge is approximately

$$B_H \approx \frac{\mu_0 I_H^T}{2\pi a}$$

ωηερε a is the minor cross section dimension scale and I_H^T is the toroidal component of the halo current. For stabilization, we require $B_R \sim B_H$ or

$$\frac{I_H^T}{I_p} \approx |n| \left(\frac{a}{R}\right)^2 \left(\frac{Z}{a}\right) \qquad (2)$$

The ratio of the toroidal to the poloidal halo current is approximately given by

$$\frac{I_H^T}{I_H^P} \approx \Delta\theta \left(\frac{a}{R}\right)^2 \left(\frac{RB_T}{\mu_0 I_P}\right) \qquad (3)$$

where $\Delta\theta$ is the poloidal angular extent (in radians) of the halo current in the plasma. Solving Eqns. (2) and (3) for the poloidal halo current gives

$$I_H^P = I_p \left(\frac{\mu_0 I_P}{RB_T}\right)\left(\frac{Z}{a}\right)\left(\frac{|n|}{\Delta\theta}\right) \qquad (4)$$

For the geometry studied here, we have $\left(\frac{\mu_0 I_P}{RB_T}\right) = 0.57$, $\left(\frac{Z}{a}\right) = 0.03$, $\Delta\theta = \pi / 2$, $|n| = 3$. Insertion of these values into Eq. (4) gives $I_H^P = 0.03\ I_p$, in good agreement with the maximum currents calculated in the MHD simulation.

4.6.2 Hardware Implementation

This proposed control of halo current for vertical stabilization can make immediate use of the available FSX electrically isolated and biasable outer passive plates as electrodes for applying edge biasing as shown in Fig.1, and available bias power supplies. This can be done under feedback control in concert with the core stabilization techniques discussed above.

***** J. A. Schmidt and S. C. Jardin, Princeton Plasma Physics Laboratory, Princeton University, Princeton, NJ, 08543.

References:

[1] F.Najmabadi, R. Conn, et al., "The ARIES-I Tokamak Reactor Study", UCLA-1323 (1991).

[2] Schmidt, J.A., and Jardin, S.C., Bull. Am. Phys. Soc, **41**, 1435 (1996).

[3] Rutherford, P.H., Journal of Fusion Energy, **13**, 83 (1994).

[4] Jardin, S.C., DeLucia, J., and Pomphrey, N.,J. Comput. Phys **66**, 481(1986).
[5] Sayer, R.O, Peng, Y.M., Jardin, S.C., *et. al*., Nucl. Fusion **33**, 969 (1993).
[6] Jardin, S.C., Pomphrey, N., and Bell, M, Nucl. Fusion **33**, 371 (1993) .
[7] Jardin, S.C., Larrabee, D.A., Nucl. Fusion **22**, 1095 (1982).

FIG.1 in Section 4 See Figure Folder

FIG.2a in Section 4 See Figure Folder

FIG.2b in Section 4 See Figure Folder

4.7 Edge Plasma Feedback Control by Electrostatic Biasing*+

4.7.1 Introduction

We propose to use the segmented passive stabilizer shell in FSX for feedback control of ballooning and kink modes by poloidal edge current drive. The poloidal segmentation of the stabilizer plates allows coupling to m=1 and/or m=2 modes. Poloidal current in the scrape-off layer can be driven between the inner and outer divertor strike point in a single-null divertor configuration (m=1). In a double-null divertor configuration, current can be driven between the lower and upper outboard strike points as well as between the lower and upper inboard strike points. Depending on the polarity of these currents, either m=1 or m=2 configurations can be realized. A feedback signal derived from magnetic probes can be used to control the potential on the stabilizer plates and the resulting poloidal scrape-off layer current, thus counteracting the intrinsic current perturbation associated with MHD modes. The existing UCSD bias power supply (2.5 MW) is suitable to drive edge currents of up to 5 kA.

We have previously shown that the plasma potential in the plasma edge and scrape-off layer can be controlled with very moderate applied voltages (≥ 25V) and very low (≤ 25 A) currents. We have demonstrated that symmetric biasing (inboard versus outboard strike points in a double null configuration) allows control of the edge plasma pressure profile, the radial particle transport in the scrape-off layer, and the poloidal rotation profile. An intriguing result has also been that the neutral beam power required to induce an H-mode could be lowered by 25% during biasing. Fig. 1 shows the modification of the plasma potential (a), the edge plasma density (b), and the fluctuation-driven radial particle flux (c) with positive bias applied to the outboard divertor strike points. Indirect evidence for changes in the poloidal E_rxB plasma flow were obtained from the dispersion of plasma fluctuations as well as from divertor H_α signals indicating plasma accumulation in either the upper or lower divertor, depending on the bias polarity and the direction of poloidal flow.

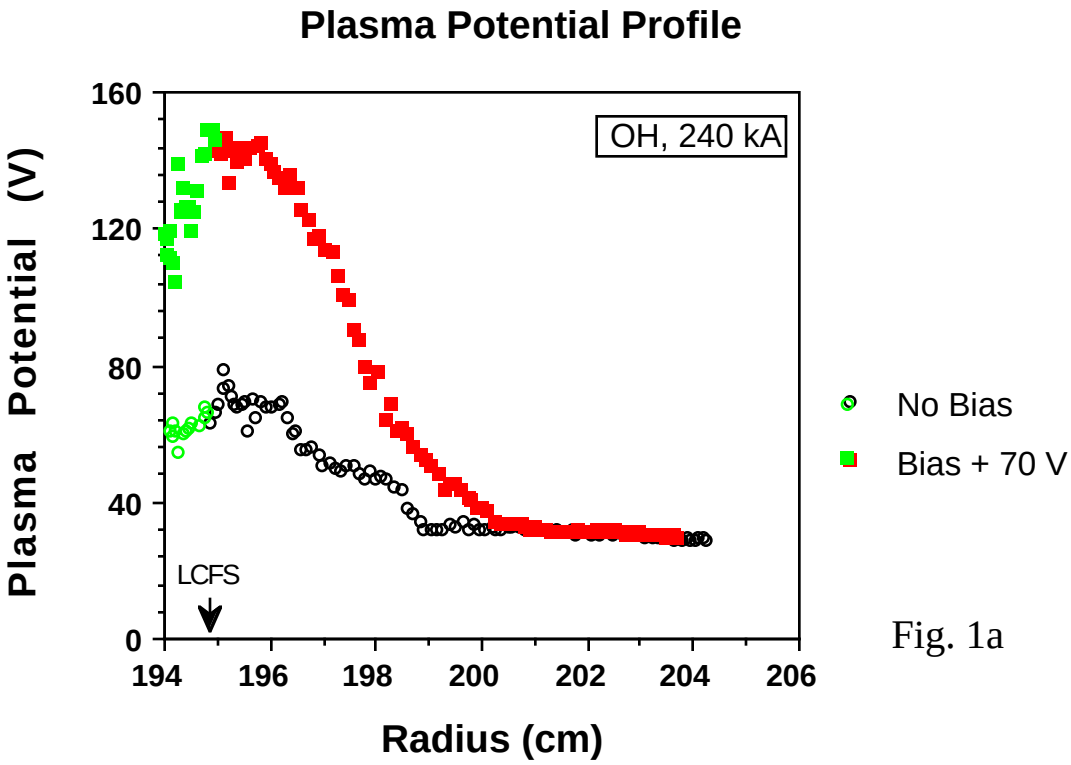
Plasma Potential Profile
OH, 240 kA
Plasma Potential (V)
160
120
80
40
0
LCFS
194
196
198
200
202
204
206
Radius (cm)
No Bias
Bias + 70 V

Fig. 1a

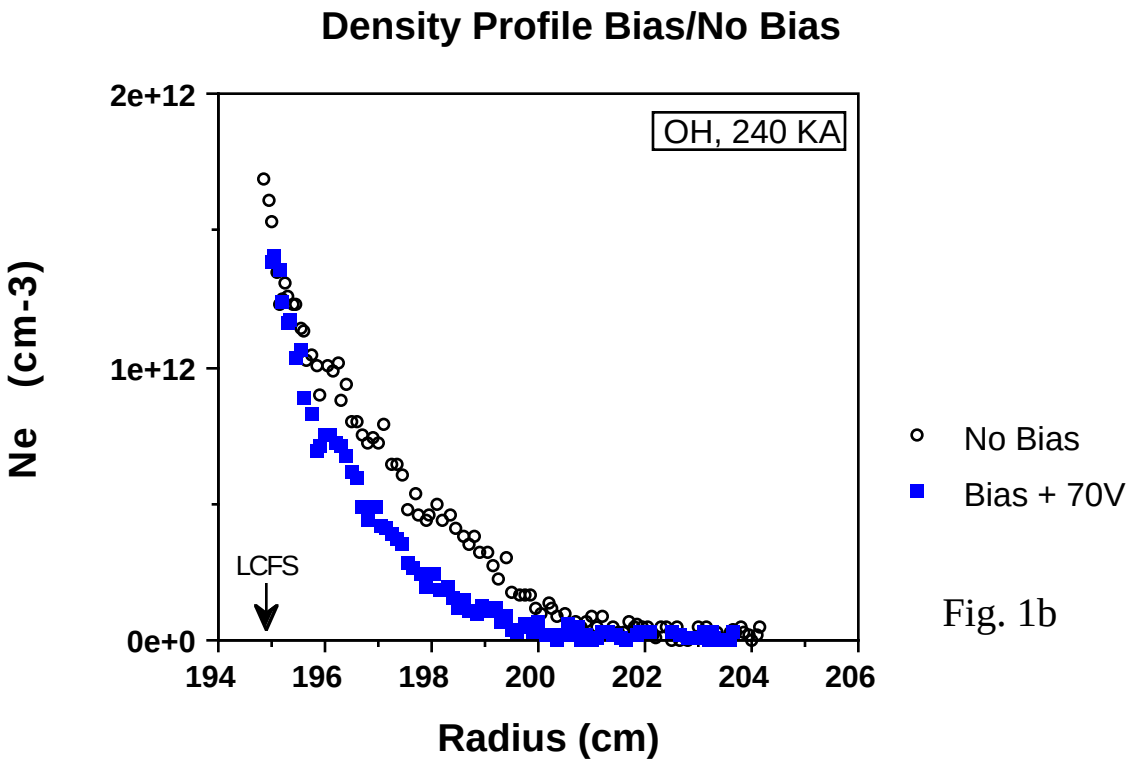
Density Profile Bias/No Bias
OH, 240 KA
Ne (cm-3)
2e+12
1e+12
0e+0
LCFS
194
196
198
200
202
204
206
Radius (cm)
No Bias
Bias + 70V

Fig. 1b

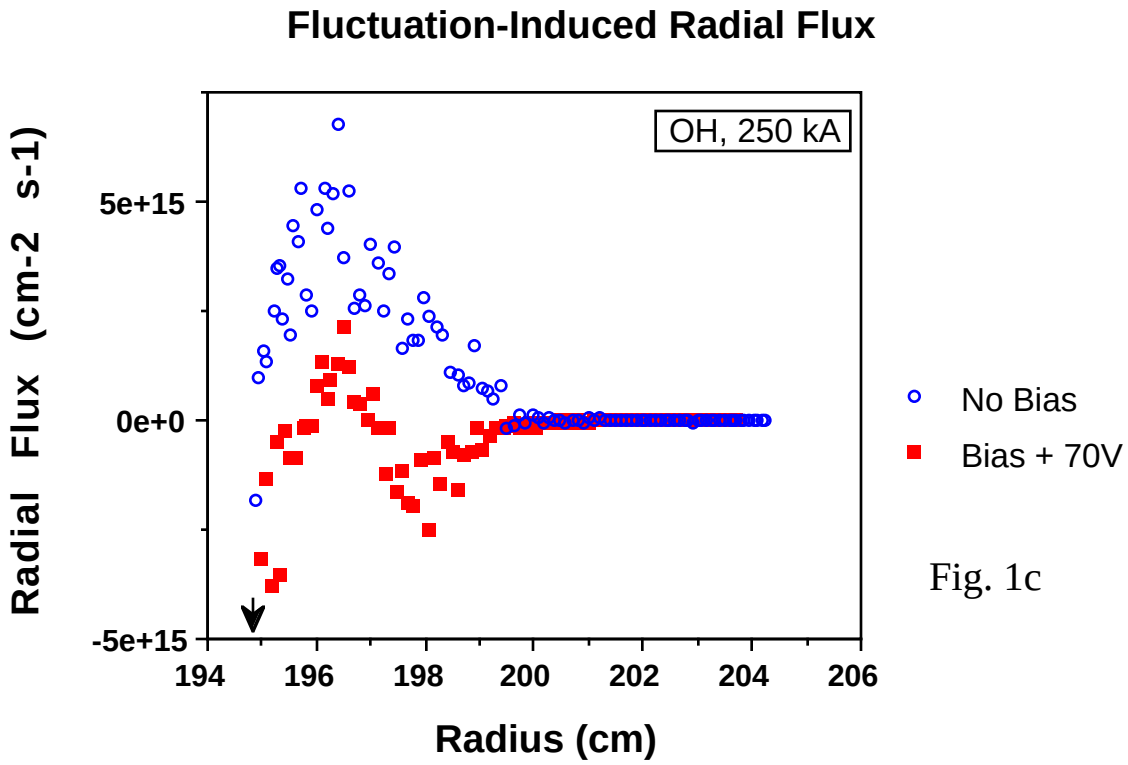

Fig. 1c

The bias configuration described above thus allows modulation of the scrape-off layer thickness, radial edge transport, and the poloidal ExB flow direction and speed. Feedback control of these parameters may enable us to significantly improve core plasma performance. We give two examples. Dissipative divertor operation in future tokamaks requires establishing a stable radiative layer either in the divertor or at the core plasma boundary. Typically, neither the total radiated power nor the location of the radiative layer can be well controllel. Edge impurity control is essential for regimes with strong rf auxiliary heating and enhanced core confinement (VH-mode, ERS-mode, CH-mode).

We propose to control the scrape-off layer thickness (and thus, SOL impurity screening) and/or the poloidal impurity flow speed in the edge plasma by passive stabilizer plate biasing. Impurity line intensities may be used as feedback signals. Feedback control of the radiative power loss (and the location of the radiation layer) may be achieved via modulating the bias voltage (and the impurity flow).

As a second example, we consider the role of the edge plasma for rf coupling. Modulated passive plate biasing may allow us to optimize the edge plasma density

and density gradient for optimum rf coupling while the core plasma parameters evolve in time.

4.7.2 Fast Reciprocating Edge Probe Diagnostics

The existing UCSD fast reciprocating probe will be used to characterize edge plasma response to biasing and edge current drive. The probe allows simultaneous measurements of plasma density, electron temperature, and floating potential during each insertion (round-trip insertion time ≥ 100 ms). In addition, the density and potential fluctuation levels as well as the relative phase between density and potential fluctuations are measured and used to calculate the radial particle flux.

This probe has been extensively and reliably used in PBX-M to characterize the plasma boundary and to observe edge plasma modifications in enhanced confinement regimes (such as the H-mode), in particular during rf heating. Edge pressure profile modifications due to RF ponderomotive force have been observed with IBW heating. During feedback stabilization experiments, the probe will be crucial to assess the local modulation of edge plasma parameters and transport. Alternatively, probe signals (with the probe held stationary) may be used as input signals for feedback control. In addition to the parameters listed above, the plasma flow velocity will be measured directly by a specialized (Mach) probe tip attached to the existing UCSD fast reciprocating probe drive.

L. Schmitz*[+], J. Boedo[+], S. Luckhardt[+]
* Institute of Plasma and Fusion Research, University of California, Los Angeles, CA,
[+] Fusion Energy Research Program, University of California, San Diego, CA.

4.8 Current Injection*

4.8.1 Description of Principle

A negative current in the scrape-off region beyond the separatrix of a diverted tokamak can improve MHD stability for kink and pressure driven modes. Additionally, if the current generates turbulence in the scrape-off layer, it may serve to radially spread the scrape-off layer heat flux and thereby reduce the peak heat flux onto the divertor target plates. By injecting thermionic current, for example, or current from other electron sources, a current of up to 25% of the plasma current can be driven in the scrape-off region.[1] If the thermionic current, for example, is emitted at only one end of the open field lines, a current will flow in the absence of a potential bias. The heat to maintain the electron emission that drives the scrape-off current could be supplied by the plasma outflow and no additional power is needed.[1] The ability to apply edge biasing in the active feedback loops described above will give additional control capability.

4.8.2 Hardware Implementation

Sections 3 and 6 describe the FSX biasable passive plate and divertor systems. We propose to use the relatively accessible and spacious FSX divertor region for the installation of suitable thermionic emitters, and possibly other sources [2], to investigate embodiments of these concepts for the feedback stabilization of kink and pressure driven modes.

*S. C. Luckhardt[1], J. Boedo[1], L. Schmitz[1,2], J. Kesner[3], J.J. Ramos[3], H. Kugel[4]

[1] Fusion Research Program, University of California, San Diego, CA.

[2] Institute of Plasma and Fusion Research, University of California, Los Angeles, CA.

[3]Massachusetts Institute of Technology, Cambridge, MA.

[4] Princeton University, Plasma Physics Laboratory, Princeton, NJ.

References

[1] J. Kesner, J.J. Ramos, S.C. Luckhardt, "Scrape-off layer Current in Diverted Tokamaks", Nucl. Fus. **34**, (6),795 (1994).

[2] D. J. Hartog, *et al*., "Gun Spectroscopy: Impurities, Temperature, and Density in a Miniature Plasma and Current Source", Bull. Am. Phys. Soc., **41** (7), 1538 (1996).

4.9 Toroidally Segmented Divertor Biasing and Current Injection*

4.9.1 Introduction

Numerous experiments have addressed the role of scrape-off layer (SOL) currents in magneto-hydrodynamic stability [1]. In this Section, we propose the use of non-axisymmetric, time-varying SOL currents to suppress the growth of resistive-wall modes and possibly resistive tearing instabilities, through the generation of time and space varying magnetic pressure. Time-modulated non-axisymmetric currents are driven in the scrape-off layer (SOL), with the purpose of generating a modulated poloidal field, capable of providing sufficient magnetic pressure for feedback stablization of slowly growing MHD modes. Estimates of required currents and voltages are provided for the proposed Feedback Stabilization Experiment (FSX) and for the International Thermonuclear Experimental Reactor (ITER). The requirements are found to be reasonable, justifying an early test of this concept.

4.9.2 Modes to be stabilized

This approach is to use non-axisymmetric currents in the SOL to inject helical flux into what would otherwise be considered, from an MHD point of view, the "vacuum region" surrounding the plasma. This helical flux would be phased in such a manner as to provide a restoring force on a growing instability. For the force to be maximum, it is advantageous if the injected helical flux is contained between the plasma edge and a conducting wall or vacuum vessel. Thus it is necessary that the mode to be stabilized rotate fast compared with the resistive penetration time of a relatively nearby conducting wall. This is generally the case even for unstable resistive wall modes, in a plasma rotating at a speed too far below the Alfvén velocity for stabilization by ion-acoustic effects. For the case of unstable resistive tearing modes, even modest plasma rotation makes wall penetration times and resistive island growth times long compared with rotation speeds. The technique discussed here could, in principle, be applied to tokamaks, spheromaks, RFP's, or even FRC's.

4.9.3 Configuration

The proposed configuration is a toroidally segmented divertor electrode on the outer side of a single-null plasma, or on the outer top or bottom of a double-null plasma (see Fig. 1). The divertor segments (4 segments to provide control for an n=1 instability at any phase, 8 segments for an n=2, etc.) must be independently

biasable. In the single-null configuration an unsegmented inner divertor could be solidly grounded, while in the double-null case the opposite outer divertor as well as the inner divertors would be unsegmented and grounded to the vacuum vessel. (This electrical configuration could be achieved in the absence of divertors through use of appropriately located toroidal belt limiters.) By using the divertor segments as electrodes, one can inject helical flux into the crucial region between the outer edge of the plasma and the surrounding conducting wall. Resistive links or other special techniques might be required to control breakdown between adjacent electrodes, and to provide well-defined paths for halo-currents during plasma disruptions. It is possible that the best location for the electrodes would be in a region somewhat removed from the highest heat flux on the divertor plate, in order to separate the functions of flux injection and power and particle removal.

It is interesting to note that the helical flux injection pattern which comes naturally with this technique is almost ideally shaped for control of external kinks, in that the helicity of the injected flux will match nearly exactly the dominant eigenmode of the kink. For the case of the resistive tearing mode, the poloidal mode structure will not match the instability precisely, but it may be desirable in any case to tailor the structure of the feedback fields by the inclusion of higher n and/or m components to constrain the island motion and thus minimize the “phase-flip” instability.

4.9.4 Current Requirement

The requirement for feedback power depends in a complex way on sensing capabilities, the physics of the mode to be controlled, and the frequency response and phase stability of the feedback circuit. For present purposes we will characterize the required response capability in terms of dB_q/B_q. For practical estimates of required currents and voltages, we will assume $dB_q/B_q \sim 5\%$, consistent with other experimental and theoretical studies of plasma feedback [1]. Now we consider a single helical “stripe” of current, running from the biased divertor plate, along the field lines, to the grounded plate. This stripe has, by construction, radial width I_r, poloidal width I_q, and parallel length $I_{||}$. The radial width, I_r, we will consider to be a control variable, depending on the SOL width and the width of the electrodes employed, but much smaller than any of the other characteristic lengths of the system. For an instability of poloidal mode number m (~ nq) we can estimate $I_q \sim \pi a/(k/m)$, and $l_{||} \sim \pi R q$. This allows us to estimate dI, the current in this stripe required to achieve the desired dB_q/B_q.

For FSX, operating at 750 kA, this corresponds to a "stripe" current of about 7.5 kA. For ITER operating at 21 MA, this corresponds to about 200 kA per stripe.

It is interesting to ask the question as to whether this current density can be provided by simple biasing of the divertor electrodes, or if some more complex form of current injection is required. The ion saturation current will be $B_q \sim \mu_0 I_p$ / (2πa/k)

$$dB_q \sim \mu_0 dI / (2I_q) \quad (1)$$

giving

$$dI / I_p \sim dB_q / (\mathrm{m}B_q) \sim 1\% \quad (2)$$

In the of limit simple current injection at sheath voltages of over a few times the local electron temperature. We estimate that for a deuterium plasma

$$j_{sat} \sim 0.6\ \mathrm{n_e C_s} \sim 10^{-15} n_e / T_{\mathrm{ev}} \quad (3)$$

where we take $T = T_i \sim T_e$. injection. The current density in the injected "stripe" is estimated at

$$dI\ (I_r\ I_q) \sim I_p\ (dB_q/B_q) / (I_r\ a\ \pi / \mathrm{k}) \quad (4)$$

If for FSX we estimate I at 0.1 m, and take $a \sim 0.4$ m, k ~ 2 for FSX we find a requirement on the plasma properties at the electrode of

$$n_e / T_{ev} \sim 2 \times 10^{20} \quad (5)$$

which can be achieved, for example, with a density of 6×10^{19} at the divertor plate and a temperature of 10 eV. A similar estimate for ITER, using $I_r \sim 0.2$ m gives a requirement on $n_e / \mathrm{T_{ev}}$ of 5×10^{20}, which is in the range of what is expected.

There is not a great deal of extra "room" in these estimates, however, and it may be desirable for a near-term experiment to include methods to enhance the emissivity of the electrodes. One possibility might be the use of the small 1 kA current injectors recently developed for use in the MST reversed-field pinch [2,3]. 20 such injectors

distributed toroidally around the FSX experiment, just outside the highest heat-flux region on the divertor, would provide adequate current injection capability.

4.9.5. Voltage Requirements

First we estimate the resistive voltage drop along the field. The parallel Spitzer resistivity in the SOL can be estimated at:

$$h_{||} \sim 1.7\text{x}10^{-3} (T_{ev})^{-3/2} \qquad (6)$$

assuming $Z_{eff} \sim 2$, giving a voltage drop of

$$V \sim 1.7\text{x}10^{-3} (T_{ev})^{-3/2} (dB_q/B_q)\, I_p\, R\, \text{q} / (I_r\, a / \text{k}) \qquad (7)$$

If we assume the electron temperature in most of the SOL for FSX is about 30 eV, this gives a very reasonable of 45 V for the resistive drop in the FSX case, and depending on the SOL electron temperature, similar or even lower for ITER. The RMS resistive power dissipation in the SOL, counting 2 "stripes", would be ~350 kW for FSX, and ~10 MW for ITER. A similar power dissipation would be expected in the sheath, for the case of simple plate biasing.

Next we estimate the inductance of a current stripe, from an estimate of the stored poloidal field energy.

$$(1/2)\, \text{L}\, (dI)^2 \sim (I_I\, I_q\, I_{||})\, (dB_q)^2 / 2\, \mu_0 \qquad (8)$$

$$\text{L} \sim (I_r\, I_{||} / I_q)\, \mu_0 / 4 \sim (\mu_0\, \text{m}\, R\, \text{q}\, I_r / 4\, a / \text{k}) \qquad (9)$$

For FSX parameters this gives $\text{L} \sim 1.3 \times 10^{-6}$ H; in ITER the inductance could be perhaps twice higher. If we wanted to limit the reactive power to be no greater than 2x the resistive power, this would limit the frequency range to about 4 kHz in FSX, and about 50 Hz in ITER. These frequency ranges are appropriate for stabilization of resistive-wall modes and tearing modes in these devices.

4.9.6 Hardware Implementation

The toroidally segmented divertor configuration required for work proposed in this Section is similar to available hardware required for a previously proposed toridally segmented divertor biasing concept involving electrostatic stabilization of the edge

boundary [4]. The work proposed in this Section can be implemented in the near term by modifying available hardware to provide biasable toroidally segmented divertors. In addition, the current injection hardware discussed in Section 5.9.3 can be used to aid this work. Fig. 1 shows a schematic of the proposed geometry.

4.9.7 Conclusion

Modulated non-axisymmetric SOL currents could provide a reasonable "actuator" for feedback control of slowing-growing MHD modes in a near-term experiment such as the proposed FSX, and in the ITER device. These currents have the advantage of providing a nearly ideal field pattern for control of the external kink / resistive wall mode. The n-spectrum should be optimized to limit the phase-flip instability of the tearing mode. Current, voltage, and power requirements, as well as frequency range, are all reasonable both for FSX and ITER.

* R. J. Goldston, *et al*., Princeton Plasma Physics Laboratory, Princeton University, Princeton, NJ 08543.

References

[1] Refer for example to the "Proceedings of the IAEA Technical Committtee Meeting on Tokamak Biasing", Montreal, Canada, 8-10 September, 1992 (IAEA, Vienna, Austria, 1993), and references therein.

[2] D. Craig, *et al*., Bull. Am. Phys. Soc. **41**(7), 1407 (1996).

[3] G. Fiksel, *et al.*, Bull. Am. Phys. Soc. **41**(7), 1407 (1996).

[4] "Tokamak Plasma Stabilization and Disruption Avoidance Using Segmented Divertor Biasing", H. W. Kugel, M. C. Chance, J. Manickam, M. Okabayashi, L. Schmitz, and L. E. Zakharov, U.S. DOE Invention Disclosure, M576, July 2, 1993.

Fig. 1 in Section 4 See Figure Folder

4.10 Plasma Edge Ergodization Using Segmented Divertor Biasing*

4.10.1 Introduction

A major goal of tokamak fusion research is to reduce steady concentrated thermal loads, and bursting loads, on divertors, vessel walls, and other internal hardware.[1] In recent tokamak fusion reactor design studies, divertors, in particular, are expected to undergo severe or calamitous heat loading if the plasma strike points are incident on conventional hardware.[1] Radiative divertor concepts, in which the plasma strike points undergo a soft landing in a dense neutral pressure region, may require normal plasma operation and may not be effective during strong edge instabilities and plasma current disruptions. A promising method for reducing divertor heat loads is to produce a controlled turbulence at the plasma edge so as to distribute the outwardly transported plasma power over a large area.[2] This turbulence is produced by creating an ergodized edge region in which any point is magnetically directed to the vessel wall. Plasma diffusing radially outward encounters the ergodic region at the edge, and then flows along the ergodized flux lines to the wall rather than along flux lines connected to the divertors. In addition, counter flowing impurity influxes from the wall are impeded by the pressure gradient of the outward flowing plasma. Residual inward flowing impurities that reach the ergodized edge layer are swept toward the divertors by the edge parallel flow.

Experimental investigations on small tokamaks have applied magnetic perturbations via auxiliary coils to create edge ergodization.[3,4] This magnetic method may not be applicable to reactor size tokamaks due to difficulties involved with locating auxiliary coils close to the plasma edge. These design issues include thermal, electrical, and radiation shielding, adequate support structures, and operational limitations arising from the need to design for selected types of perturbation. In addition, the resulting operation of the ergodization coil system should not destabilize edge modes or increase their resistance to damping mechanisms.

A single, outer radius divertor target, segmented into 6 sections was proposed for DIII-D to drive spatially periodic helical currents in the plasma edge.[5] These currents would create overlapping magnetic islands and the resulting turbulence would yield an ergodic edge plasma. This type of configuration is designed for diverted plasmas with a single-null in which the outer strike point is incident on a

insulated segmented electrode and the inner strike point is incident on an inner continuous divertor structure at vessel potential. In this Section we propose to investigate helical current driven edge ergodization for both large single null and large double-null fusion devices using toroidally segmented divertors [6].

4.10.2 Edge Ergodization Using Segmented Divertor Biasing

Several embodiments of this proposed concept for ergodization are possible depending on the particular device design. As a specific heuristic example, consider a diverted, double-null plasma, for which the outer strike points receive about 4 times greater power density than the inner strike points.[1] Fig.1a shows, as an example, a torodially segmented biased divertor for twisting the magnetic field lines in the outer scrape-off layer so as to broaden the effective deposition area of the incident outer strike points, thereby lowering the incident power deposition on the divertor plates about an order of magnitude. Shown in Fig.1b is a partial schematic of one divertor segmented into a separate electrodes with bias of opposite polarity applied to each segment. The opposite divertor segments are connected together electrically so as to form one unsegmented electrode. The spatially alternate biasing of one divertor plate without segmentation of the opposite plate drives the currents along the field lines in the scrape-off layer (SOL). These currents cause an alternate twisting of the magnetic field lines in the flux tubes thrusting into the respective biased segments. As a result, the projection of the SOL on the divertor segments, deviates from an initially axisymmetric line and forms spikes, perpendicular to the initial strike line (Fig.1a). Taking into account the plasma motion in the plane of the scrape-off layer across the magnetic field, the energy deposition will be averaged over a larger area, the width of which is determined by the length of the spikes (l_n). This averaging makes l_n to be the characteristic width of the energy deposition onto the divertor plate, resulting in substantial reduction of peak power density if the spike lengths exceed the initial width of the SOL. The length l_n of the spikes on the divertor plate may be estimated by neglecting the curvature of the geometry of the SOL

$$l_n = \frac{0.8 I_s}{l_\phi B \sin \alpha} \quad \text{L}$$

Here, I_s is the current through each segment, B is the main magnetic field, α is the angle between the magnetic field line and the divertor plate in the plane of the

magnetic surface, and L is the length of the magnetic field line between the middle of the plasma and the strike line on the divertor plate.

In terms of total current $I_{tot} = \Sigma|I_S|$ through the divertor plate, l_n may be expressed as

$$l_n = \frac{0.8\, I_{tot}\, q_{SOL}}{B\, sin\, \alpha} \; L\,, \qquad q_{SOL} \equiv \frac{L}{2\pi R}$$

For ITER [1], B = 5 T, q_{SOL} @ 2, $sin\, \alpha$ @ 0.5 and I_{tot} = 0.2 MA corresponding to the available ion current from the plasma deposit, the resulting l_n is 13 cm, which is an order of magnitude larger than the initial value of ~ 1 cm.

Other bias configurations are possible for providing varying degrees of toroidal symmetry, helicity, and ergodization. Applied bias currents will tend to follow the near surface flux lines. Bias currents applied in the direction of the plasma current will provide stabilization, however, the simultaneous application of edge bias currents in the counter direction will cause coexisting and overlapping island regions of increased turbulence. Edge currents that flow between adjacent segments of opposite polarity in the same divertor will also contribute to this turbulence. This total increased stochasticity provides can effective ergodization of the edge plasma. The plasma edge pressure gradient will cause increased outward power flow through these ergodic regions and thereby reduce divertor heat loads. In addition, plasma particle flows to the wall are expected to inhibit counter-flowing impurity influxes from the wall. Residual impurities reaching the ergodized layer are expected to be swept to the divertor by the edge parallel flows. Varying the strength of the counter bias currents allows for an adjustments for the degrees of desired edge stabilization and of ergodization.

4.10.3 Hardware Implementation

The toroidally segmented divertor configuration required for work proposed in this Section is similar to available hardware required for the toroidally segmented divertor work proposed in Section 5.6.4. Toroidally segmented divertors with external buses can be connected in a number of different ways to provide different biasing configurations. The sensing diagnostics available on FSX can be used to detect changing edge conditions, and allow the configuration control circuit to select the most appropriate biasing symmetry for providing in real-time both edge

stabilization and ergodization. The work proposed in this Section can be implemented in the near term by modifying available hardware and using available biasing power supplies.

* L. E. Zahkarov, M. S. Chance, H. W. Kugel, J. Manickam, M. Okabayashi, Princeton Plasma Physics Laboratory, Princeton NJ 08543, and L. Schmitz, IPFR, University of California, Los Angeles, CA 90024

References

[1] K. Tomabechi, *et al*., "ITER Conceptual Design", Nuc. Fus. **31**, 1135 (1991).

[2] A. Samain, A. Grosman, and W. Feneberg, "Plasma Motion and Purification in an Ergodic Divertor", J. Nucl. Mater. 11&112, 408 (1982).

[3] S. Takamura, et al., "Electric and Magnetic Structure of an Edge Plasma in a Tokamak with a Helical Magnetic Limiter", Phys. Fluids **30**(1) 144 (1987).

[4] S. C. McCool, et al., "Electron Thermal Confinement Studies with Applied Resonant Fields on TEXT", Nucl. Fus., **29**(4) 547 (1989).

[5] M. A. Mahdavi, et al., "Applications of Divertor Biasing to the Next Generation Tokamaks", in Proceedings of the IAEA Technical Committee Meeting on Tokamak Plasma Biasing, p. 562, 8-10 September 1992, Montreal,(IAEA, Vienna,1993).

[6] H. W. Kugel, M. S. Chance, J. Manickam, M. Okabayashi, L. E. Zahkarov, Princeton Plasma Physics Laboratory, Princeton NJ 08543, and L. Schmitz, IPFR, University of California, Los Angeles, CA 90024, "Tokamak Plasma Edge Ergodization Using Segmented Divertor Biasing", U. S. DOE Invention Disclosure, M577, July 2, 1993.

Fig.1 in Section 4 (See Figure Folder)

Section 5: Control of Internal Modes (Tearing modes)

5.1 Mode identification for internal MHD

In conventional tokamaks, including ITER's standard operating mode, advanced tokamaks, spherical toruses, and reversed field pinches, the resistive and neoclassical tearing modes are important for stability and confinement. In addition, for these devices control of the disruption or internal reconnection is a critical issue. Also, benchmarking of computer codes for analysis, development of diagnostic sensors for feedback control, and demonstration of advanced feedback control is needed both for tokamaks and high-β alternates.

The FSX facility will use a combination of existing PBX-M capabilities and new hardware additions to implement feedback stabilization schemes. Up to 1.2 megawatts of radio frequency (RF) power can be supplied by a lower hybrid (LH) waveguide. By this technique, local currents can be driven to counteract instabilities in the regions where they develop.

Another technique for driving local currents is to use "mode-converted" waves. We propose to install a novel antenna, developed at General Atomics, called a "combline" because of its appearance. Unlike other schemes, this design is relatively insensitive to the distance from the plasma for good coupling. The combline antenna can thus be placed on the inboard wall of FSX, without using space on the outer wall that is needed for other purposes (Fig. 1 in Sec. 3.3).

5.2 Feedback-processing and generation

The m/n=2/1 island can in principle be asymptotically stabilized to "decay" to zero by superposing on it an externally generated magnetic field which has a similar spatial structure and which partly cancels that of the island. Actual feedback stabilization of the m/n=2/1 island using actively controlled external magnetic coils requires that the applied fields must be maintained spatially in phase with the island and must be reduced in magnitude as the island disappears.

Expected island motion is in the toroidal direction and approximately matching the plasma's rotation speed, which on the FSX q=2 flux surface is expected to reach a maximum of 20,000 complete revolutions per second during unbalanced neutral beam injection. The time interval needed to accelerate an initially

stationary plasma to this full rotation rate is roughly estimated to exceed 100 milliseconds, based on neutral beam deposited torque (5 newton-meters) and expected plasma density ($4.5 \times 10^{19}/m^3$). Within its own rotating frame of reference the island evolves slowly, with expected characteristic times in the "tens of milliseconds" range.

The control computer must perform both state estimation and control generation. The state estimation task is to continually estimate the island's changing size and location , based on various sensor measurements (including but not limited to magnetic measurements). The control generation task is to continually and appropriately command the external magnetic field coils ' electrical power supplies based on the estimated state.

The 2/1 island state estimation task using magnetic measurements is difficult for several reasons. The plasma is likely to have fluctuations with many different spatial m/n numbers, all of which may contribute magnetic "noise" to the magnetic measurement coils. (Of course, dynamic range considerations require that magnetic measurements must be combined in analog signal processing to generate signals proportional only to the n=1 field components; this will help somewhat.) The main poloidal field coils are driven by chopper power supplies which induce "noise" currents in various tokamak structures. And it's also necessary to estimate and subtract out from the sensor measurements those fields produced directly and indirectly by the controlled feedback currents driven in the feedback coils . These effects include the direct "vacuum" field of the external coils, the field produced by eddy currents induced in nearby metallic structures by the external coil currents, and the field produced by image currents induced on rational surfaces within the plasma by the external coil currents.

A "brute force" approach for the control computer would require that several times during each plasma rotation (e.g., 10 times or more) the control computer reexamine all sensor measurement input signals associated with the 2/1 tearing mode, calculate the new location and magnitude of the island, and issue new power supply commands. In addition to its conceptual simplicity, this approach might have the advantage of maximizing the structural flexibility of the control system for experimenting with novel feedback control algorithms.

Unfortunately, it would require completing each full control cycle (including all data acquisition, state estimation and control calculations, and data transmission) in only 5 microseconds or less, which may not be practical and would likely be expensive.

The less expensive alternative approach being considered for FSX tearing mode stabilization incorporates analog phase-lock loop signal processing to reduce control computer requirements to a more conventional computer control cycle time near one millisecond. (Indeed, it may be possible to implement the computer algorithms within the an existing control computer which is already on-site.) The computer continually outputs (once per millisecond) a digital "rate" command which causes the contents of an external digital register circuit , representing an angle "theta," to advance at that rate.

For input signals from magnetic sensors and any other analog sensor devices, this digital "theta" value is wired to address PROM lookup tables preprogrammed with the functions , sin(theta) and cos(theta), which are used to separately multiply each analog input signal via multiplying -digital-to-analog-convertor (MDAC) chips . The resulting "heterodyned" analog signals drive low-pass filters whose outputs are sampled by the computer once per millisecond. If the "rate" command output by the computer commands a frequency close (as determined by the bandwidth of the lowpass filters) to the actual rotation frequency of the 2/1 island, then the two signals examined by the computer for each source signal are directly proportional to the sine and cosine of the phase difference between "theta" and the actual island's phase location. The computer continually (once per millisecond) determines this phase difference from the two input signals and continually modifies its output "rate" command as necessary to drive the phase difference to zero, thus "locking on" to the island's phase.

For each toroidal array of external field coils, the computer continually outputs (once per millisecond) a phase angle command and a current magnitude command. External hardware forms the sum of the commanded phase angle and the rapidly changing "theta" angle, forms the sine and cosine of that rapidly changing angle via lookup tables in additional PROM chips, and multiplies their output by the commanded current magnitude via additonal MDAC chips. The

resulting rapidly varying analog signal is connected as the setpoint command for the external feedback field coil power supplies.

By removing from the control computer the necessity of performing extremely high speed but simple calculations, it will be possible to practically implement various more complicated algorithms to better estimate the state or generate better control commands. Instances of possible improvement include (1) LQG optimal control. or other optimal control, (2) implementing an extended Kalman Filter or other "observer" algorithm which incorporates a nonlinear dynamic model of how the island evolves (including possible "phase-flipping" if the relative phase to the external feedback field is nonzero), (3) deliberately misadjusting the control (e. g., turning it off periodically for a few milliseconds, or e.g., temporarily rotating the applied external field at a frequency different from the island rotation rate) in order to automatically measure and adapt to changes in couplings between the feedback coils and the sensors.

5.3 MHD control techniques with magnetic fields: Tearing mode coils

Feedback stabilization of internal MHD modes using active feedback and external coils has been attempted as early as 1975 on the ATC facility[1] and in 1978 on TO1[2]. In the ATC experiments some effect (≈20%) on the mode amplitude was observed. More recently very promising results were obtained with this technique on ohmically heated plasmas on DITE[3]. The (2,1) tearing mode precursor to density limit disruptions was controlled by the feedback system and the disruptive density limit was thereby increased by 10-20%. The DITE plasma was high density and ohmic so that neoclassical effects on the mode stability are assumed to be small. A similar feedback system was installed on JET[4]. It has been used to demonstrate open loop feedback effects on the m=2, n=1 tearing mode in ohmic plasmas and the complexity of assessment of the adaptive digital network on large tokamaks. A program similar to that on DITE is underway at Columbia on the HBT-EP facility[5].

The FSX experiment will extend the DITE results to higher temperature and pressure plasmas on a shaped tokamak. The neoclassical corrections to the tearing stability are estimated to be significant, thus FSX will offer the first opportunity to study feedback stabilization of neoclassical tearing modes with external coils.

The linear theory of tearing modes can be used to estimate the necessary current required to stabilize a (2,1) tearing mode[6-8]. An equation describing the growth of tearing modes can be written in a form describing the rate of change of the island width. In its' simplest form it depends only on the shape of the equilibrium current density through the parameter $\Delta'(w)$:

$$\tau_{res}/r_s \, \partial w/\partial t = r_s \Delta'(w)$$

The stability is also affected by mode coupling, inertial squeezing, neoclassical (bootstrap current) effects, by other non-inductive currents (e.g., ECCD or LHCD) and by boundary conditions at the plasma wall (e.g., conductors or active feedback coils). The last of these effects are incorporated in this equation through additional terms, resulting in the expression:

$$\tau_{res}/r_s \, \partial w/\partial t = r_s \Delta'(w) + r_s \Delta_{neo}' + r_s \Delta_{fb}'(w) + r_s \Delta_{cd}'(w)$$

The second term arises from the change in plasma bootstrap current as the island flattens the density and temperature gradients across the 'O' point. This happens to have the proper phase to destabilize the island. As the island needs some finite size to begin flattening the gradients, this term tends to not affect linear stability, but can make a linearly stable island nonlinearly unstable or an unstable island bigger. The strength of this term, Δ_{neo}', is proportional to the local bootstrap current, J_{bs} relative to the average plasma current density within the rational surface, $\langle J_o \rangle$ and the magnetic shear, s, at the rational surface:

$$r_s \Delta_{neo}' = 12.8 \, J_{bs}/(s \langle J_o \rangle) \, r_s \, w/(w^2 + w_d^2)$$

This term is typically the largest positive (destabilizing) term. Comparisons of experimental data with this theoretical expression suggest that there is some uncertainty in the factor of 12.8.

The third term describes the impact of active feedback using coils to change the boundary conditions. Alternatively, the feedback system can be viewed as driving image currents at the mode rational surface. Either way, for the specific case of

the m=2, n=1 tearing mode an approximate analytical expression can be found for $\Delta_{fb}'(w)$.

The feedback term is derived as follows. The perturbation to the eigenfunction shape is calculated with a numerical Δ' code by using the boundary condition at the rational surface of $\psi(r_s) = 0$, $\psi'(r_s)$ finite. This calculation assumes timescales long compared to the Alfvén time. For the (2,1) mode this is pretty close to a straight line, so the shape may be approximated as the change in Δ', Δ_{fb}' due to the feedback coils located at a minor radius r_c, as:

$$\psi_{fb}'(r_s) \approx \psi_{fb}(r_c)/(r_c-r_s)$$

$$\Delta_{fb}' = \psi_{fb}'(r_s)/\psi_{2,1}(r_s)$$

$\psi_{2,1}(r_s)$ can be written in terms of the island width as:

$$\psi_{2,1}(r_s) = r_s\, \delta B_r(r_s)/m = e\, s\, B_\phi\, (w/4)^2 / r_s\, q$$

and $\psi_{fb}(r_c) = r_c\, B_r(\text{coil})/m$. The expression is then written in terms of the amplitude of the m=2, n=1 component of the applied radial field at the coil location. As perturbed magnetic field from the tearing mode scales as the island width squared, the quantity $B_r(\text{coil})/w^2$ can be viewed as a gain parameter for the feedback system. The expression has the form:

$$r_s\Delta_{fb}'(w) = 16q/(n\, \varepsilon_s\, s_s)\; r_c/(r_c-r_s)\; B_r(\text{coil})/B\phi\; (r_s/w)^2$$

As might be expected, a given level of feedback current (B_r) is much more effective in stabilizing a small island. However, that implies a high gain for the feedback amplifier, which must rely on a input signal which is roughly proportional to the island width squared.

The first, second and third terms are shown in Figure 1. The maximum feedback signal was assumed to be 2-3 x 10^{-4} B_ϕ, which is adequate to stabilize the mode for the assumptions made for this PBX-M plasma.

A rough comparison to the requirements estimated for the JET feedback system can be made. The power supplies for the JET coils were rated at about 18 MVA, with the assumption that the mode frequency would be 1 kHz or less. Assuming that the relative geometry and plasma configurations are similar between FSX and JET, the power requirements should scale as the volume of field, l^3, as the energy density in the magnetic feedback field, B^2 and as the frequency. JET dimensions are about twice those of FSX, R= 3m vs. 1.5m, likewise the typical JET toroidal field is about 3T compared to 1.5 for FSX. The mode frequency for FSX is assumed to be an order of magnitude higher than that on JET, 10 kHz vs 1 kHz. Thus the power requirements scale as:

$$P \alpha \; l^3 B^2 \omega \; = \quad 8 \times 4 / 10 = 3.$$

By this simple argument, FSX should require about 6 MVA to match the performance of the JET feedback system. A similar comparison can be made for the DITE system. DITE has a minor radius of about 1/2 that of FSX, but is not elongated. The major radius is 1.2m, or comparable. The ratio of the volumes is then about that between JET and FSX. The mode frequencies and toroidal fields are comparable. The DITE power supplies each put out a peak current less than 1 kA at a peak voltage of 60 V, or <60kVA. I guess there were 2 or 4 supplies, or about 0.125 - 0.25 MVA. This would scale to a requirement of about 1-2 MVA for FSX.

The required power for feedback stabilization may be somewhat higher in FSX due to the pressure drive. Thus, the FSX feedback system is designed with a 5-10 MVA capability.

There will be a total of 20 high frequency (20 kHz) tearing mode suppression coils added; a toroidal array of ten coils on the outboard midplane in the gap between the passive plates and ten on the inboard midplane. The tearing mode suppression coils will have five power supplies with a bandwidth of ≈20 kHz and a total of ≈5MVA. The coils will have ? turns driven at up to 500(?) A. The (2,1) component of imposed magnetic field will have an amplitude of about 5 Gauss at the plasma surface, and in vacuum will have about 2.5 Gauss at the location of the (2,1) mode. The inboard/outboard coil currents can be balanced to reduce the (1,1) component at the q=1 surface to an arbitrarily low number. The n=10

toroidal symmetry will allow nearly complete elimination of n>1 components, up to n=9.

References

[1] K. Bol et al., in Plasma Physics and Controlled Nuclear Fusion Research 1976 (Proc. 6th Int. Conf. Tokyo, 1975), Vol. 1, IAEA, Vienna (1975) 83.

[2] V. V. Arsenin, L. I. Artemenkov, N. V. Ivanov, et al., in Plasma Physics and Controlled Nuclear Fusion Research 1978 (Proc. 7th Int. Conf. Innsbruck, 1978), Vol. 1 IAEA, Vienna (1979) 233 and Yu. V. Gvozdkov, N. V. Ivanov, A. m. Kakurin, Fiz. Plazmy **6** (1980) 234 [Sov. J. Plasma Phys. **6** (1980) 130].

[3] W. Morris et al., Phys. Rev. Lett. **64** (1990) 1254.

[4] A.Santaguistina, et al.,European Physical Society Meeting, Bournemouth (1995), V19C, pIV,p.461. and P. Savrukhin, S. AliArshad, D. J. Campbell, et al., European Physical Society Meeting, Kiev (1996).

[5] M. Mauel , E. Eisner, A. Garofalo, et al., in Eddy-current Characterization and plasma rotation control in wall-stabilized tokamak discharges, 16th IAEA Fusion Energy Conference, Montréal, Canada (Oct 7-11,1996) paper IAEA-CN-64/AP1-19.

[6] D. A. Monticello, R. B. White, M. N. Rosenbluth in Plasma Physics and Controlled Nuclear Fusion Research 1978 (Proc. 7th Int. Conf. Innsbruck, 1978), Vol. 1, IAEA, Vienna (1979) 605.

[7] E. Lazzaro and M. F. F. Nave, Phys. Fluids **32** (1988) 1623.

[8] G. Bosia, E. Lazzaro, Nucl. Fusion **31** (1991) 1003.

5.3.1 Tearing Mode Coil Design

Computer calculations were performed for the design of the tearing mode coils. A particular computed plasma equilibrium was chosen as typical for FSX, and then used in tearing mode coil conceptual design calculations to establish the geometrical shape of several important equilibrium flux surfaces and their poloidal magnetic coordinates. (Future studies concerning the tearing mode coils' design sensitivity to changes from this assumed plasma equilibrium should be performed as part of a FSX final design process.)

The six flux surfaces represented in this fashion in conceptual design calculations were those having "safety factor" values of q=1, q=1.5, q=2, q=2.5, q=3, q=4. The geometrical shape of each flux surface was represented by 128 neighboring

points on the closed curve intersection of that flux surface with a meridian (poloidal) plane, and was numerically tabulated as a sequential list of ordered pairs in cylindrical coordinates, $\{(R_i, Z_i)\}_{i=1}^{128}$. The algorithm selecting the 128 points chose them so that they were equally spaced in the "poloidal angle" magnetic coordinate of the computed equilibrium. Figure 1 shows a plot of the discrete points selected from the computed plasma equilibrium for each of these flux surfaces.

Fig. 1. Flux surface points distributed in magnetic coordinates.

For each important flux surface, a special interpolating curve was fitted using subroutines from IMSL's math library. With the convention that $(R_{129}, Z_{129}) \equiv (R_1, Z_1)$, periodic cubic spline functions r(s) and z(s) were calculated so that the resulting smooth closed curve $\{(r(s), z(s)), 0 \le s \le s_{129}\}$ matched each of the points of $\{(R_i, Z_i)\}_{i=1}^{129}$ at calculated parametric values $\{s_i\}_{i=1}^{129}$, where the parametric variable s represents the arc length integrated counterclockwise along the curve from the initial (R_1, Z_1) point, and where s_{129} is the closed curve's total perimeter arc length.

The algorithm is iterative, and alternates in its k^{th} iteration between using provisional arc length values $\{s_i^{(k)}\}_{i=1}^{129}$ to calculate periodic cubic splines $r^{(k)}(s)$ and $z^{(k)}(s)$ which precisely fit the points $\{(s_i^{(k)}, R_i)\}_{i=1}^{129}$ and $\{(s_i^{(k)}, Z_i)\}_{i=1}^{129}$ respectively, and then refining the arc length values by numerically evaluating the integral $s_i^{(k+1)} = \int_{s=s_1^{(k)}=0}^{s=s_i^{(k)}} \sqrt{(\frac{d}{ds} r^{(k)}(s))^2 + (\frac{d}{ds} z^{(k)}(s))^2}\, ds, \ \forall i \ , 1 \le i \le 129,$ for use in the next iteration. Convergence $(r^{(k)}(s), z^{(k)}(s)) \to (r(s), z(s))$ is rapid. Among the nice properties of the resulting special functions r(s) and z(s) is that $(\frac{d}{ds} r(s), \frac{d}{ds} z(s))\Big|_{s=s_i}$ are unit vectors tangent to the smooth curve at the selected flux surface points, a geometric property used subsequently to determine magnetic field components of interest for the tearing mode, i.e., field components perpendicular to the flux surface.

To scan magnetic field toroidally, the toroidal angle variable, Φ, $0 \le \Phi \le 2\pi$, was divided into 80 equal increments. Each flux surface was then represented for field

calculations in three dimensions by two-dimensional arrays of 128 poloidal X 80 toroidal =10240 total field evaluation point locations, each specified by its cylindrical coordinate location, (R_i, Z_i, Φ_j), or equivalently by rectangular $(x_{(i,j)}, y_{(i,j)}, z_i)$ coordinates.

The tearing mode coil system was selected to have ten-fold toroidal symmetry in order to avoid interference with 10-fold symmetry structures of the FSX tokamak (e.g., 20 TF coils and various vacuum vessel internal structures), while also providing the ability to avoid spatial "aliasing" and thus resolve toroidal mode numbers up through n=4. For numerical field computations, the shape of one of the ten identical coils was specified as a closed sequence of point locations in three dimensions, following the coil current filament's geometric path. The magnetic field produced by 1 ampere-turn in that coil was then calculated at each of the 10240 field evaluation points on each of the six important flux surfaces by numerically integrating the Biot-Savart law over the specified filament current path, using straight line segments between specified points. Each "perpendicular" field component, i.e., perpendicular to the flux surface at each field evaluation point, was then determined using the unit vector directions previously calculated from the cubic spline functions, and stored in an array. Since interest for FSX in tearing mode feedback centered on control of the m/n=2/1 and 3/2 modes, excitation with the two "n" values for toroidal coil excitation in the calculations were handled differently. For n=1 excitation, coil excitation current was distributed among the 10 coils as $I_k = \cos(\frac{2\pi k}{10} + \theta)$ where k, 1<k<10, represents the coil's toroidal location. For n=2 excitation, coil current was distributed as $I_k = \cos(\frac{4\pi k}{10} + \theta)$. For either excitation case, a final array of 10240 "perpendicular" field components on each flux surface for a 10-fold symmetry coil set was calculated from the perpendicular field components previously stored by summing values for appropriately rotated toroidal locations.

As an example of the result, Fig. 2 plots the perpendicular field distribution on the q=2 flux surface as produced by 10 "window frame" coils located on the outer midplane when they are powered with n=1 excitation. (The shapes of the vacuum vessel ports and the internal passive plates almost completely dictate the allowable shape of these coils. In particular, these coils cannot be "tilted" to follow field lines because of interference with the neutral beams. The resulting flux

surface field pattern of Fig. 2 is seen to be quite locally concentrated in the poloidal magnetic coordinate.)

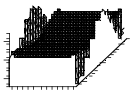

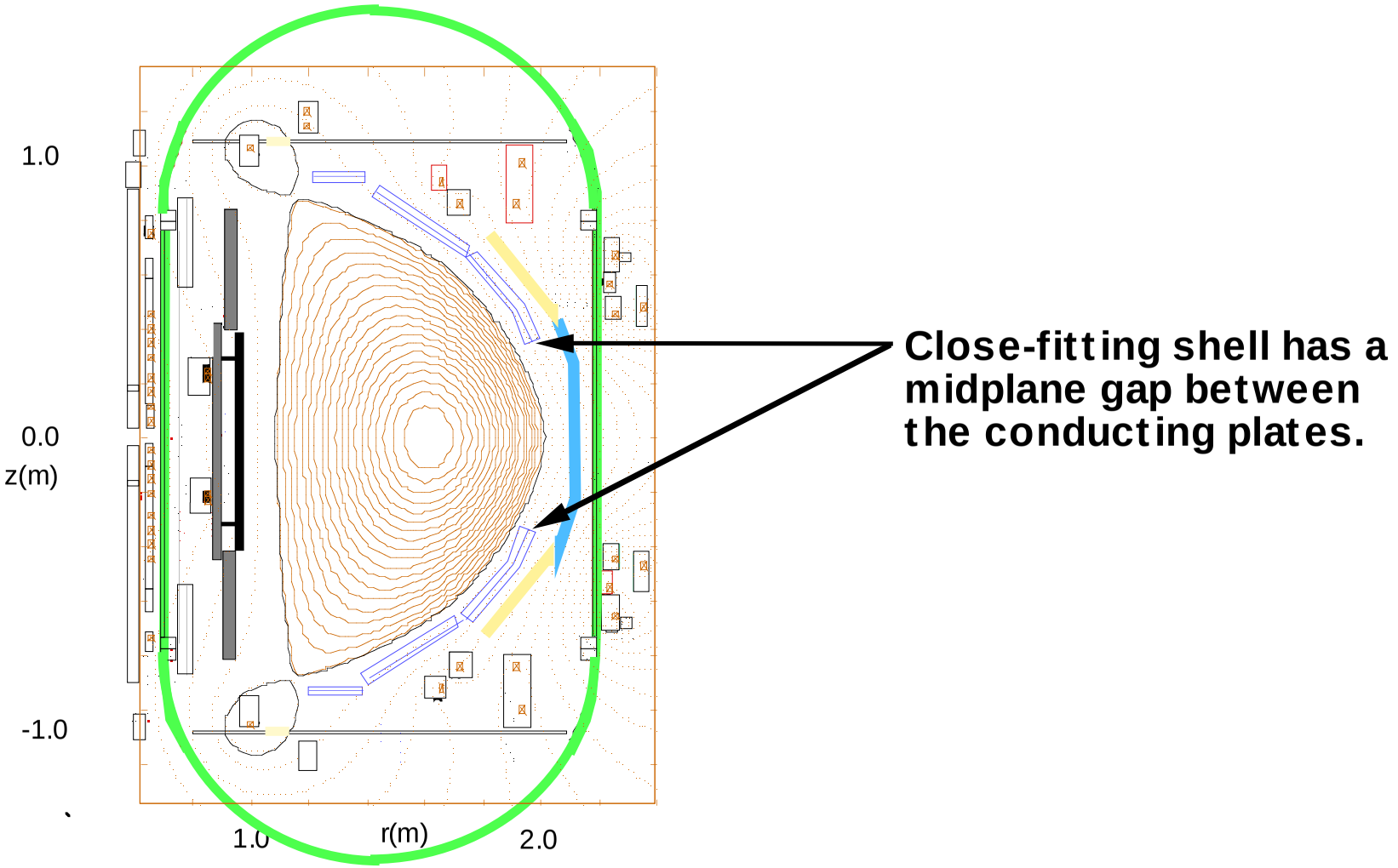
1.0
0.0
z(m)
-1.0
1.0
r(m)
2.0
Close-fitting shell has a midplane gap between the conducting plates.

Fig. 1

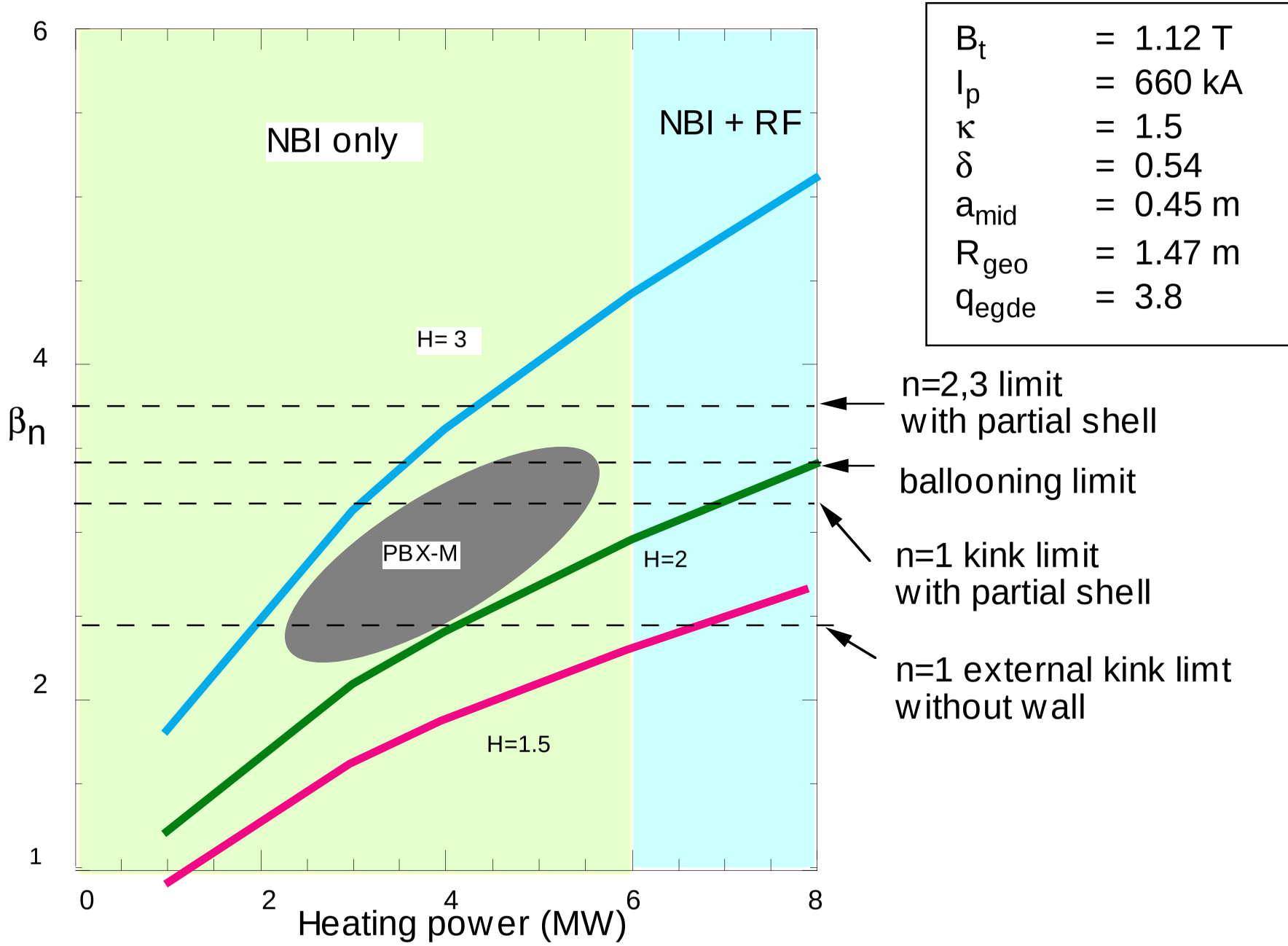
6
4
2
1
β_n
NBI only
NBI + RF
H= 3
H=2
H=1.5
PBX-M
0
2
4
6
8
Heating power (MW)
B_t = 1.12 T
I_p = 660 kA
κ = 1.5
δ = 0.54
a_{mid} = 0.45 m
R_{geo} = 1.47 m
q_{egde} = 3.8
n=2,3 limit
with partial shell
ballooning limit
n=1 kink limit
with partial shell
n=1 external kink limt
without wall

Fig. 2

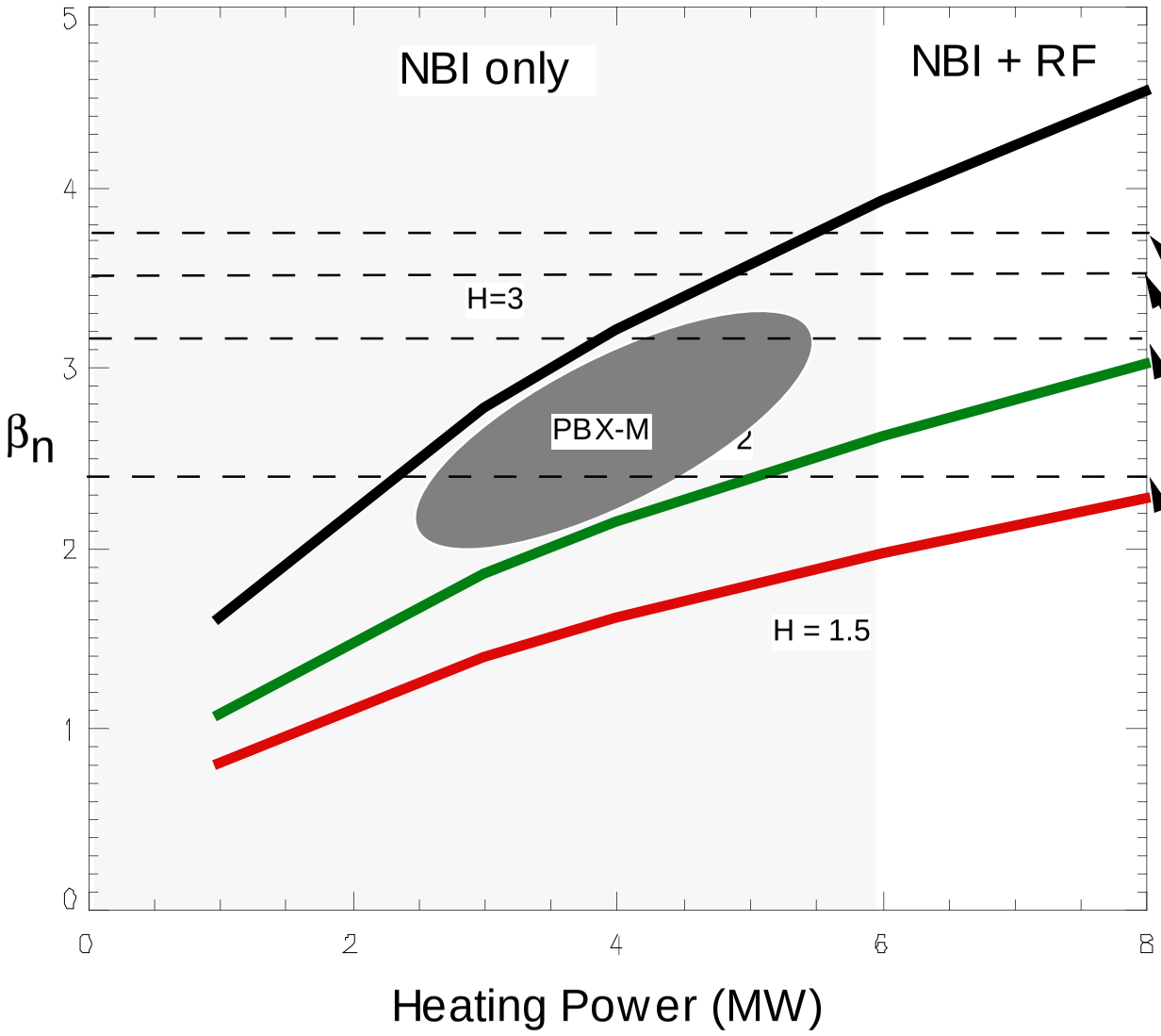

B_t	= 1.5	T
I_p	= 1.0	MA
κ	= 1.6	
δ	= 0.54	
a_{mid}	= 0.45	m
R_{geo}	= 1.47	m
q_{edge}	= 3.4	

n=2,3 limit with partial wall

ballooning limit

n=1 external kink limit with partial shell

n=1 external kink limit withouit wall

Fig. 3

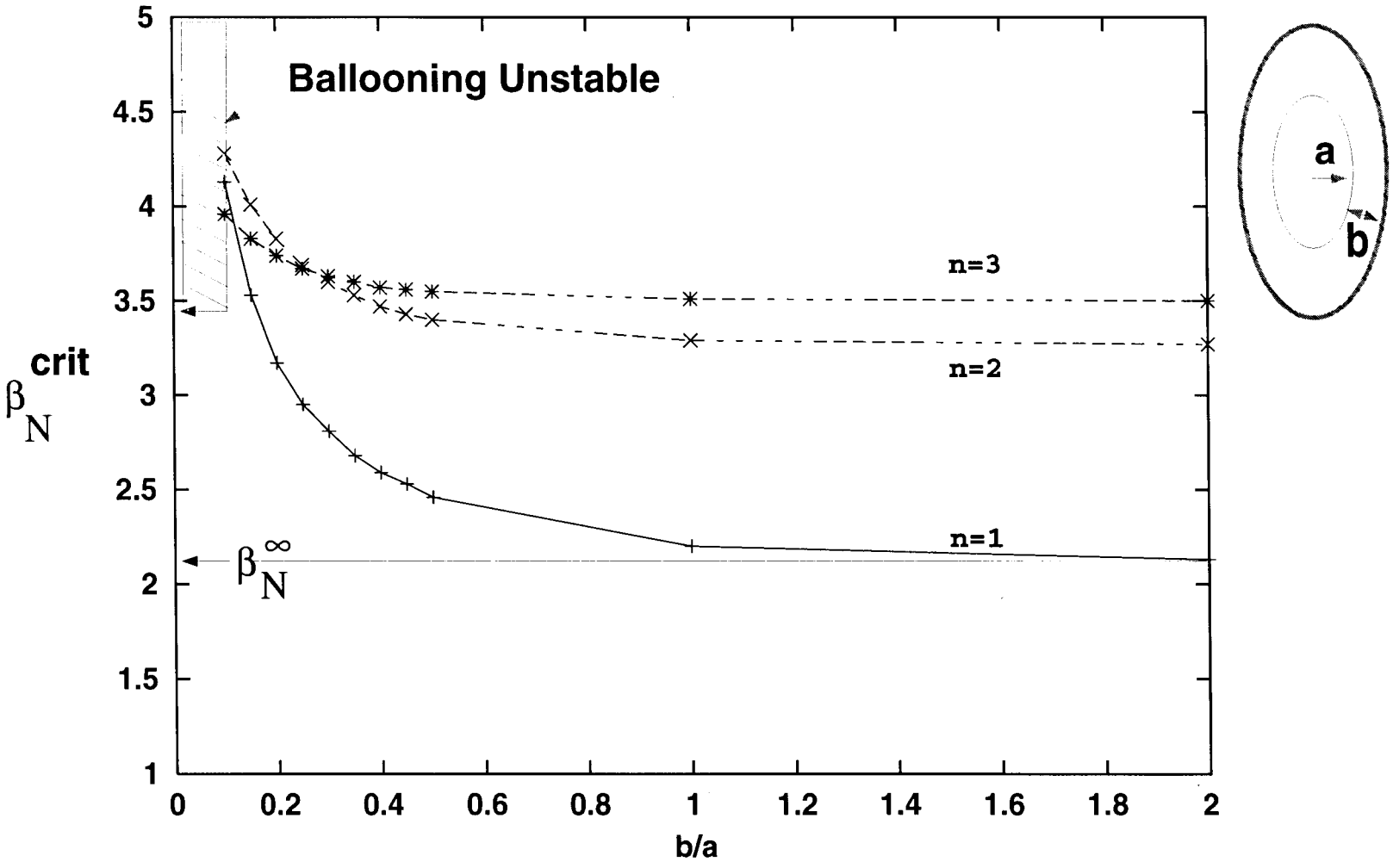
Ballooning Unstable
β_N^{crit}
β_N^{∞}
n=3
n=2
n=1
b/a
a
b
5
4.5
4
3.5
3
2.5
2
1.5
1
0
0.2
0.4
0.6
0.8
1
1.2
1.4
1.6
1.8
2

Fig. 4

```
Q0    0.90
QE    3.84
QMIN    0.90
P(0)/<P> =
 2.814
LI/2=
 0.347
I(Q=1)/I(TOT) =
      0.790

ASPECT RATIO=
    3.231
CURRENT
(I/AB)=
    1.402
VOL. AVG. BETA
    4.338
BETA (B-MID)=
    4.965
G=(BETA/I/AB)=
    3.540
BETA-POLOIDAL=
    1.048
BETA-STAR =
    6.751
G-STAR =
    4.814
TRANSP VALUES:
BTEQ=   4.471
BPEQ=   1.731

R=      1.450
A=      0.449
XMA=     1.512
ELLIP=     1.690
TRIAN=     0.620
```

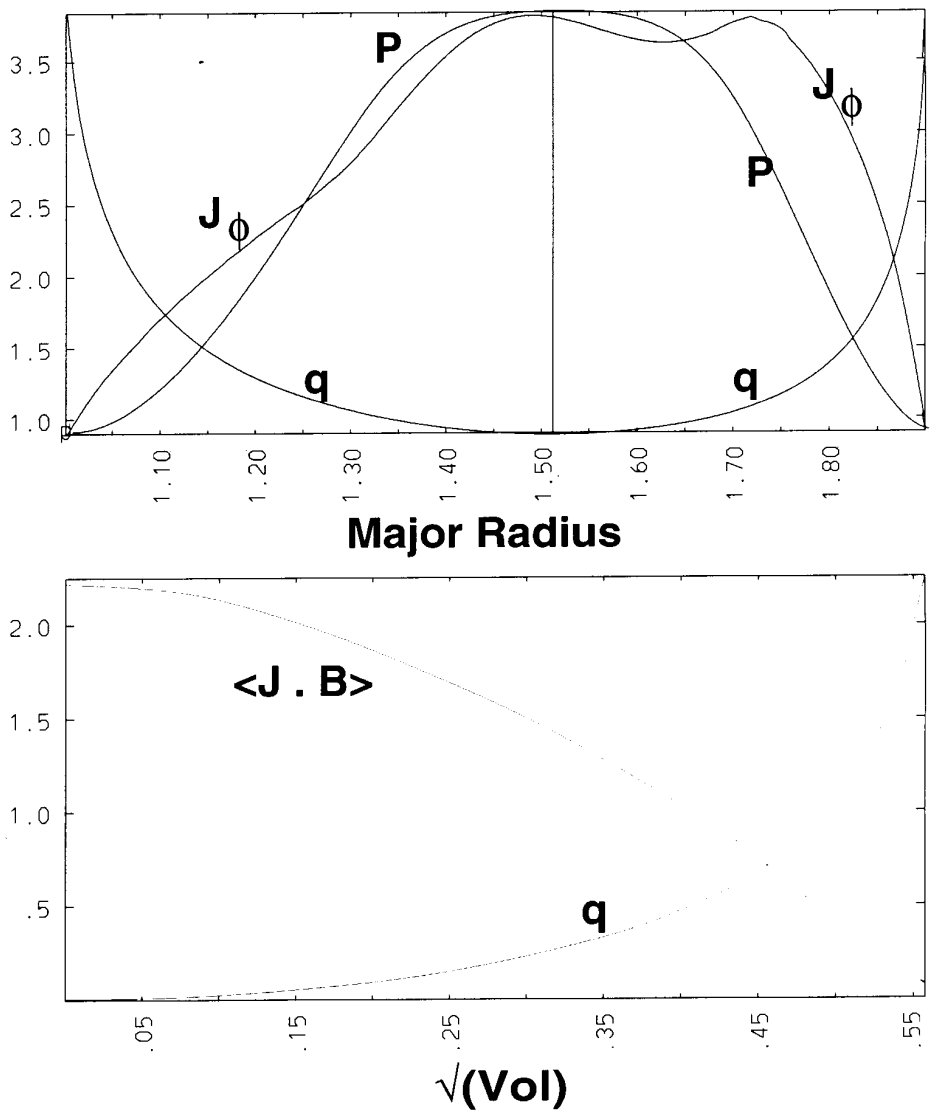

P = Pressure, J_ϕ= Toroidal Current Density, q = Safety Factor, <J . B> = Parallel Current

Fig. 5

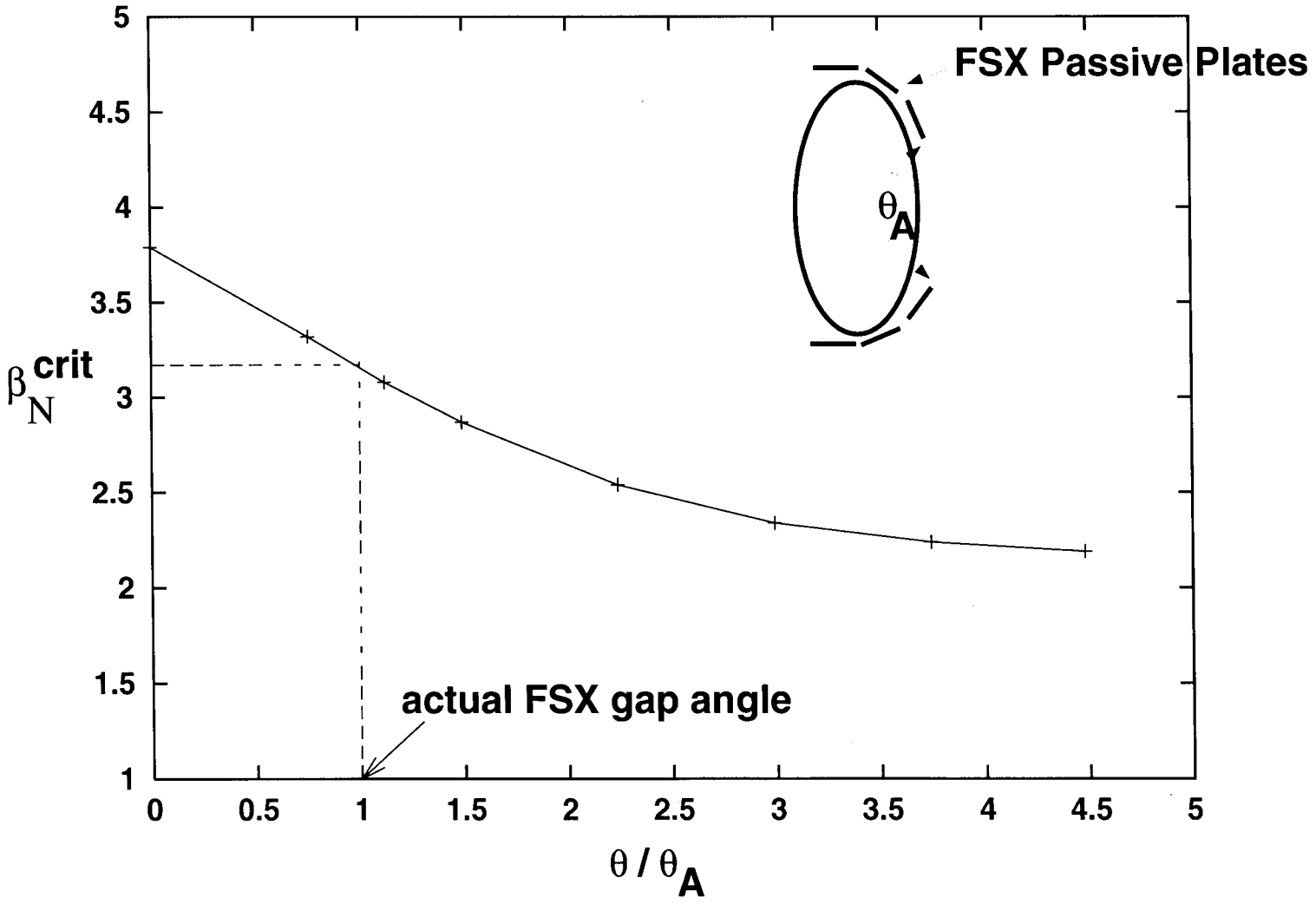
FSX Passive Plates
θ_A
β_N^{crit}
actual FSX gap angle
θ / θ_A
5
4.5
4
3.5
3
2.5
2
1.5
1
0
0.5
1
1.5
2
2.5
3
3.5
4
4.5
5

Fig. 6

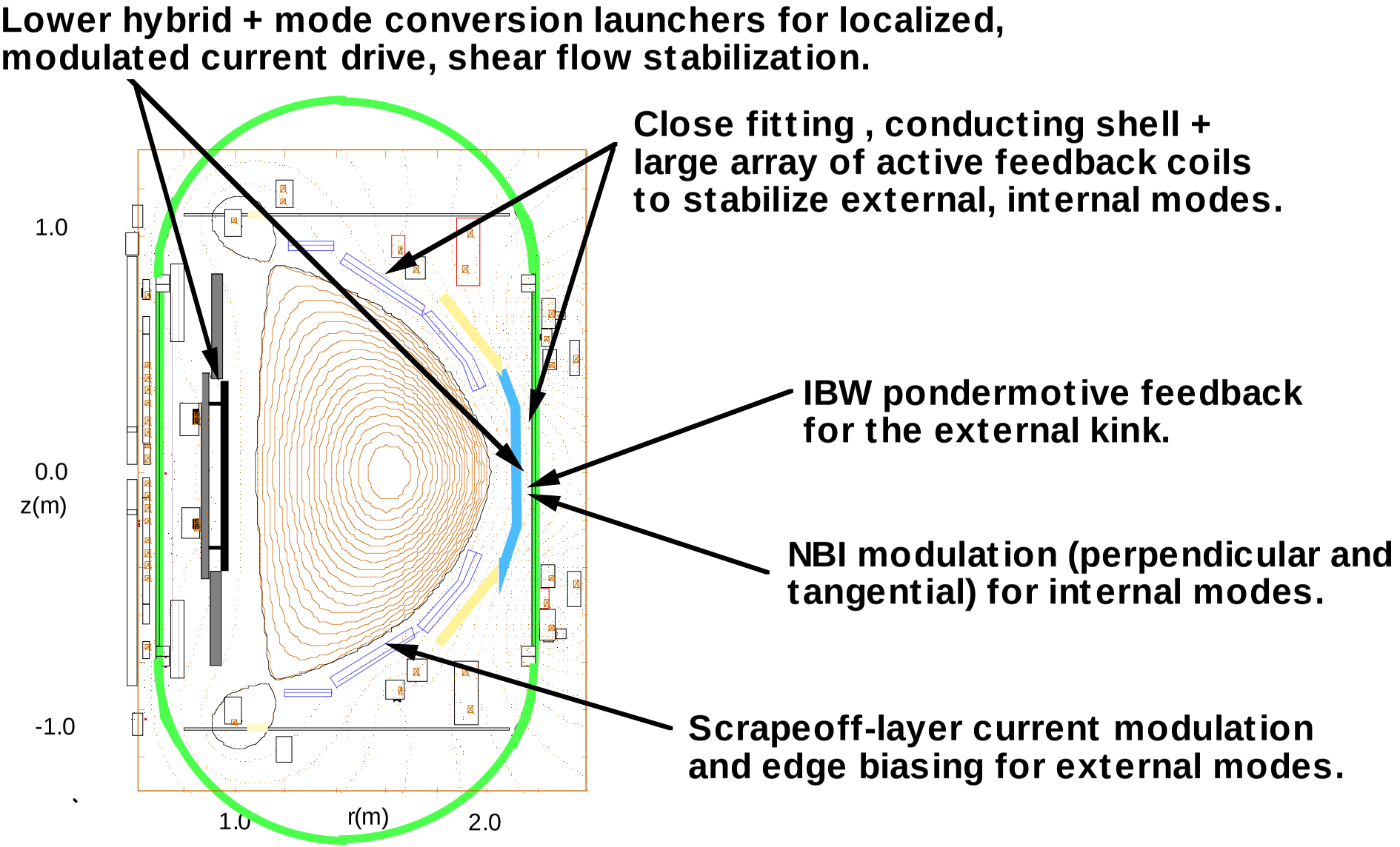
Lower hybrid + mode conversion launchers for localized, modulated current drive, shear flow stabilization.
Close fitting , conducting shell + large array of active feedback coils to stabilize external, internal modes.
IBW pondermotive feedback for the external kink.
NBI modulation (perpendicular and tangential) for internal modes.
Scrapeoff-layer current modulation and edge biasing for external modes.
1.0
0.0
z(m)
-1.0
1.0
r(m)
2.0

Fig. 1

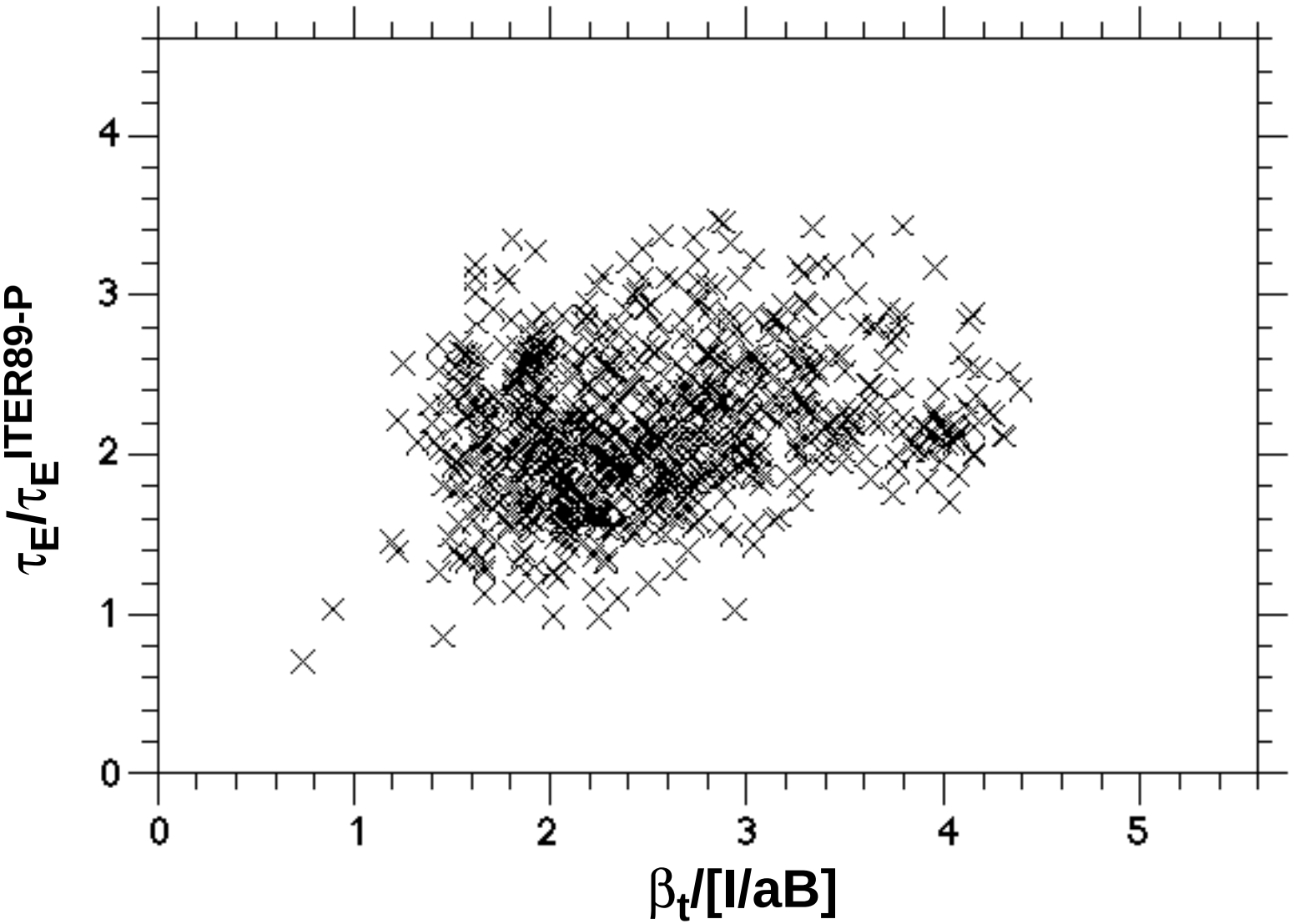

Fig. 2

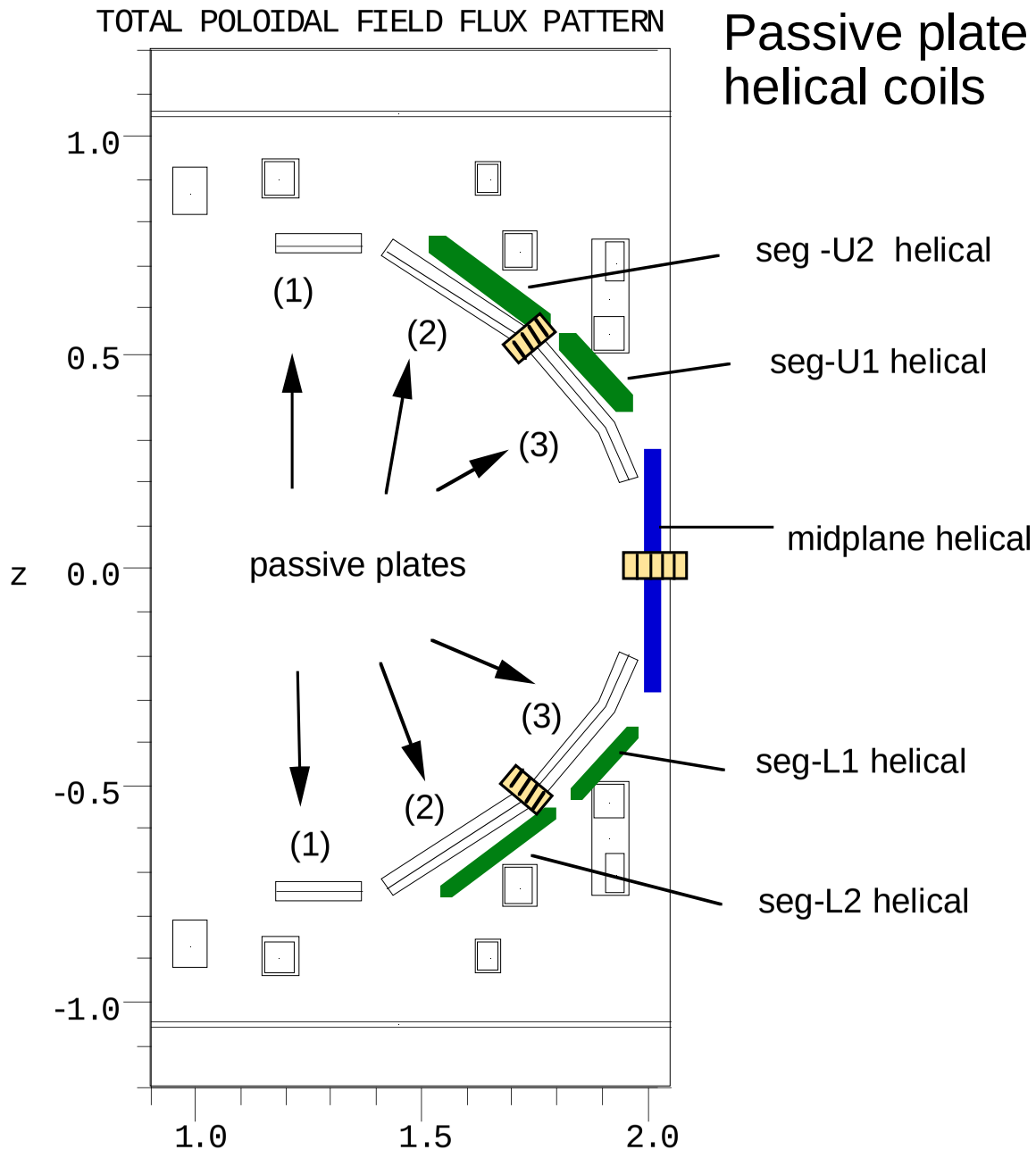

Fig. 1 Schematic diagram of passive and active elements for resistive wall mode stabilization.

Schematic of Mode Identification Process

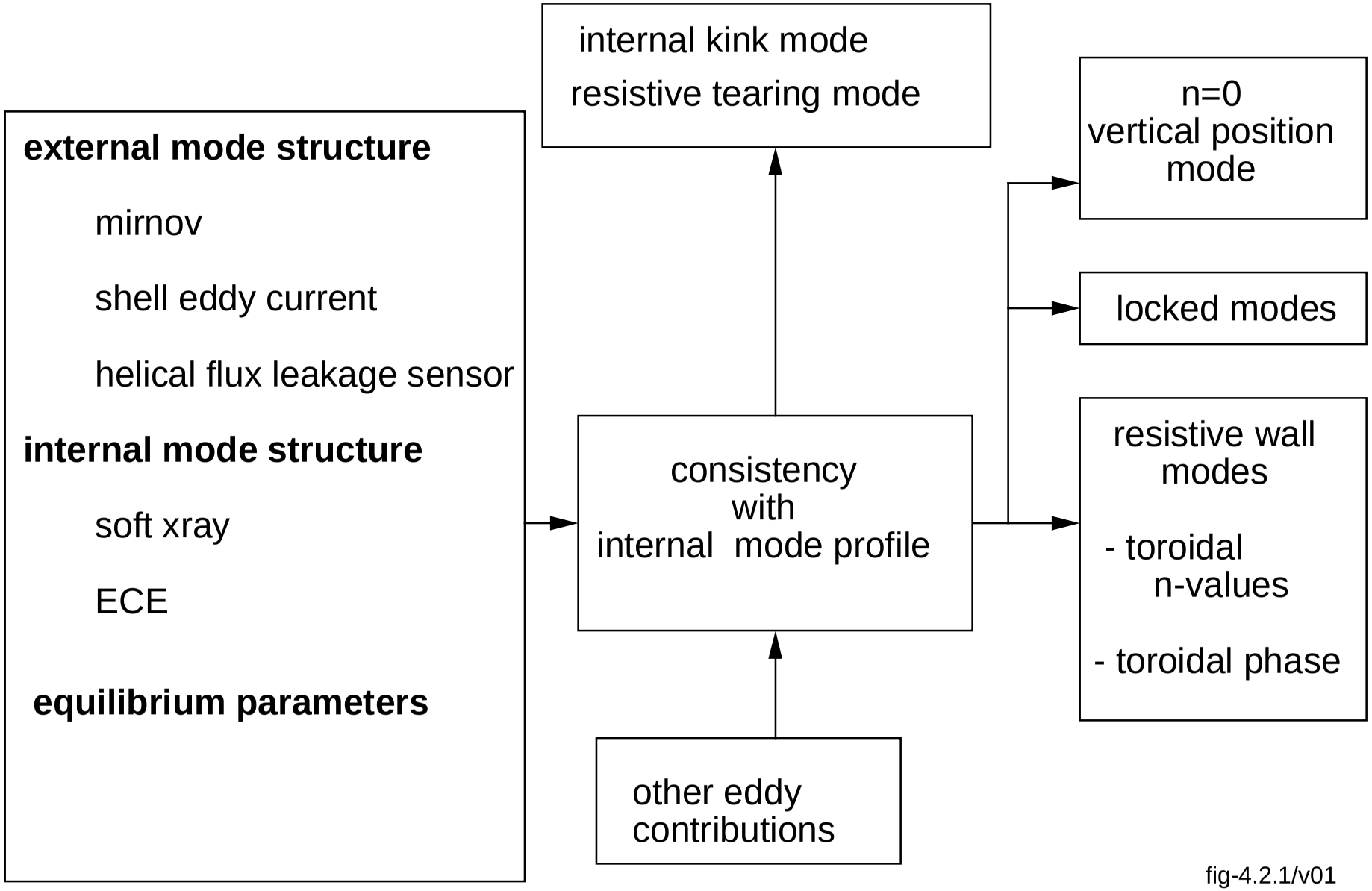

Fig. 1

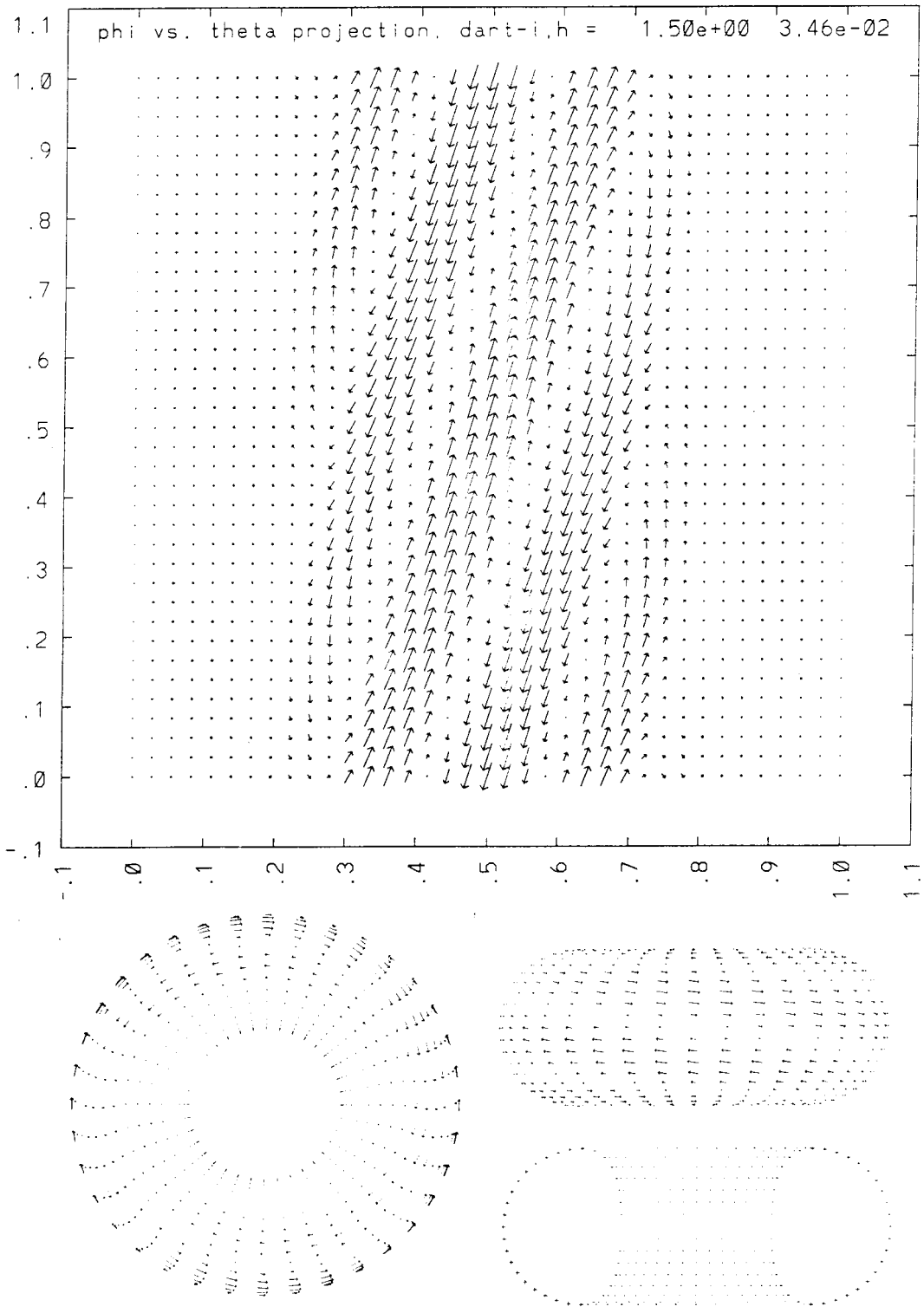

Figure 1: Projection in the (L_ϕ-L_θ)plane of the induced current on a conforming shell at 0.5a due to an ustable n=1 kink mode. The coordinate axes are physical lengths and normalized to unit length. The top and side views of the outer and inner sides are also shown.

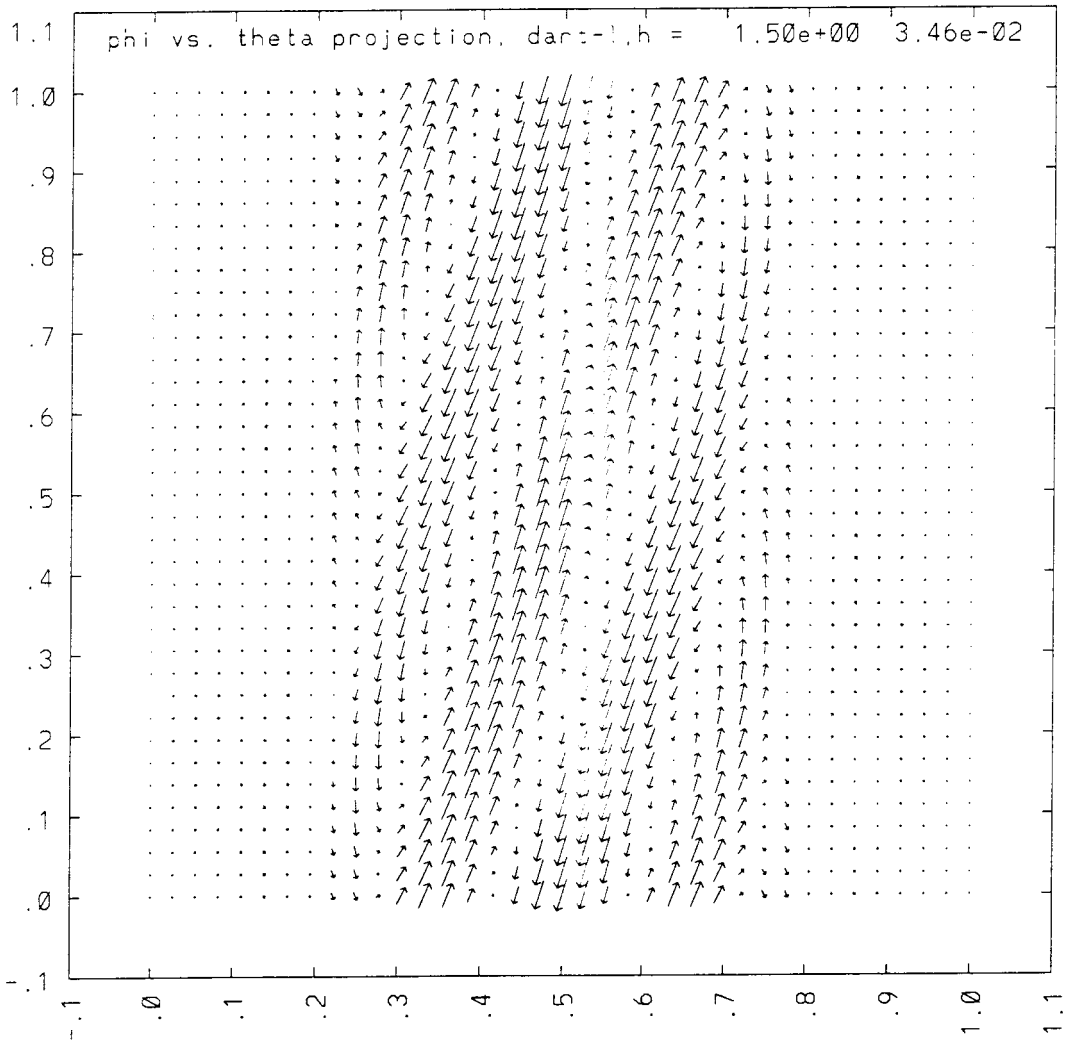

Figure 2: Projection in the L_ϕ - L_θ plane of the induced current on a conforming shell, artificially placed at 0.1a, due to the unstable n=1 kink mode of Fig. 1.

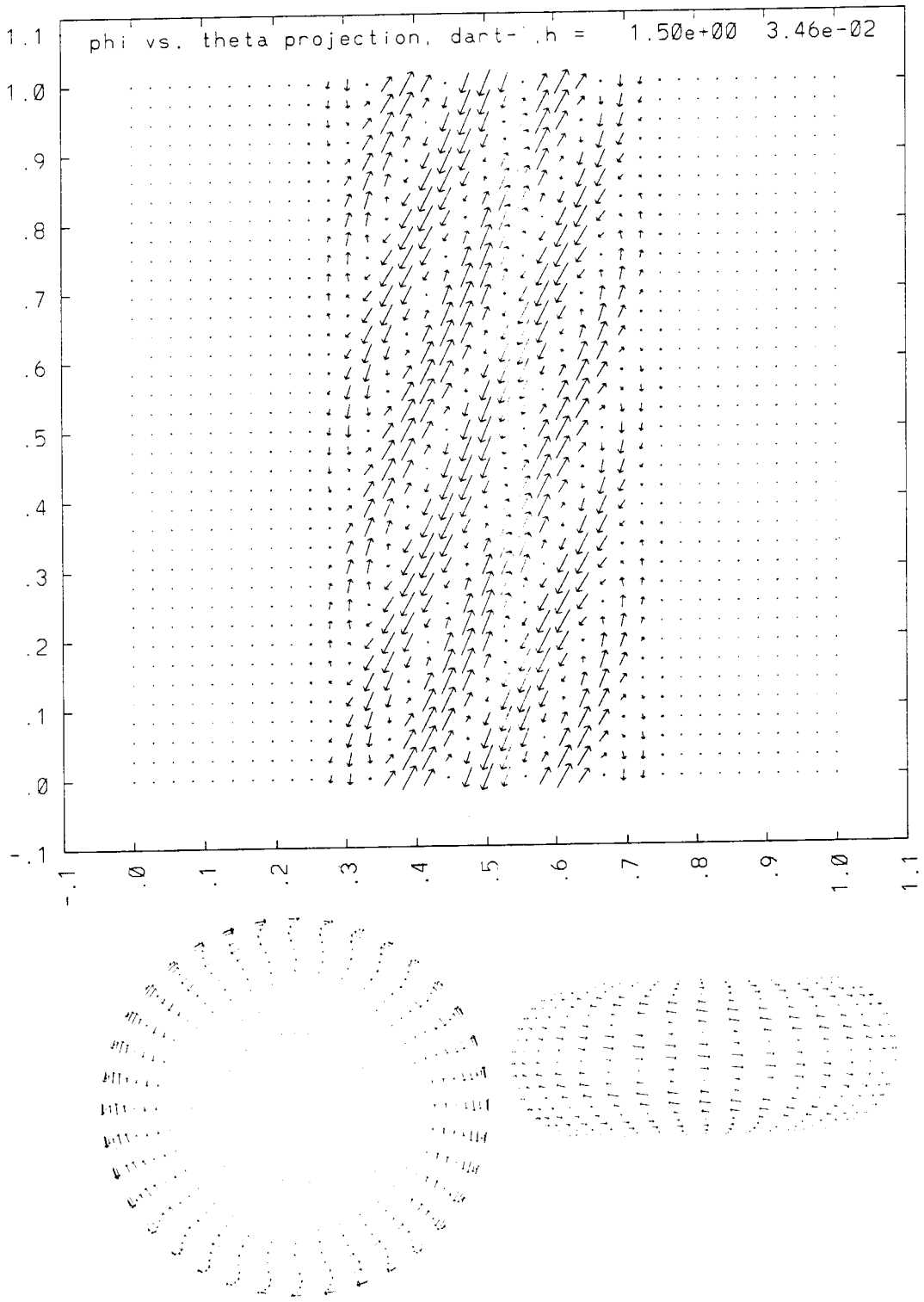

Figure 4: Projection in the (L_ϕ-L_θ) plane of the induced current on a conforming shell at 0.5a due to the unstable n=2 kink mode of the same equilibrium of Fig. 1. The coordinate axes are each normalized to unit length. The top and an outer side view are also shown.

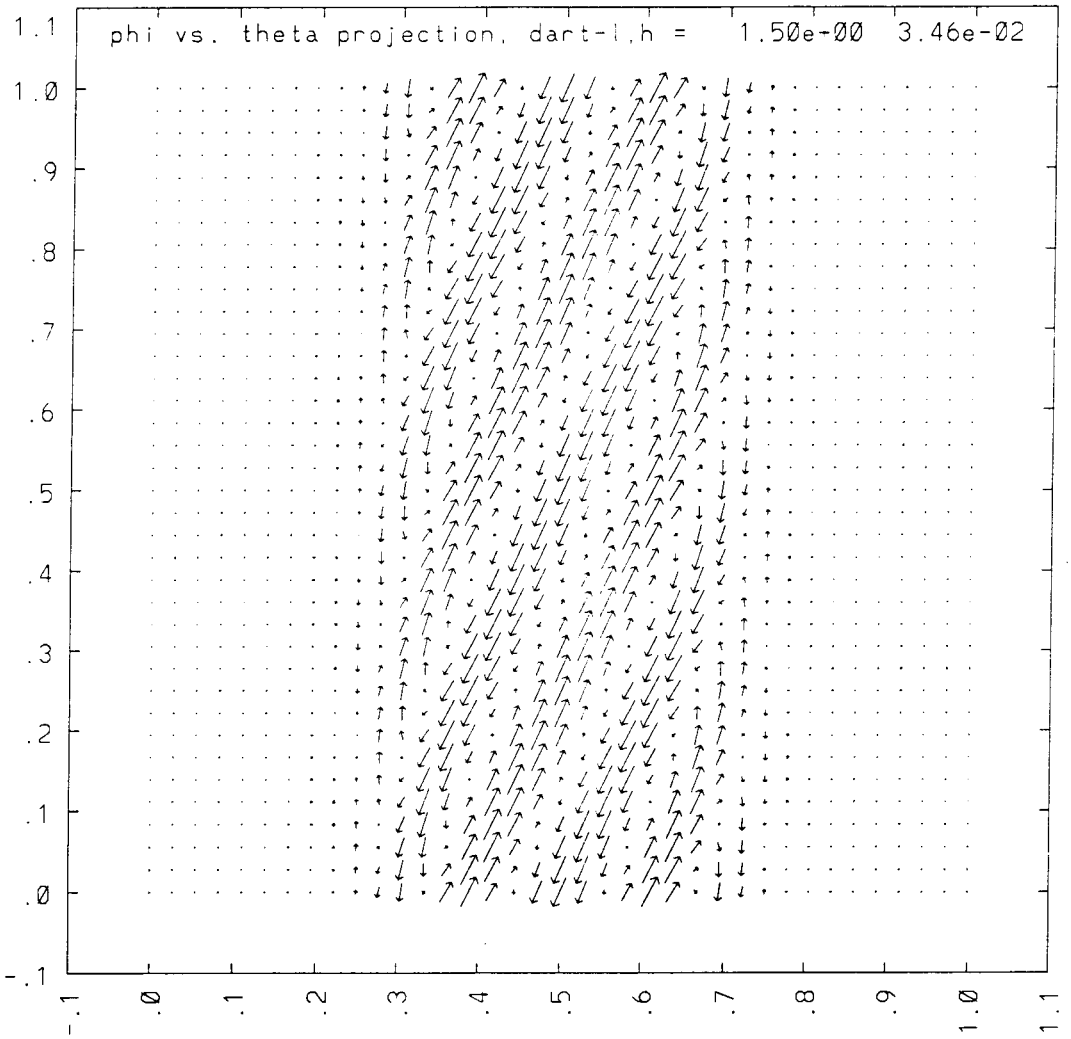

Figure 5: Projection in the $(L_\phi\text{-}L_\theta)$ plane of the induced current on a conforming shell, *artificially placed* at 0.1a, due to the unstable n=2 kink mode of Fig. 1.

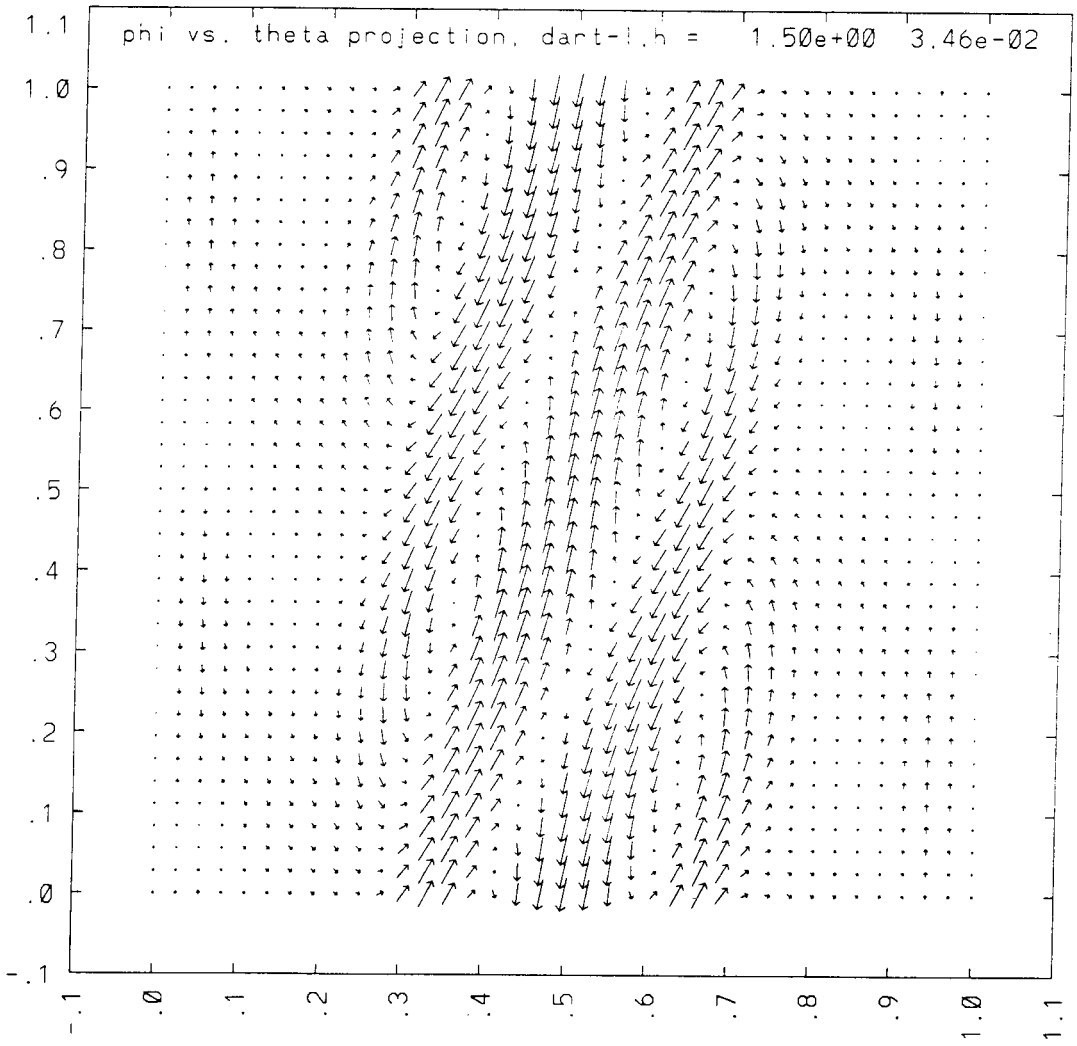

Figure 7: Projection in the (L_ϕ-L_θ) plane of the induced current on a conforming shell at 0.5a due to an unstable n=1 kink mode for a case in which q_{edge} = 3.82. The coordinate axes are physical length and each normalized to unit length.

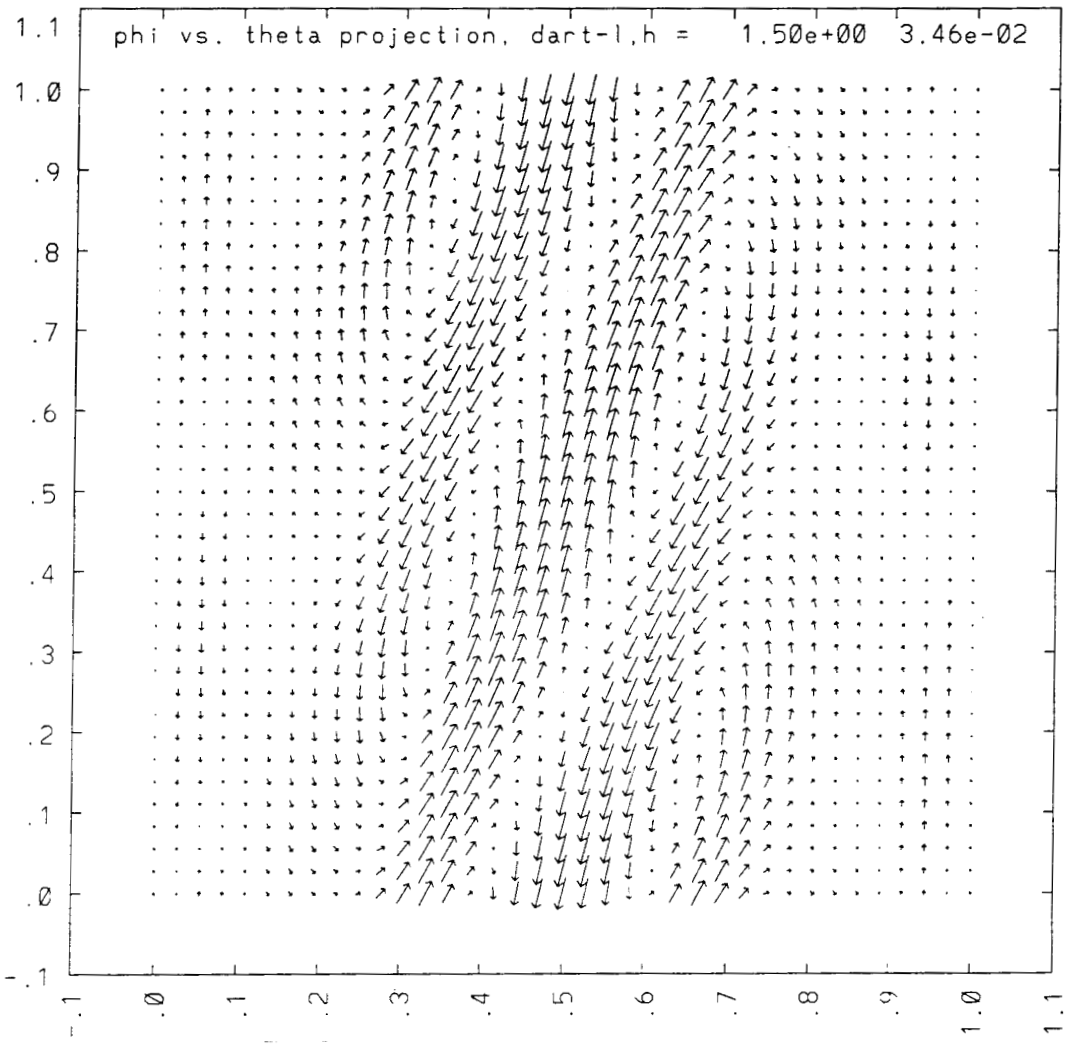

Figure 8: Projection in the ($L\phi$-$L\theta$) plane of the induced current on a conforming shell at 0.5a due to an unstable n=1 kink mode for a case in which $q_{edge} = 2.83$. The coordinate axes are each normalized to unit length.

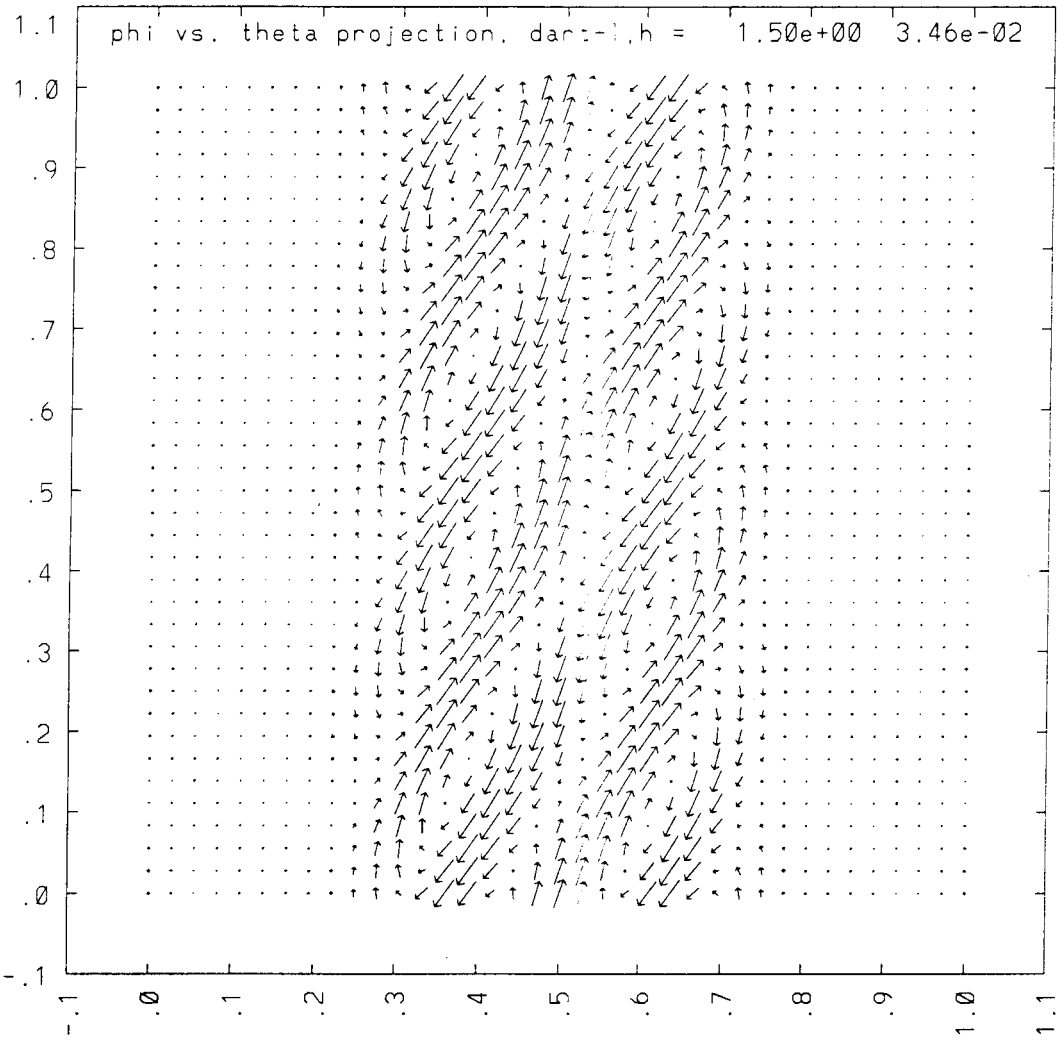

Figure 9: Projection in the (Lϕ-Lθ) plane of the induced current on a conforming shell at 0.5a due to an unstable n=2 kink mode for the case in which q_{edge} = 2.83. The coordinate axes are each normalized to unit length.

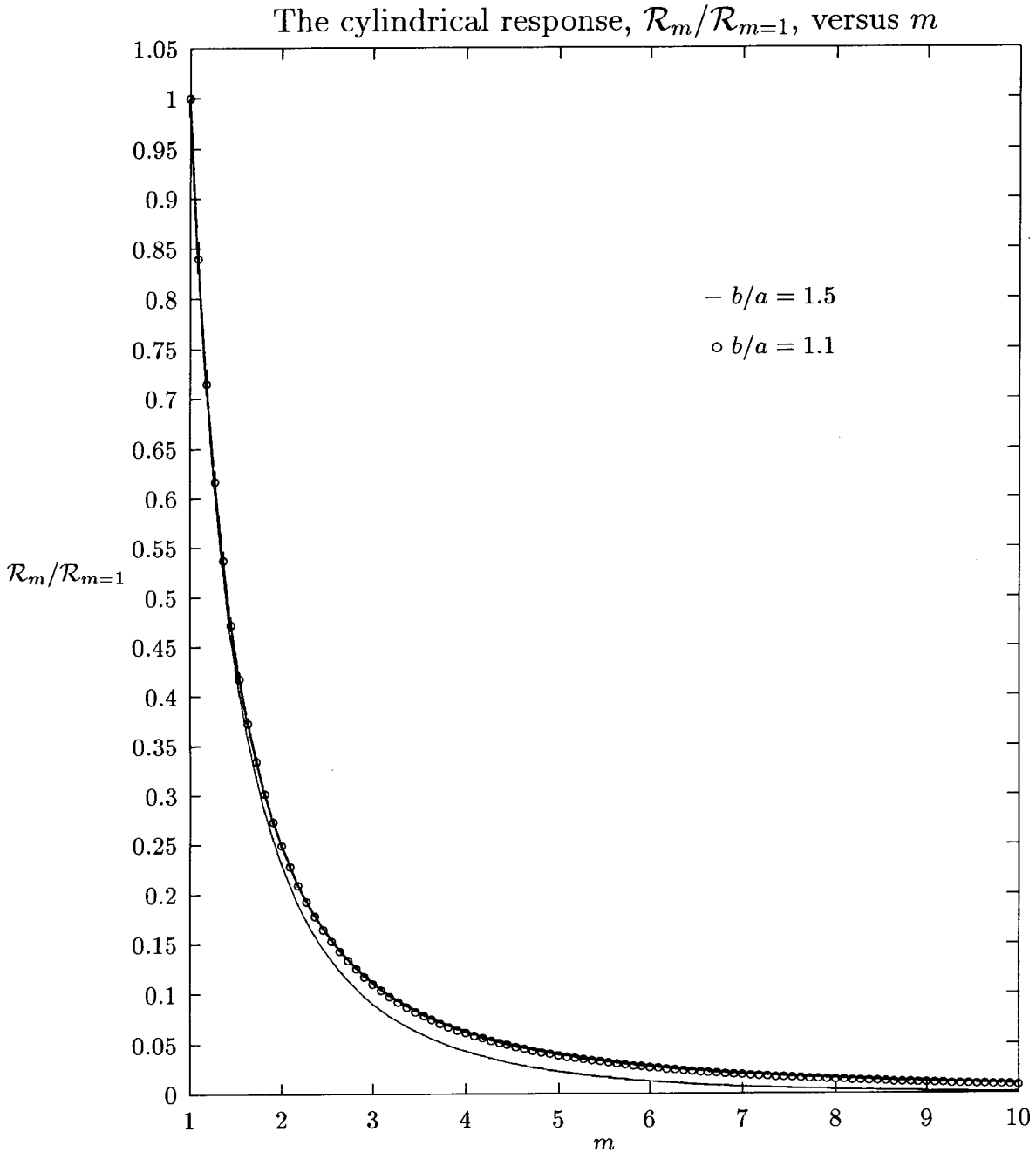

Figure 10: The Fourier harmonics of the response, R_m at r=b, to the cylindrical plasma perturbation, normalized to the m=1 component, plotted as a function of m. In the limit where b/a = 1, $R_m / R_{m=1}$ = m-2. This limiting curve almost overlaps that for b/a = 1.1.

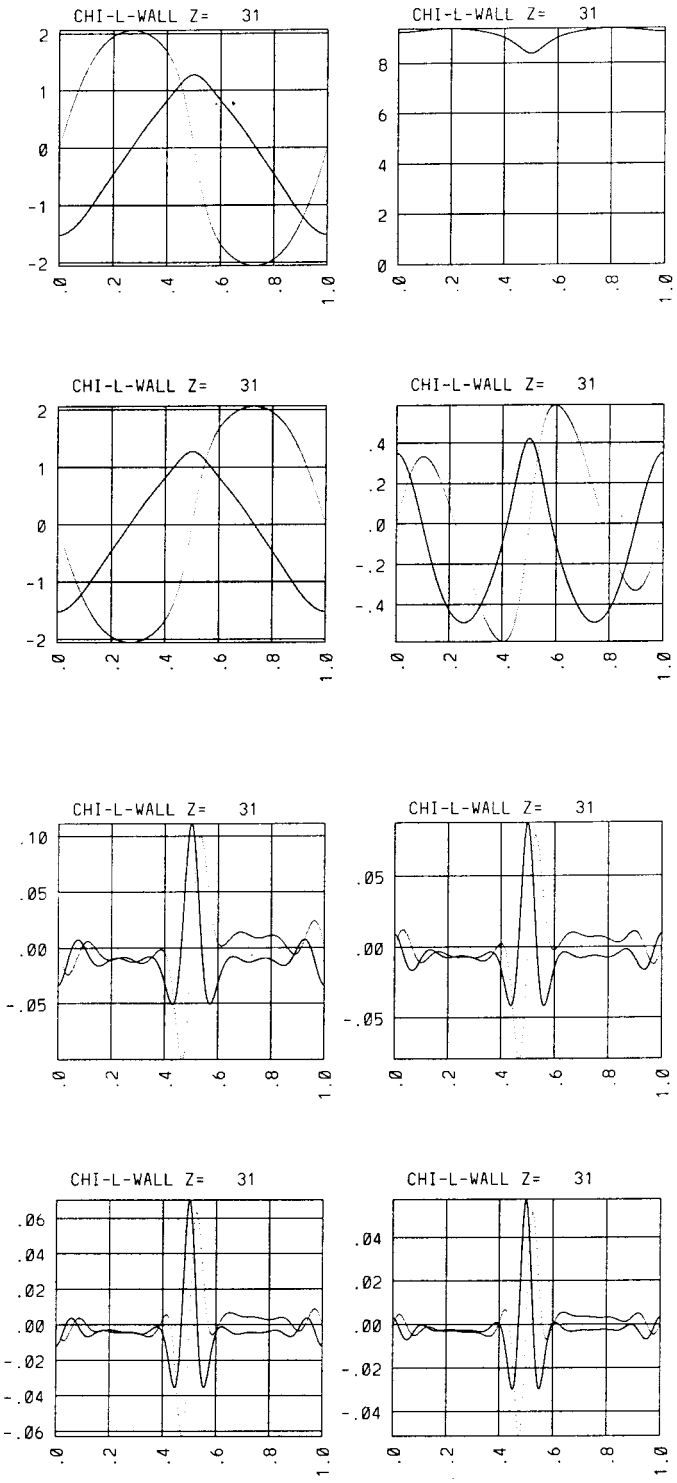

Figure 11: The decreasing two dimensional response, $R(\theta)$ at the shell for the m=-1, 0, 1, 2, 7, 8, 9 and 10th harmonics of the plasma perturbation for the unstable kink mode of the case described in Fig.1.

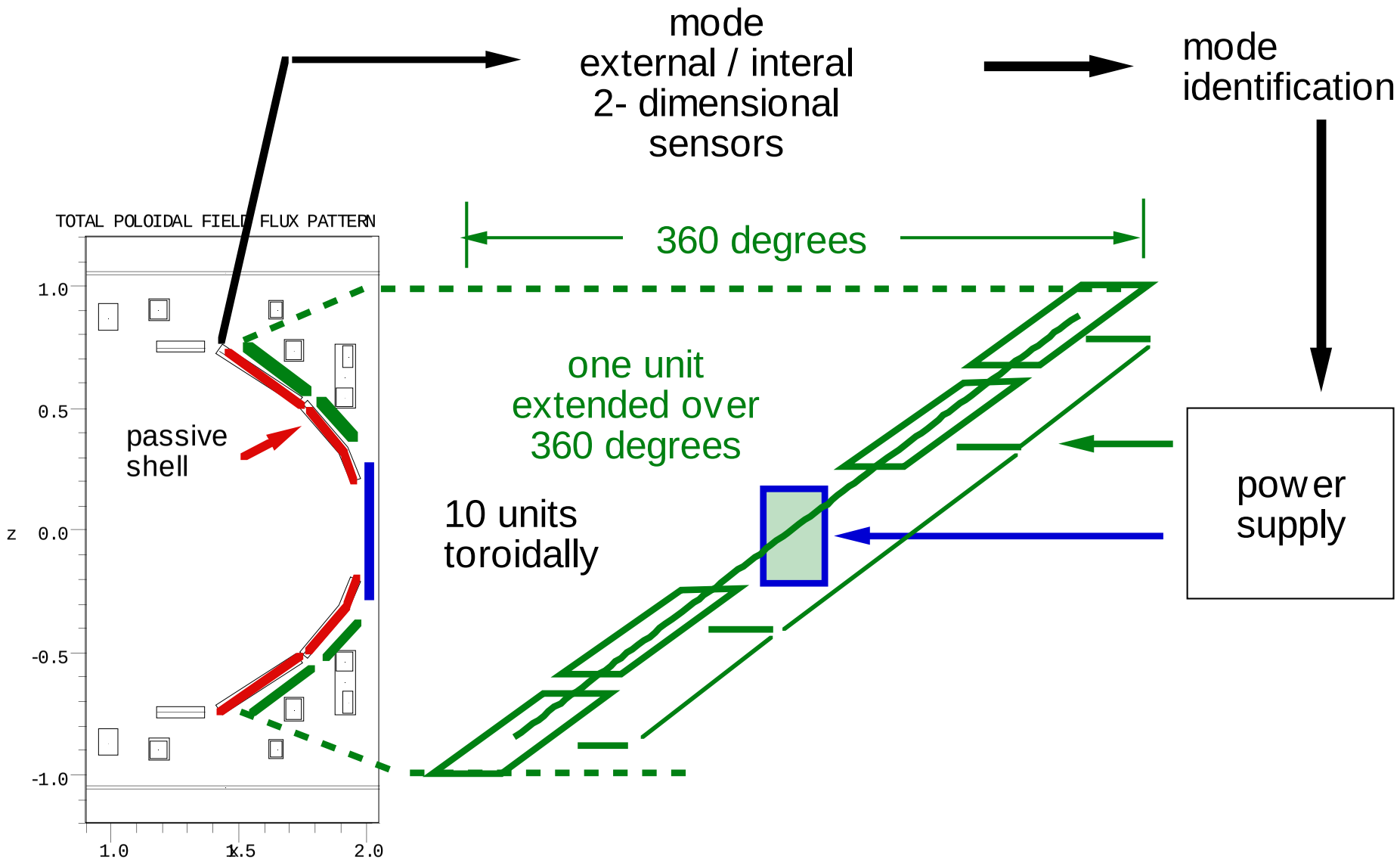

Fig. 1 Integrated shell scheme for resistive wall mode stabilization. One set of active coils is lined up along the eddy current flow pattern. One unit stretches toroidally over 360 degrees. The two power supply systems energize the midplane coil section and the section at the off-midplane independently. Total of 10 units covers uniformly the domain of the outboard plane.

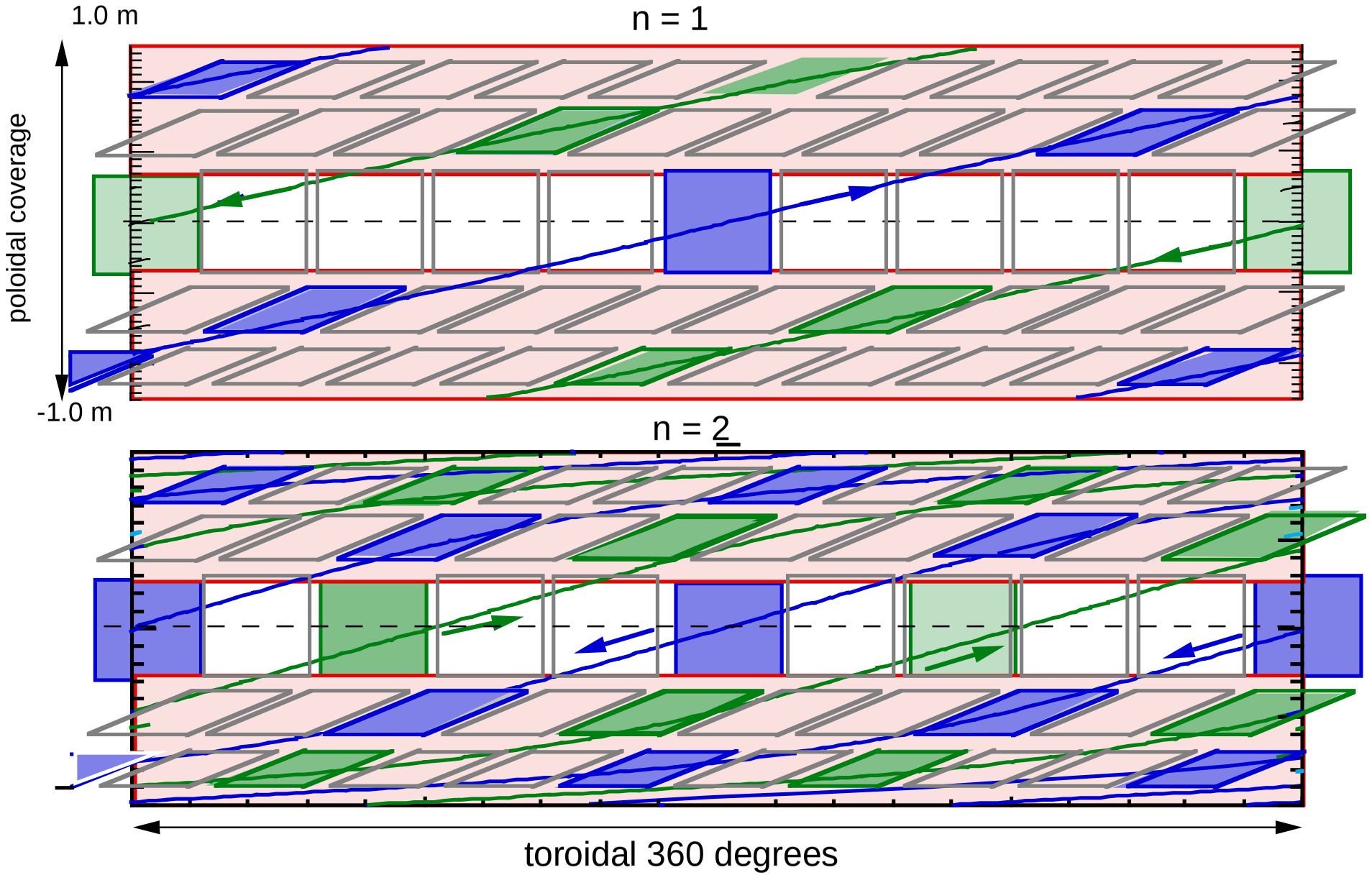

Fig. 2 The actual coil location shown in comparison with the eddy current pattern for n = 1 and n =2. The solid line represents the toroidal location of the maximum and minimum eddy current in the poloidal components, which is discussed in Sec. 4.3.1

Passive / active shell covers major poloidal domain excited by resistive wall mode

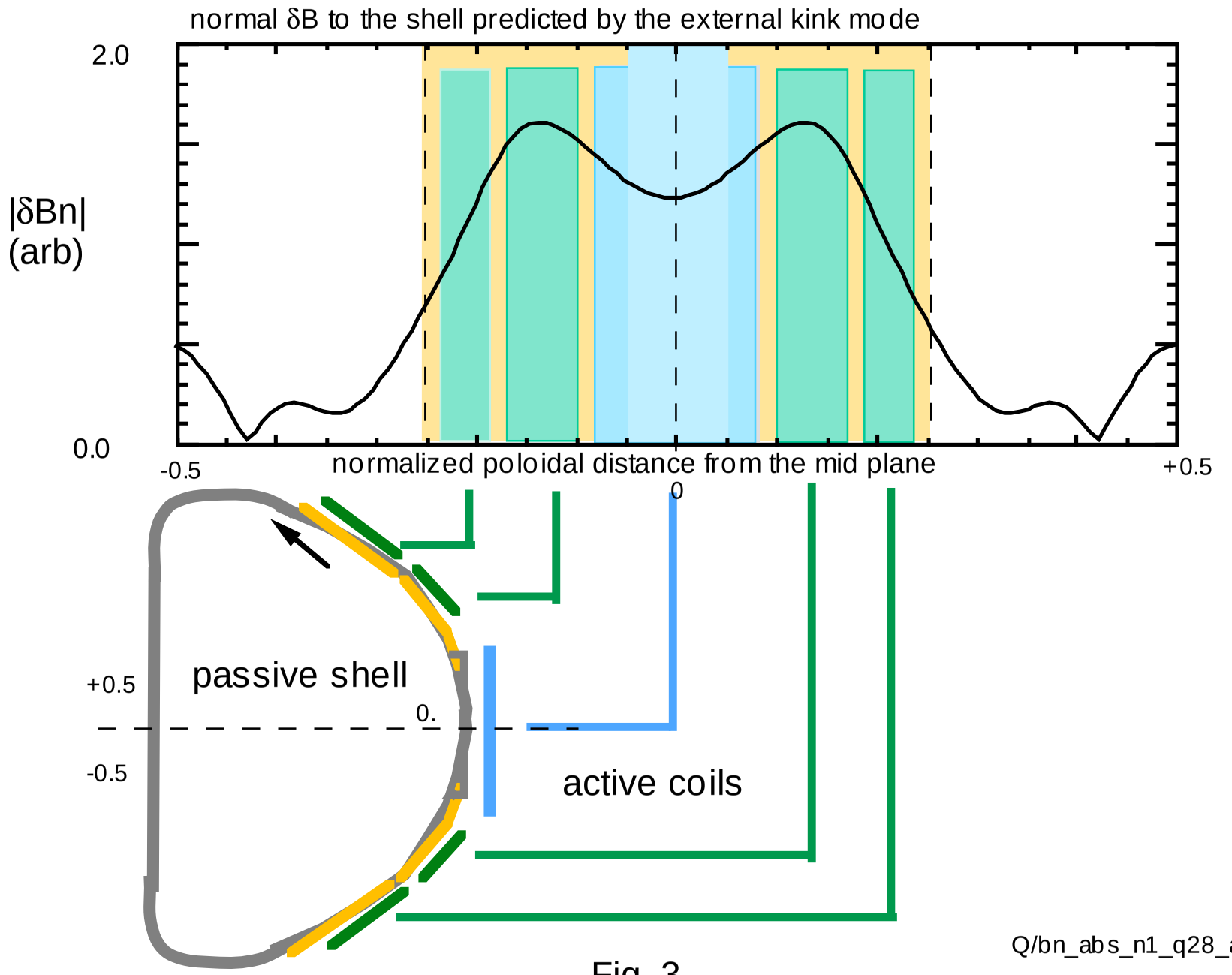

Q/bn_abs_n1_q28_a02

Fig. 3

Helical flux leakage sensor loop and fake rotating shell approach

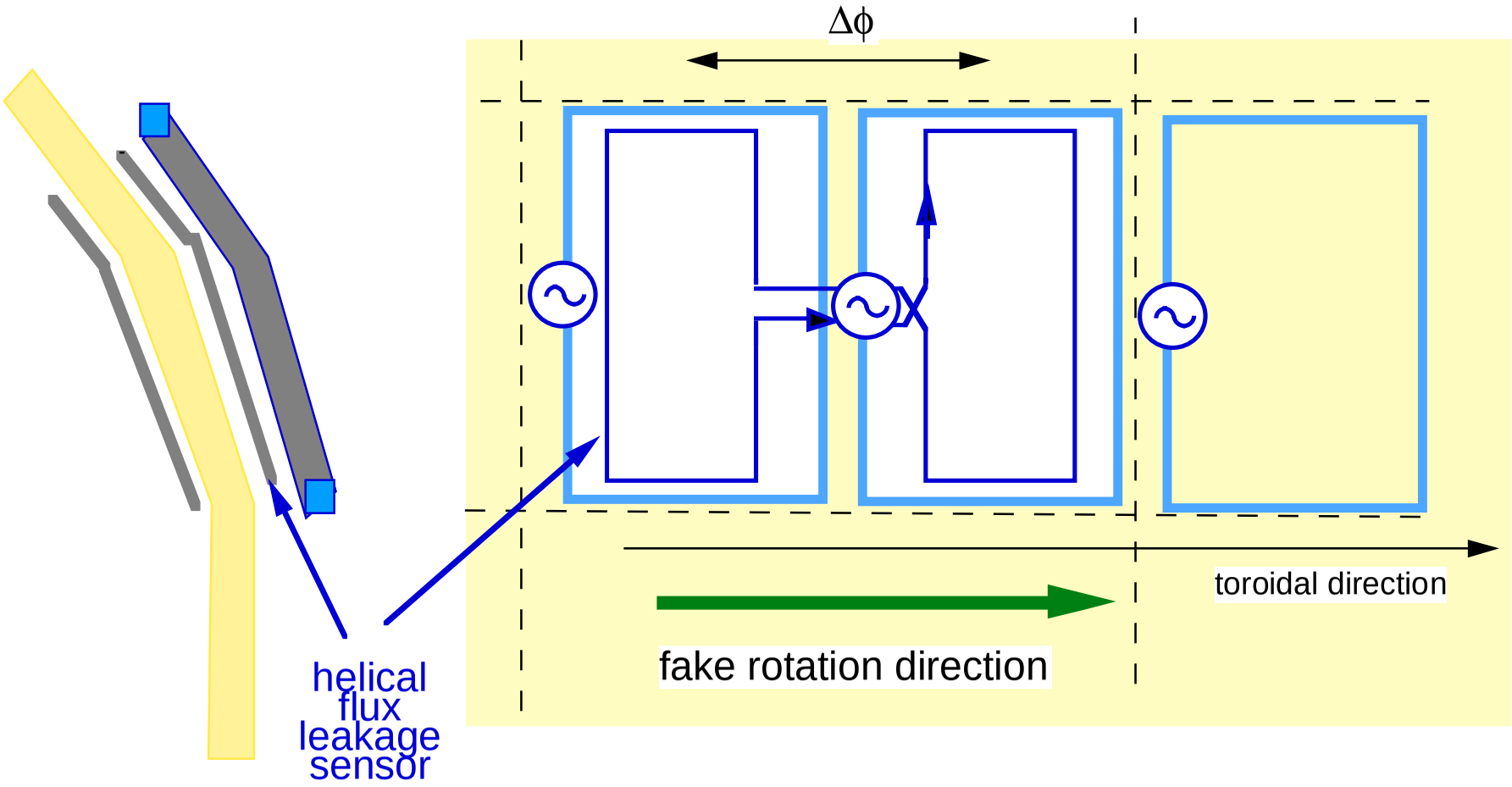

• Fake Rotating Shell Network (by R. Fitzpatrick and T. Jensen) can be implemented by measuring the spacial difference of the toroidal phasing

• Sensors located front & back of "thick alminum shell" assesses the advantage of the "thick highly conducting first wall" like ITER

Fig. 4

57 MHZ FOLDED WAVEGUIDE FOR FSX
ORNL/PPPL

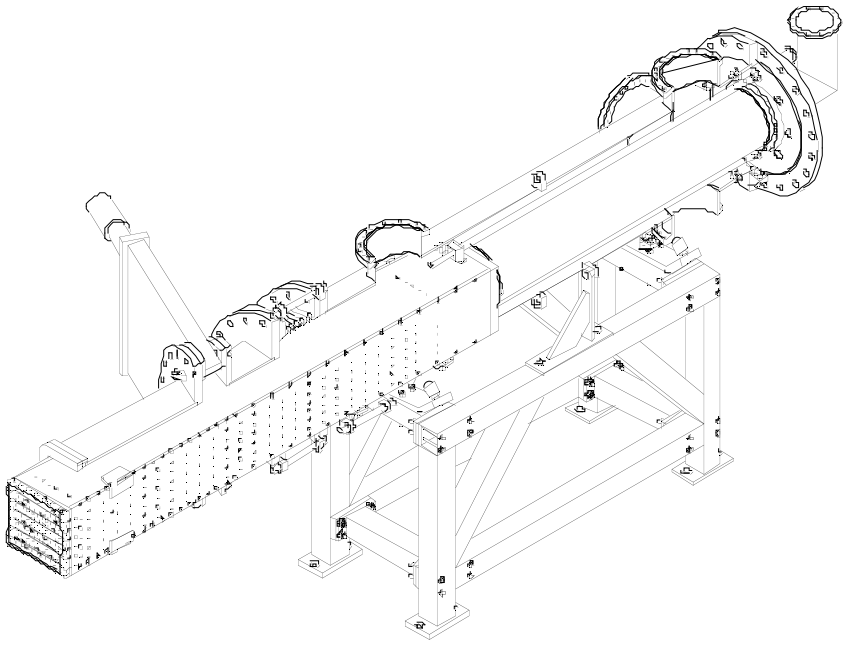

Fig.1. View of ORNL Folded Waveguide. The gate valve and duct allow the waveguide to be removed while torus is under vacuum and adjusted for polarization changes or oriented for IBW or Fast Wave operation.

FSX IBW System

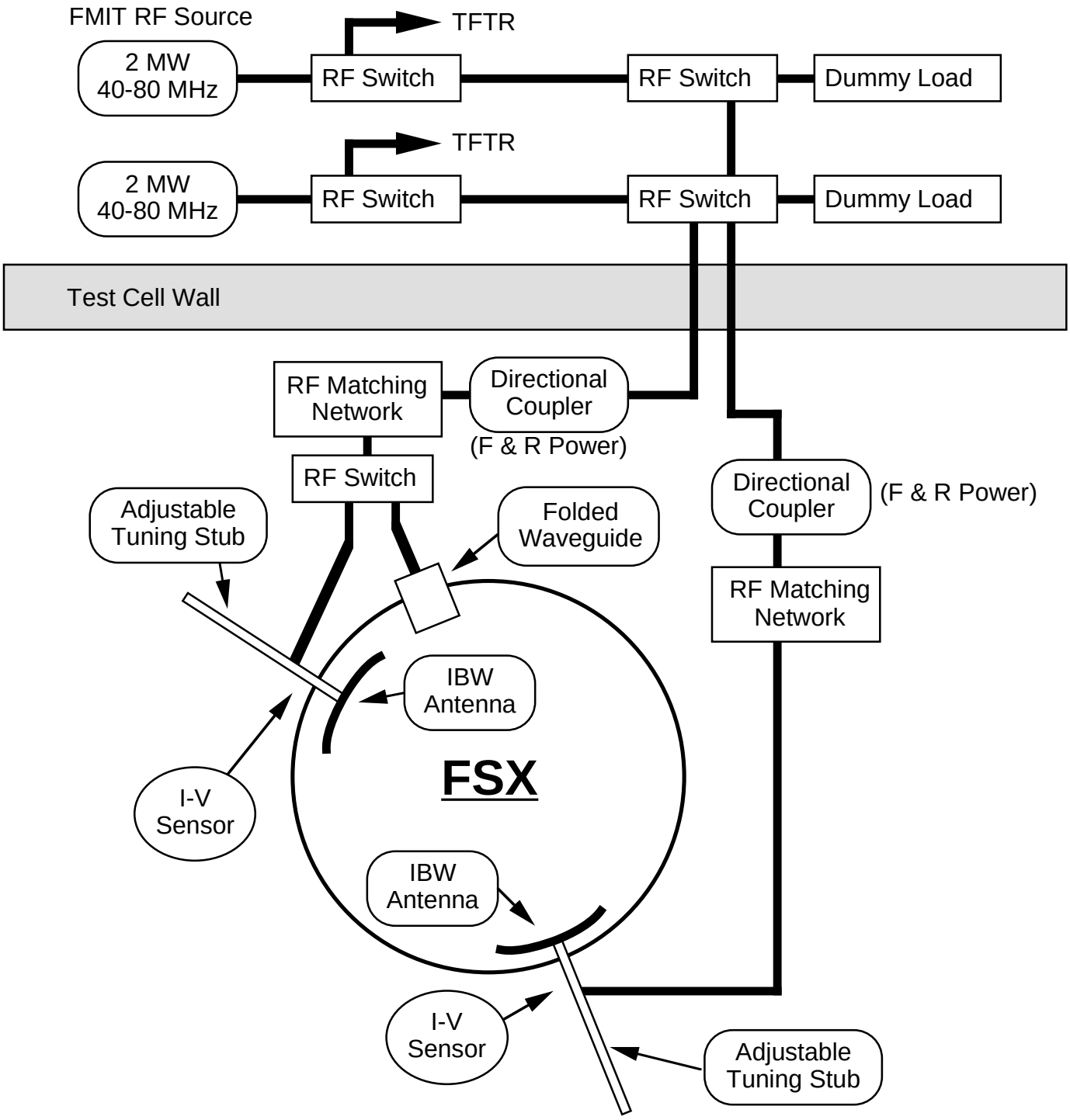

Fig.2. Schematic of FSX IBW System showing antennae and Folded Waveguide

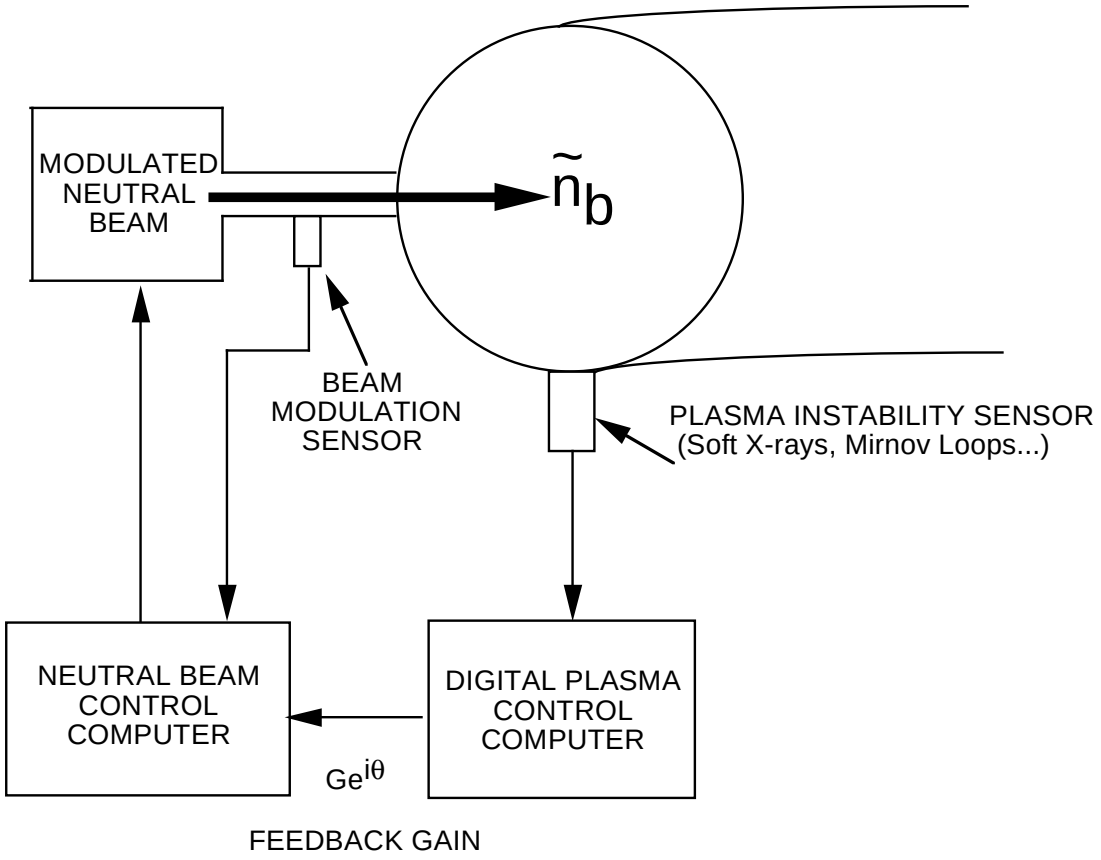

Fig.1. Feedback Suppression of Disruption Modes
Using Neutral Beam Modulation

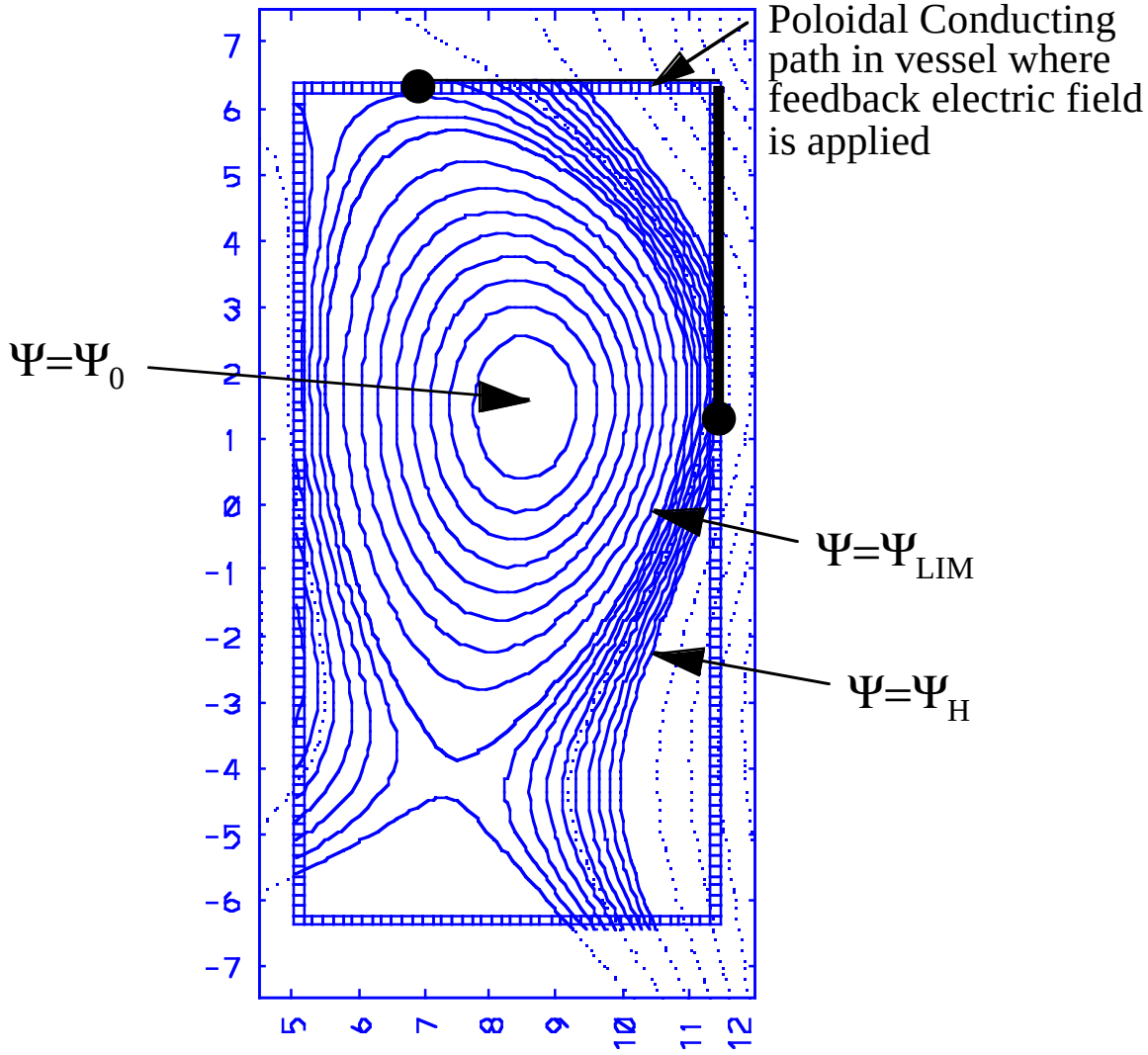

Fig.1. The volume inside the vessel is divided into 3 regions: The plasma region, the halo region, and the vacuum region. The upper right corner of the vessel has a voltage difference proportional to the plasma vertical displacement.

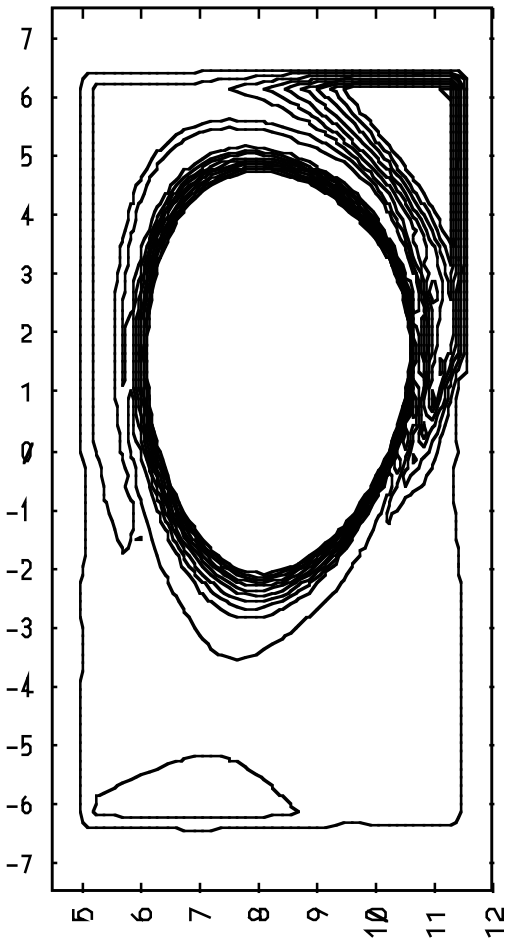

Fig.2a. Poloidal current streamlines at a fixed time for halo feedback calculations with halo width WH = 0.4. The other parameters for these runs were TH = 20 eV, a = 266, EMAX = 40 V/m and TV = 0.1 eV. Streamlines deep inside the plasma region are not shown.

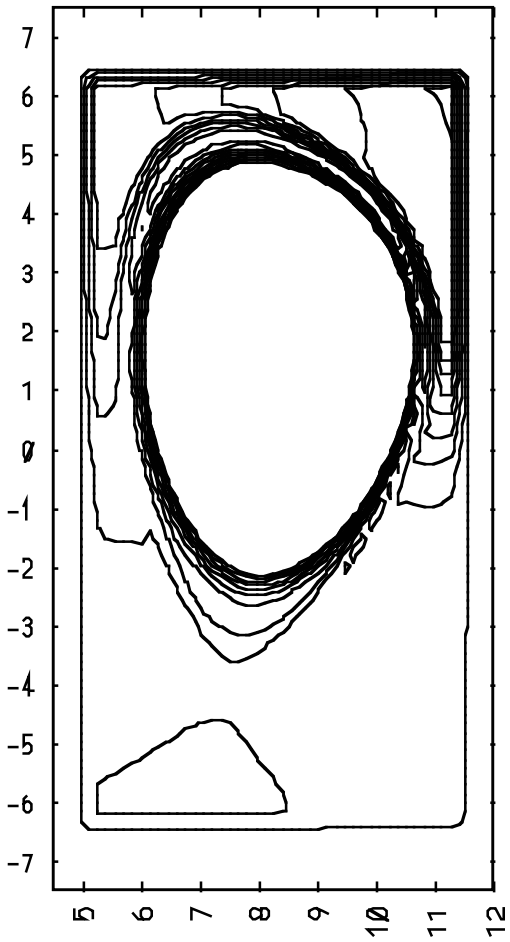

Fig.2b. Poloidal current streamlines at a fixed time halo feedback calculations with halo width WH = 0.01. The other parameters for these runs were TH = 20 eV, a = 266, EMAX = 40 V/m and TV = 0.1 eV. Streamlines deep inside the plasma region are not shown.

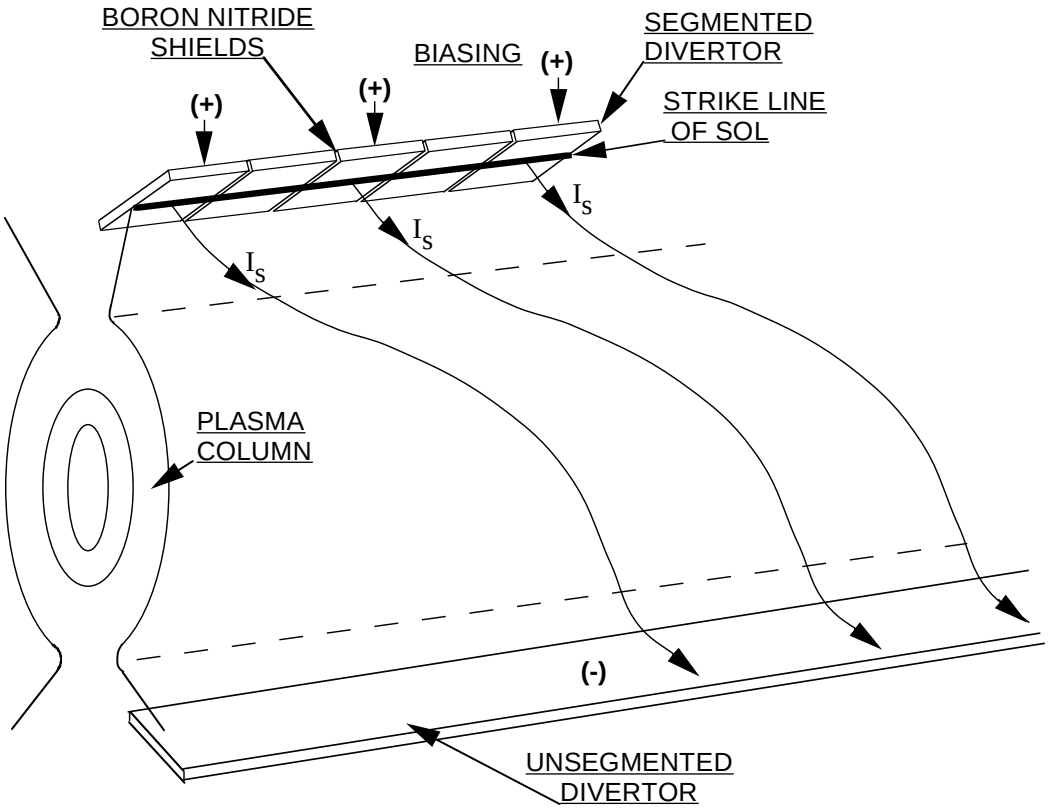

Fig.1. Toroidally segmented upper outer divertor for feedback control of SOL currents. Bias is applied to different segments by the feedback stabilization control system.

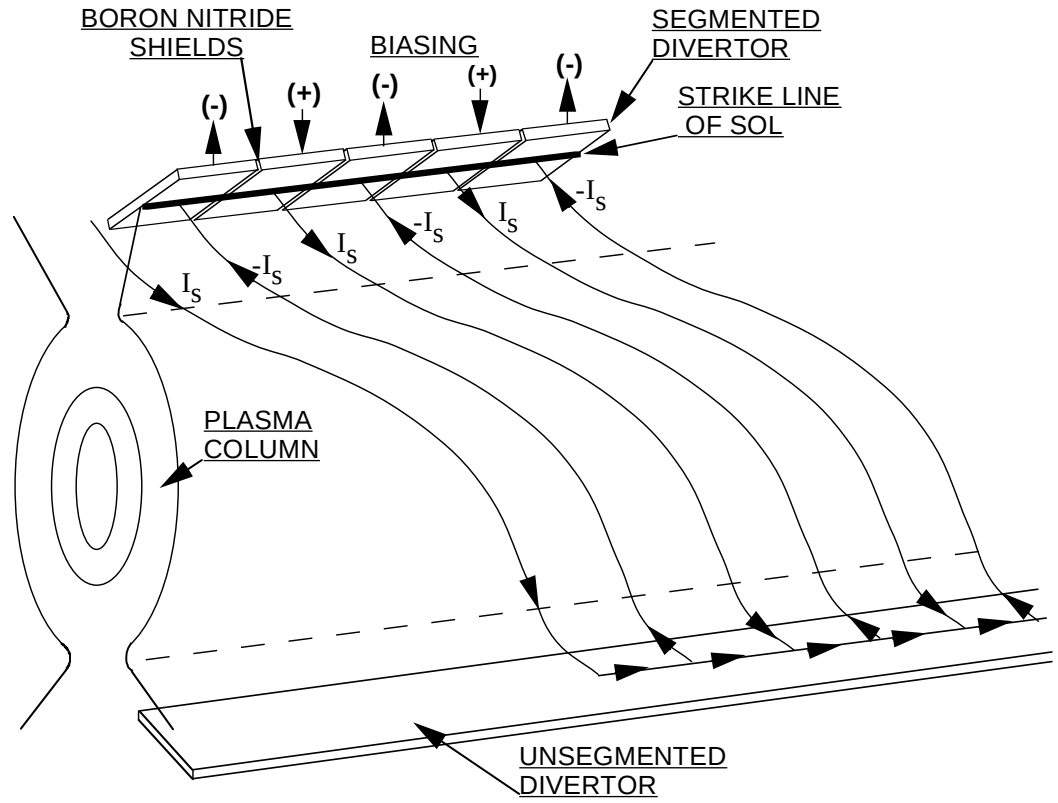

(b)

Fig.1b Upper outer divertor toroidally segmented into separate electrodes with bias of opposite polarity applied to each segment.

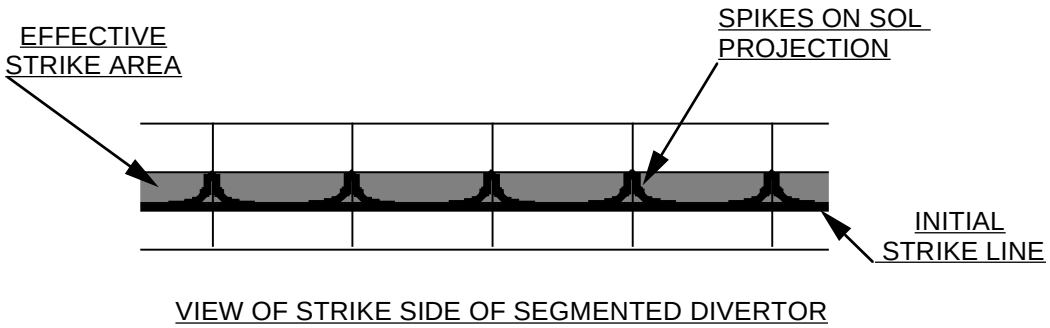

(a)

Fig.1a View of strike side of a toroidally segmented divertor for twisting the magnetic field lines in the outer scrape-off layer so as to broaden the effective deposition area of the incident outer strike points.

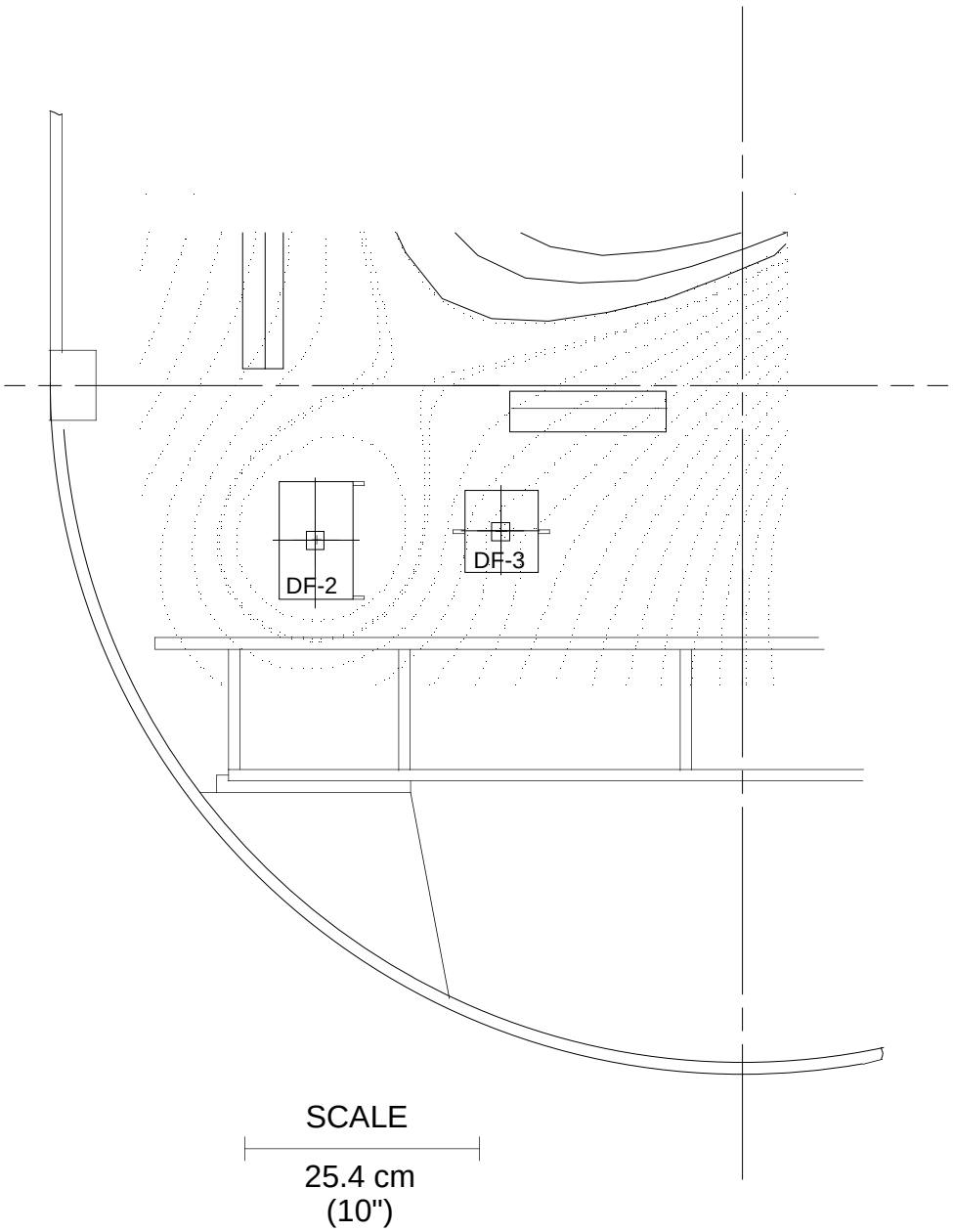

• Reference Equilibrium: Double-Null, TF = 1.5T, Ip = 660 KA, IDF-3 = 1 KA

• Increasing IDF-3 Moves Divertor Lobe Away from X-Point.

Fig.1. FSX Divertor Region Flux Equilibrium Calculation

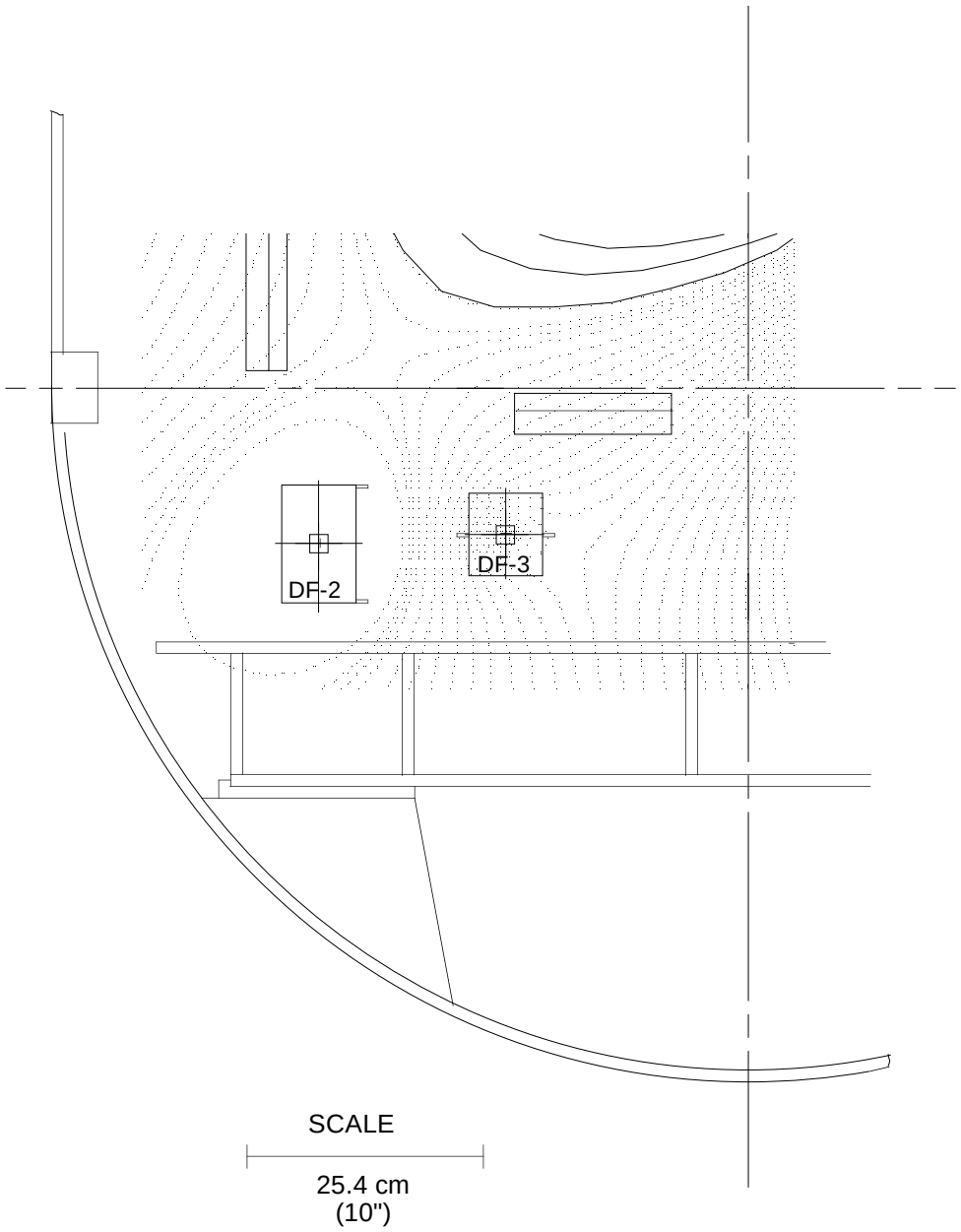

- Reference Equilibrium: Double-Null, TF = 1.5T, Ip = 660KA, IDF-3 = 4 KA.
- Increasing IDF-3 Moves Divertor Lobe Away from X-Point.

Fig.2. FSX Divertor Region Flux Equilibrium Calculation

FSX Divertor Design Concept

• Deep ITER-Like Vertical Targets,
Baffled, Low Fueling, Biasable, Flexible

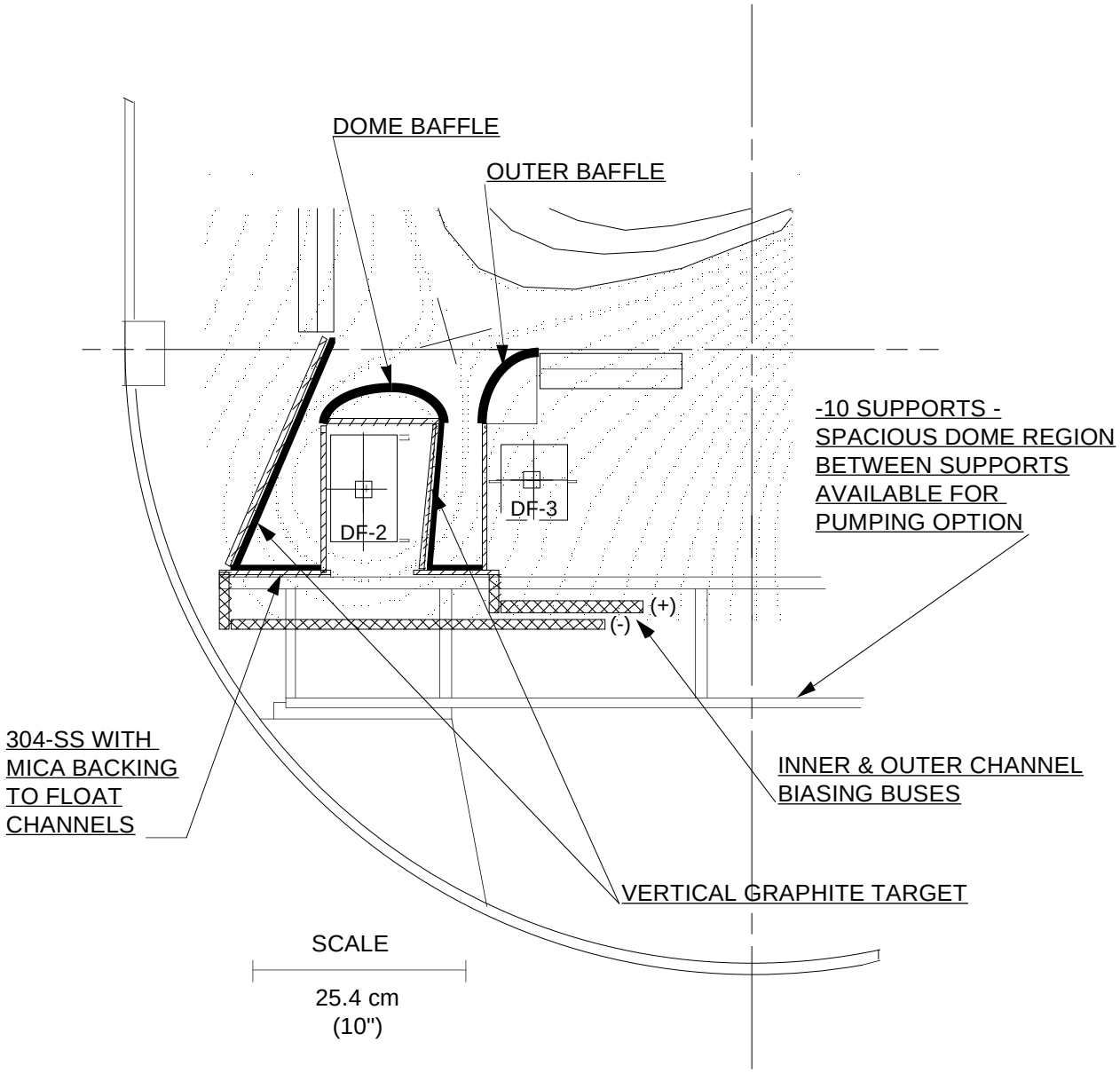

10 TOROIDAL UNITS, CONVENIENTLY REPLACABLE

• Reference Equilibrium: Double-Null, TF =1.5T, Ip = 660KA, IDF-3 = 1KA.
• Increasing IDF-3 Adjusts Strike Points Away from X-Point.

Fig. 3. FSX Divertor Design Concept